ÖZYEĞİN UNIVERSITY

NANO-SCALE CHEMICALLY MODIFIED THIN FILM CHARACTERIZATION FOR CHEMICAL MECHANICAL PLANARIZATION APPLICATIONS

A Dissertation

By

Ayşe Karagöz

Department of Mechanical Engineering
Özyeğin University
Istanbul

Submitted to the
Graduate School of Sciences and Engineering
In Partial Fulfillment of the Requirements for
the Degree of

Doctor of Philosophy
in the

Department of Mechanical Engineering

Özyeğin University
January 2015

Approved by:

_____

Assoc. Prof. Dr. G. Bahar Başım, Advisor
Department of Mechanical Engineering
Özyeğin University

_____

Prof. Dr. M. Pınar Mengüç,
Department of Mechanical Engineering
Özyeğin University

_____

Assoc. Prof. Dr. Göksenin Yaralıoğlu,
Department of Electrical and Electronics Engineering
Özyeğin University

_____

Assoc. Prof. Dr. Güray Erkol,
Department of Natural and Mathematical Sciences
Özyeğin University

_____

Assist. Prof. Dr. Bülent Akgün
Department of Chemistry
Boğaziçi University

Date Approved: 09.01.2015

This work is dedicated to my family, especially my mother Fatma Karagöz and my father Recep Karagöz, for their endless support, encouragement, and patience...

ABSTRACT

Abstract of Dissertation Presented to the Graduate School
of the Ozyegin University in Partial Fulfillment of the
Requirements for the Degree of Doctor of Philosophy

NANO-SCALE CHEMICALLY MODIFIED THIN FILM CHARACTERIZATION FOR CHEMICAL MECHANICAL PLANARIZATION APPLICATIONS

By

Ayşe Karagöz

January 2015

Chair: Dr. G.Bahar Başım

Department: Mechanical Engineering

The aim of the microelectronics industry has historically been achieving increasing functionality through decreasing the device sizes while simultaneously reducing the unit manufacturing costs. This objective has been achieved by the implementation of multilevel metallization (MLM) based on the development of advanced photolithography processes and the chemical mechanical planarization (CMP) process that enabled the successful patterning through photolithography by planarization of the wafer surfaces.

The projected targets of the Integrated Circuit (IC) manufacturing are facing some physical barriers with the current and forthcoming needs of the semiconductor industry

to develop future metal oxide semiconductor field effect transistors (MOSFET). These challenges entail the introduction of new and more difficult materials to achieve better device performance such as use of Germanium due to its higher electron mobility to build faster microprocessors, as well as the use of III-V semiconductors such as GaN, GaAs or InAs which are being tested for high power device applications. Furthermore, new ideas such as reduced power consumption and ability of energy harvesting introduced ferroelectric and magnetic memories, as well as piezoelectric transducers which involve variety of materials harder to integrate to conventional semiconductor manufacturing.

Chemical Mechanical Planarization process is one of the key enablers for the integration of the new materials into the current semiconductor fabrication processes. CMP functions on the principle of chemically modifying the surface to be polished while this surface is continuously abraded mechanically by the Nano-particles homogeneously suspended in the slurry environment. Development of new CMP processes require a robust slurry formulation that can provide high material removal rates (MRR) to promote high volume manufacturing throughput with low dissolution rates (DR) to achieve topographic selectivity and global planarity, in addition to creating minimum surface defectivity surface roughness values. Hence, it is important to understand the chemical and mechanical nature of the CMP process to better control the process and design future processes for the new generation materials.

This dissertation focuses on the characterization of the chemically modified thin films which form during the CMP applications through the exposure of the surface to be polished to the slurry chemicals to optimize the process performance at a Nano-scale. The overall study is presented in two main sections the first part focusing on the findings on the chemically formed metal oxide thin films on metal CMP applications

and the second part focusing on the chemically modified thin film characterization on the nonmetal CMP applications. On metal CMP applications, chemically modified thin films are required to be protective oxides to achieve topographic selectivity. Therefore, the chemically modified thin films of the metal (tungsten) substrates were characterized for thickness and composition as well as their protective nature by calculating their Pilling-Bethworth (P-B) ratio comparing the volume of oxide to the volume of the metal underneath. The analyses have shown a layered oxide film formation with the very top oxide film was detected to be a hydroxyl compound of the tungsten followed by W/WO_x combination in the lower layers until a pure W substrate is reached. Furthermore, it has also been demonstrated that the surface topography of the tungsten wafers tend to change as a function of the oxidizer concentration. The observed changes in the surface topography were also found to affect the wettability and the total surface energy. Hence, it is obvious that the protective nature, as well as the surface nano-topography of the metal oxide thin films need to be studied to assess the metal CMP performance at a nano-scale. Changes in the surface roughness and topography with the oxidizer concentration were also studied through a mathematical modeling approach using Cahn-Hilliard Equation (CHE) approximation. CHE explains the formation of surface nano-structures in terms of reverse diffusion principal and expected to shed light to understanding the changes in the material removal rate mechanisms as a function of the CMP process variables.

In the second half of the dissertation, slurry formulations are evaluated to characterize the chemically modified thin films to enhance selectivity for germanium/silica (Ge/SiO_2) CMP systems. The chemically modified thin films are mainly the hydroxyl layers formed by the dissolution of the materials such as silicon, silica or germanium in front end applications of the CMP. To evaluate the impact of

chemically modified thin films of the Ge/SiO_2 system, it is necessary to modify these chemically modified films with oxidizers and surface active agents (surfactants) since the function of the chemically modified layers in these applications is to achieve optimal removal rate selectivity. Therefore, initially selectivity analyses were conducted by wear rate responses measured at a single particle-surface interaction level through Atomic Force Microscopy (AFM) with and without the use of surfactants. Both anionic (sodium dodecyl sulfate-SDS) and cationic (cetyl trimethyl ammonium bromide-C_{12}TAB) surfactants were evaluated at their sub-micelle and above critical micelle concentrations (CMC) as a function of pH and oxidizer concentrations. CMP performances of Ge and SiO_2 wafers were evaluated in terms of material removal rates, selectivity and surface quality.

This dissertation is composed of seven chapters. The first chapter discusses the importance of nano-scale chemically modified thin films for chemical mechanical planarization process by an introduction to CMP process. Chapter 2 reviews the main components of the CMP process, its integration at the front end, middle section and back end of the line applications, as well as the importance of the characterization of the chemically modified thin films in CMP development. Chapter 3 discusses metal oxide protective thin film characterization for metal CMP applications by focusing on the growth and protective nature of the metal oxide thin films on CVD deposited tungsten wafers pre and post polishing in the presence of an oxidizer. In Chapter 4, CMP performance of the tungsten wafers are evaluated based on the material removal rate and surface quality analyses as a function of the changes in the slurry solids loading and H_2O_2 concentration as an oxidizer. Chapter 5 focuses on germanium/silica CMP through wear rate testing as a preliminary predictive approach as well as through standard CMP MRR evaluations to define a suitable slurry formulation with sufficient

selectivity and removal rate performance. Chapter 6 extends the current knowledge base on the use of surfactant systems from standard shallow trench isolation (STI) CMP to Ge- based STI CMP. CMP results are reported with slurries made of silica particles with 3 wt % solids loading and 200-300 nm particle size in the presence of surfactants and 0.1 M H_2O_2 as an oxidizer. The optimal conditions for slurry formulations are presented as a function of pH and oxidizer concentration on Ge/SiO_2 selectivity statistically through design of experiments (DOE). Finally, Chapter 7 provides a summary of the reported findings of this dissertation, and the suggested future work.

ÖZET

Mikroelektronik endüstrisinin amacı giderek küçülen cihaz boyutlarına rağmen fonksiyonelliğini arttırmayı başarıp, birim üretim maliyetini azaltmaktır. Bu amaç ileri fotolitografi proseslerinin geliştirilmesi ile çok katmanlı metalizasyon işlemine uygulanarak başarılmıştır ve kimyasal mekaniksel düzlemleme (CMP) prosesi de pul yüzeylerin düzlemlenmesi ile fotolitografi desenlerinin başarılı bir şekilde uygulanmasına olanak sağlamaktadır.

Hedeflenen entegre devre (IC) üretimi gelecek yarıiletken endüstrisinde ihtiyaç duyulan metal oksit yarıiletken alan etkili transistorlerin (MOSFET) gelişimi için bazı fiziksel zorluklar ile karşılaşmaktadır. Bu zorluklar germanyum kullanımı gibi yüksek elektron mobilitesine sahip yeni ve daha zor malzemelerin kullanımıyla üstesinden gelinebilecektir, bunun yanında yüksek güçlü cihaz uygulamalarında GaN, GaAs ya da InAs gibi III-V grubuna ait yarıiletkenler kullanılmaktadır. Ayrıca, enerji tüketiminin azaltılması ve enerji depolama yeteneği gibi yeni fikirler ferroelektrik ve manyetik bellekleri tanıtmıştır, hem de çeşitli daha sert malzemelerin yarıiletken üretimine entegre edilmesini sağlayan piezoelektrik güç çeviricileri ön plana çıkarmıştır.

Kimyasal mekaniksel düzlemleme prosesi mevcut yariiletken üretim süreçlerine yeni malzemelerin integrasyonu için önemli bir prosestir. CMP işlemi sulu suspansiyon ortamında homojen olarak dagılmış nano partiküllerin mekanik olarak yüzeyi sürekli aşındırarak parlatılmış yüzeyi kimyasal olarak modifiye etmektedir. Yüksek hacimde üretime ulaşmak için geliştirilen yeni CMP prosesleri yüksek malzeme aşınım hızını sağlayabilecek etkili CMP suspansiyon formülasyonlarına ihtiyaç duymaktadır. Ayrıca topografik seçiciliği ve geniş yüzey düzlemselliğini başarmak için düşük çözünme hızı,

minimum yüzey hasarı ve yüzey pürüzlülüğü sağlamak gerekmektedir. Bu nedenle, daha iyi bir proses kontrolü sağlamak ve yeni nesil malzemeler için gelecek proses tasarımı yapmak için CMP prosesisinin kimyasal ve mekaniksel etkisini anlamak çok önemlidir.

Bu tez CMP uygulamaları sırasında suspansiyon içinde yer alan kimyasallara maruz kalması sonucu pul yüzeyinde oluşan kimyasal olarak modifiye edilmiş ince filmlerin karakterizasyonuna ve process performansının nano boyutta optimize edilmesine odaklanmaktadır. Sunulan calışma iki ana bölüme ayrılmaktadır, birinci bölüm metal CMP uygulamalarında oluşan kimyasal metal oksit ince filmlere, ikinci bölüm ise metal olmayan CMP uygulamalarında oluşan kimyasal olarak modifiye edilmiş ince filmlerin karakterizasyonuna odaklanmaktadır. Metal CMP uygulamalarında, kimyasal modifiye ince filmlerde topografik seçiciligi sağlamak için koruyucu oksit ince filmlere ihtiyaç duyulmaktadır. Bu nedenle, metal (tungsten) yüzeylerinde kimyasal modifiye ince filmlerin kalınlığı ve kompozisyonu karakterize edilmiştir, hemde yüzeyde oluşan oksit hacminin metal hacmine oranlanmasi ile Pilling-Bedworth (P-B) oranı hesaplanarak koruyucu film olup olmadıkları değerlendirilmiştir. Yapılan analizler en alt katmandaki saf tungsten yüzeyine ulaşana kadar en üst katmandaki oksit filmin tungsten hidroksil bileşiğinden oluştuğunu sonraki katmanların W/Wox kombinasyonları şeklinde devam ettiğini göstermiştir. Ayrıca, tungsten pullarinin yüzey topografisinin oksitleyici konsantrasyonuna bağli olarak değişme eğiliminde olduğu belirlenmiştir, gözlemlenen yüzey topografisi değişiminin yüzey ıslanabilirliğini ve toplam yüzey enerjisinide etkilediği sonucuna varılmıştır. Bundan dolayı, bu filmlerin koruyucu bir yapısı olduğu açıktır, ayrıca metal CMP performansını belirlemek için nano boyutta metal oksit ince filmlerin yüzey nano topografisinin incelenmesi gerekmektedir. Yüzey pürüzlülüğünün ve topografisinin oksitleyici

konsantrasyonu ile değişimi ayrica Cahn-Hillard Eşitliği (CHE) yaklaşımı kullanılarak çalışılmıştır. CHE tersine difuzyon prensibine dayanarak yüzeyde nano yapıların oluşumunu açıklamaktadır ve CMP process değişkenlerinin bir fonksiyonu olarak malzeme aşınım hızı mekanizmasındaki degişikliklerin anlaşılmasına ışık tutması beklenmektedir.

Tezin ikinci bölümünde ise, suspansiyon formulasyonları germanyum/silika CMP sistemlerinde seçiciliği sağlayabilmek için kimyasal modifiye ince filmlerin karakterizasyonu değlendirilmiştir. Kimyasal modifiye ince filmler CMP ön uç uygulamalarında silikon, silika ya da germanyum gibi malzemelerin çözünmesi sonucu başlıca hidroksil katmanlarından oluşmaktadır. Ge/SiO_2 sistemine kimyasal modifiye ince filmlerin etkisini değerlendirmek için, yüzey aktif maddeleri (surfaktan) ve oksitleyiciler ile kimyasal modifiye filmlerin modifikasyonu gereklidir çünkü kimyasal modifiye katmanlar bu uygulamalarda optimum aşınım hızı seçiciliğini sağlamanın bir fonksiyonudur. Bu nedenle, ilk olarak seçicilik analizleri yüzey aktif maddesi kullanmadan Atomik Kuvvet Mikroskubu ile tek partikül-yüzey etkileşimi seviyesinde aşınma hızına bağlı olarak analiz edilmiştir. Hem anyonik (Sodyum Dodesil Sulfat-SDS) hemde katyonik (Setil Trimetil Amonyum Bromur-C_{12}TAB) yüzey aktif maddeleri pH ve oksitleyici konsantrasyonunun bir fonksiyonu olarak misel altı ve kritik misel konsantrasyonlarında değerlendirilmiştir. Ge ve SiO_2 pulların CMP performansları malzeme aşınım hızı, seçicilik ve yüzey kalitesi açısından değerlendirilmiştir.

Bu savunma yedi bölümden oluşturulmuştur. Birinci bölüm CMP prosesine girişte nano boyutta kimyasal modifiye ince filmlerin CMP prosesinde önemi tartışılmaktadır. İkinci bölüm başlıca CMP prosesi bileşenlerinden, ön uç, orta kısım ve son uç uygulamalarına integrasyonundan, hemde CMP geliştirme calışmalarında kimyasal

modifiye ince filmlerin karakterizasyonunun önemine yer verilmiştir. Bölüm 3 oksitleyici varlığında CMP öncesi ve sonrası CVD ile işlenmiş tungten pullar üzerindeki metal oksit koruyucu ince film karakterizasyonu ve koruyucu yapısı üzerine odaklanmıştır. Bölüm 4 ise süspansiyon içinde % olarak partikül konsantrasyonunun ve oksitleyici kimyasal hidrojen peroksitin konsantasyonunun değişiminin bir fonksiyonu olarak yüzey kalitesi ve malzeme aşınım hızı temelinde değerlendirilmiştir. Bölüm 5'te ise bir ön yaklaşım olarak aşinma hızı testleri Ge/SiO_2 pulları üzerinde uygulanmıştır hem de uygun süspansiyon formülasyonları ile yeterli seçicilik ve malzeme aşınım hızı performansı değerlendirilmiştir. Bölüm 6 da bilinen yüzey aktif madde sistemleri shallow trench isolation (STI) CMP den Ge temelli STI CMP ye genişletilmiştir. CMP sonuçları 3wt% partkül konsantrasyonu ile 200-300 nm partikül boyutlu silika partiküllerinden, yüzey aktif maddesi varlığında ve oksitleyici olarak 0.1 M H_2O_2 kullanılarak rapor edilmiştir. Deney dizaynı (DOE) programı ile sayısal olarak Ge/SiO_2 seçiciliği için optimum süspansiyon formülasyonlari sunulmuştur. Son olarak, Bölüm 7 tez calışmasında raporlanmış olan bulguların özetini ve tavsiye edilen gelecek calısmalar hakkında bilgi sağlamaktadır.

ACKNOWLEDGEMENTS

First and foremost, I would like to express my sincere gratitude and appreciation to my advisor, Assoc. Prof. Dr. G. Bahar Başım, for her patient, encouragement, guidance and knowledge. It has been an honor to be her first Ph.D. student. I appreciate all her contributions of time, ideas, and funding to make my Ph.D. experience innovative and productive. The joy and enthusiasm she has for her research was contagious and motivational for me, even during tough times in the pursuit of my Ph.D. I am also thankful for the excellent example she has set as a successful woman engineer, advisor, sister and as a mom to her doughter (Doğa). I would like to thank Assoc. Prof. Dr. Göksenin Yaralıoğlu in the department of Electrical and Electronics Engineering and Assoc. Prof. Dr. Güray Erkol in the department of Natural and Mathematical Sciences for their guidance and mentoring of my research, and the through review of my dissertation. I would also like to thank Prof. Dr. M. Pınar Mengüç, and Assist. Prof. Dr. Bülent Akgün for their suggestions and comments on my research. I would also like to thank Assist. Prof. Dr. Yasemin Şengül, who helps me to complete my the modelling studies of my dissertation and also her son Oğuz for his patience when he was in his mother's womb. Moreover, I am indebted to Prof. Dr. Erhan Erkut, founding rector of Özyeğin University for the academic support and the facilities provided to me at the university.

I gratefully thank the support from the Marie Curie International Reintegration Grant (IRG) Call: FP7-PEOPLE-RG-2009 on NANO-PROX project for financially supporting this research. My dearest thanks to the people in this unique consortium.

I would like to thank Prof. Dr. Brij Moudgil, Prof. Dr. Kevin Powers, Mr. Gary Scheiffele and Dr. Gill Brubaker who guided me at Particle Engineering Research Center at the University of Florida during my visit as a research scholar at the University of Florida. I would also like to thank Dr. Valentin Craciun for his assistance in XRR analyses at Major Analytical Instrumentation Center (MAIC) at the University of Florida.

I would like to thank my undergraduate students Taylan Acar, Bora Günoven, Canay Demir and Emre Kağan Çiçek. In addition, I would also like to thank James Mal and Jacob Lum who joined OzU Nano Team for the 2014 Summer Research Programme from the Oregon States University for their contributions.

Special thanks to Professor Holger Schöenherr for making me feel like one of his own research group at the University of Siegen in Germany. My research has greatly benefited from his suggestions and kind encouragement. His technical depth and attention to detail, which I experienced as a visiting researcher at the University of Siegen, Germany. I was very lucky to have crossed paths with him and his research group.

I would like to thank Mrs. Cansu Yıldırım in the Surface Science and Technology Center (KUYTAM) at Koç University who helped me get Dynamic Light Scattering(DLS) and Fourier Transform Infrared Spectroscopy(FTIR) results on my samples.

I would also like to thank Mr. Cüneyt Bağcıoğlu in the TUBITAK-YITAL who helped me measure the thickness of my wafers by Four Point Probe technique.

Thanks to the members of the Physics lab, Wiser lab and Mechanics lab for being the ultimate lab-neighbors, providing a great work environment, and for their help and chats. Also, I would like to thank Gönül Ayci, Ziya Yılmaz, Fatih Ilgın, Barış

Işıldak, Vahid Sajadifar and Kambiz Shojaei for their skill in spreading happiness on those scientifically dark days. I'm also thankful to Murat Kırtay for his help and endless friendship and for sharing elf stories with me at many times.

For the non-scientific side of my dissertation, I particularly want to thank Melek and Davide for many evenings filled with wine and pasta. I thank my precious friend, Mustafa Kaykısız, for sharing bad days as well as good days with me. I thank Nesrin Koyuncu for being like a sister to me and also Deniz Özden for delicious bruschettas. I thank Fırat (Dude) for his persistance and encouragement, in believing me to become a PhD. I am very grateful to Serhad (Ustad) for his friendship and endless support. I would also like to extend my thanks to Ozan Cihangir, I am very pleased to meet him and admire his positive and relaxed attitude. And I also thank Mustafa Onay who was my great colleague when I was working at B/S/H. Special thanks go to Jose Angel Del Campo. I feel very lucky that, in many cases, my friendship with you have extended well beyond our shared times in Germany. Thanks to Sanem, Bilge, Özlem, Cihan and also my Cekirdek Family. I cannot forget friends whom went through hard times together, who cheered me on, and celebrated each accomplishment. Thank you all for sharing these years with me.

Finally, I would like to thank my parents, Fatma and Recep Karagöz, for their continuous support in developing my career and guidance in my life.

Thank you.

Ayşe Karagöz

Özyeğin University

January, 2015

LIST OF TABLES

LIST OF FIGURES

TABLE OF CONTENTS

CHAPTER 1

INTRODUCTION

The requirements in microelectronic manufacturing are changing as the Moore's Law (stating that transistor density on integrated circuits doubles about every two years) approached to its limits. Continuous decrease in the sizes of the transistors has almost come to atomic levels creating a fundamental barrier for the further process developments as the semiconductor manufacturing is established today [Mdu05]. The ongoing development needs are not solely based on device scaling anymore. New methodologies with better precision are needed as rapid introduction and conceptualization of new automotive, medical, implantable devices challenge the needs for improving device performances in addition to cost reduction, zero defectivity and enhanced reliability requirements [Jru06]. Although mainstream semiconductor engineering could involve tradeoffs between performance and reliability, the new applications face assessing the impact of new materials, dealing with limited margins in manufacturing, advances in processing, materials science and chemistry in addition to more rigorous customer expectations [Che08]. Figure 1.1 summarizes the evolution of the Moore's Law with the ground breaking developments and proposed limitations.

This dissertation will particularly focus on the advances on the Chemical Mechanical Planarization (CMP) process, which is one of the most important semiconductor processes in the microprocessor manufacturing. In CMP, it is critical to achieve the performance targets of the modern microprocessor and memory IC's [Bro92], while providing planarization on continuously increasing wafer sizes. CMP was first introduced as a new planarization technique in the semiconductor industry in

the late 1980's, and has been successfully implemented as a key enabling technology for integrated circuit (IC) fabrication since then. The year 2015 marks the 30 years since the initial CMP patents were filled by IBM.

As the transistor nodes continue to decrease to 32 nm, 25 nm and below, and the wafer sizes increase from 200 mm to 300 mm with 450 mm forthcoming, it becomes more challenging to develop new CMP processes. Figure 1.2 demonstrates the increase in the wafer sizes as a function of years, which can also be viewed as the percent increase in the total wafer area and the number of dies per wafer. The development of first memory chip products has started on the standard 2" wafers back in 1969. In the semiconductor industry bigger wafers mean better productivity and more profit and wafer sizes tend to change in every 10 years enabling at least twice more die to be produced as compared to the smaller wafers.

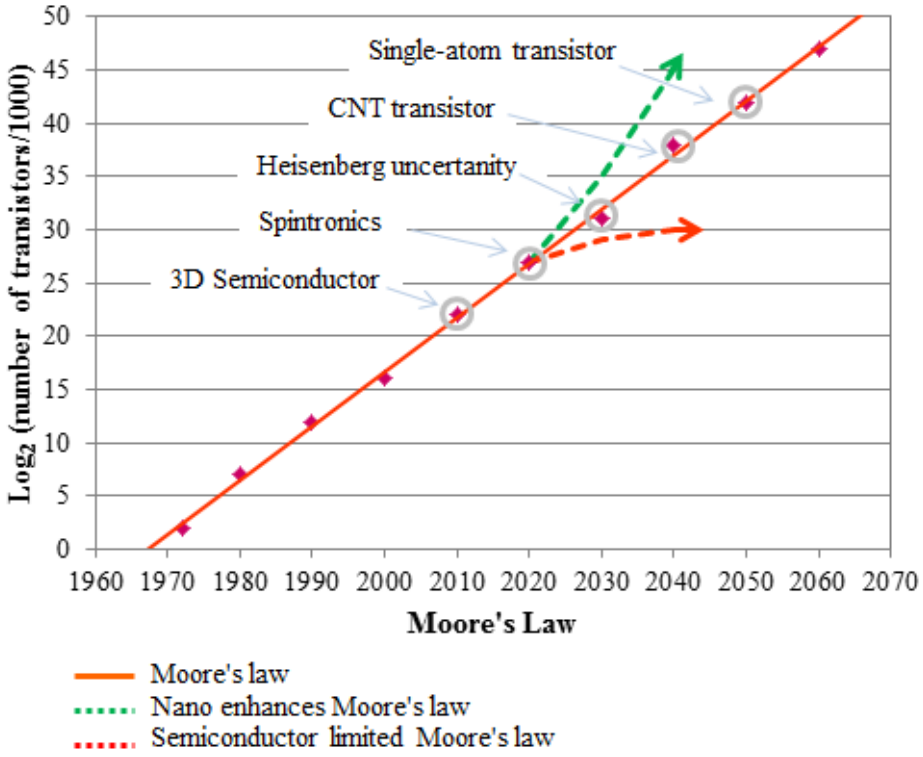

Figure 1.1. The history of Moore's Law with limited factors and projected future including nanotechnology enhancement [Jer12].

The continuous increase in the wafer sizes has been rationalized based on the increase in productivity, which is one of the enablers of the Moore's law. Productivity is the ability to decrease the manufacturing cost for each mm² of IC production increasing the diameter of wafers. The most recent need for 450 mm wafer adaptation was reinforced in 2007 based on the outcomes of an analysis conducted on 300 mm improvements, showing that the so-called "300 mm Prime" program had cycle time improvement opportunities; however, fell short of the traditional cost reduction required to stay on the Moore's Law. This realization prompted The International SEMATECH Manufacturing Initiative (ISMI) to kick off the 450 mm initiative in July 2007.

CMP is an integral part of semiconductor manufacturing in all the three stages of microprocessor architecture. Namely; (i) the transistor device level integration that is also known as the front end of the line (FEOL), (ii) the contact metallization level integration also known as the middle section of the line (MOL) and (iii) the interconnect metallization integration that is called the back end of the line. Significant challenges

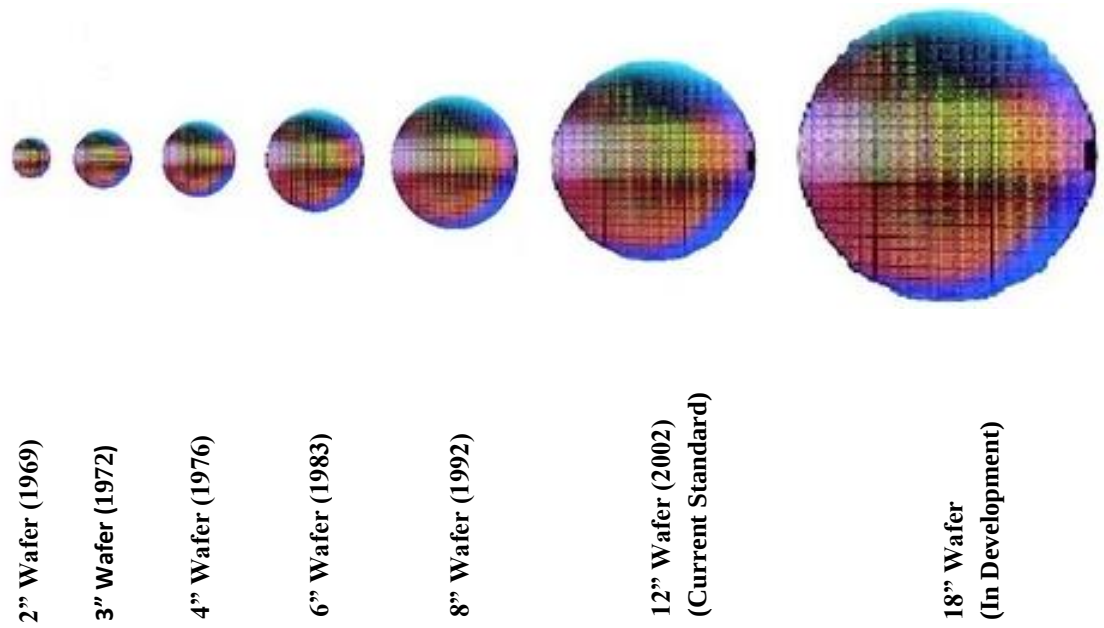

Figure 1.2. The growth of wafer diameters in years.

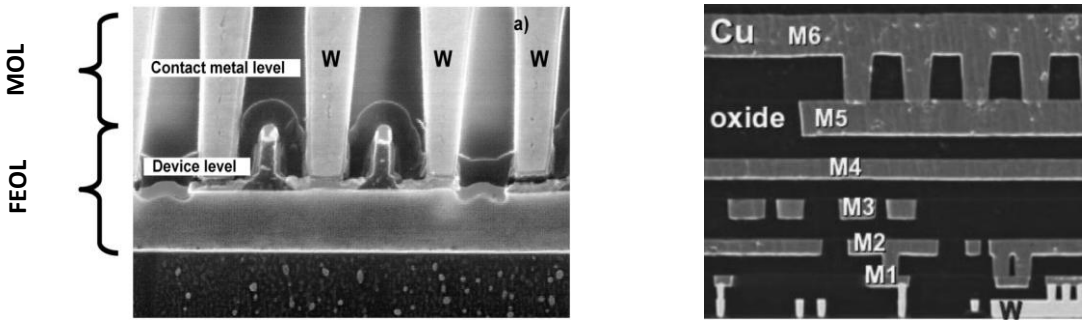

Figure 1.3. SEM cross-section a. showing device and contact metal levels and b. of six-level Cu interconnect structure.

will continue to be faced in all FEOL, MOL, and BEOL applications with the new trend of increasing wafer size while decreasing the device nodes. As the classical CMOS technology consists several hundreds of complex steps which are required to be manufactured on a silicon wafer, each integration step requires adaptations to these changes and challenges. Figure 1.3 shows the cross-sectional images of the FEOL, MOL, and BEOL integration structures. In terms of how these improvements are affecting the CMP process can be summarized through the three steps of the process integration. Shallow Trench Isolation (STI) CMP is the most important planarization application in the front end while tungsten plug CMP applied at MOL and copper CMP connecting the devices produced at FEOL to the interconnect layers in the BEOL. Depending on the step of the integration and the type of the material to be planarized through CMP, the characteristics of the chemically modified nano-layers which are continuously removed by the abrasive slurry nanoparticles vary from hydrated oxides of the semiconductor or dielectric layers to metal oxide nano-films of the metallic substrates.

The CMP applications on the non-metallic substrates, such as semiconductors or dielectrics, the primary formation of the chemically modified thin films is based on the

dissolution of the surface atoms to make hydrated nano-layers. As an example, on silicon and silica, interactions are observed between the siloxane bonds (Si—O—Si) and water. Water breaks Si-O-Si bonds and a softer hydrated layer is formed, which is removed by the abrasive slurry nano-particles during polishing while simultaneously a new layer continue to grow. The reaction for the breakage of the network forming siloxane bonds with water to form a hydrated film on the surface is as follows [Ile79].

$$H_2O + Si—O—Si \; Si—OH + OH—Si \qquad [1.1]$$

Budd explained this reaction as the attack of the solvated hydrogen ion (H3O+) on the negative oxygen sites of silica [Bud61]. The reaction is completed in three steps. First, a water molecule from the environment attaches to the Si—O—Si bond by aligning itself due to the formation of a hydrogen bond between its hydrogen and the oxygen atom of the silica surface, and interaction of the lone pair orbital's of the oxygen in water structure with the Si atom. In the second step, a reaction occurs in which proton transfer from water hydrogen to the oxygen of silica is accomplished simultaneously with electron transfer from the oxygen of water to the silica atom. At the end of these reactions, two new bonds are formed by destroying the original bond between the silica and oxygen resulting in Si—O—H bonds on the surface. The rate of this reaction is believed to be controlled by the diffusion of water into silica structure [Dor73].

In the metallic CMP applications, the nature of the chemically modified thin films is the oxides of the substrate metal. Metal oxide thin films function as a subtractive layer to achieve controlled material removal rates and minimum defectivity in CMP of metals. Furthermore, these metal oxide films are required to be protective in nature to enable topographic selectivity in metal CMP applications. CMP process employs slurries that involve an aggressive chemistry to alter the properties of the film to be polished and this film is removed by the mechanical actions of the abrasive particles in

the slurry suspension. In an optimal CMP slurry design for metal layers, the formation of the metal oxide film should be self-limiting and once formed, it must protect the underlying metal from the further attack of the slurry chemicals. This is necessary to polish the higher level metal while protecting the lower levels (in other words, to achieve topographic selectivity) and hence provide planarization [Fbk91]. Nano scale self-protective oxide thin films comply with the epitaxial stress requirements as the lattice constants match to the substrate (native metal of the oxidized film) and they are self-limiting in growth as the formation of the oxide stops the ongoing chemical reaction before a critical thickness is reached. They are continuous, pore free, adherent, non-volatile and non-reactive.

In summary, characterization of the chemically modified thin films is critical for the nano-scale control of the CMP process. Particularly chemically modified protective oxides of metal thin films are foreseen to have wide applications as (i) an interfacial layer to improve the adhesion and/or limit penetration of reactive chemicals of a deposited film and substrate as in the case for chip packaging, (ii) as a subtractive layer to achieve selective material removal as in CMP and (iii) as a nano-film with inherent self-growth limiting capability that could be used for nano-scale electronics manufacturing. Control of nano scale chemically modified thin film growth and properties using oxidizers, surface active agents, salts, etc.' in turn will lead to optimized process conditions with minimized defectivity and reliability of the current semiconductor manufacturing. In turn, the proposed study will create a basis for the new generation materials for semiconductor industry that is expected to deal with atomic level devices.

In an attempt to enhance the CMP development for the new materials and decreasing device nodes, this dissertation focuses on the characterization of the front

end and back end CMP processes through analyses on the chemically modified thin films and it is organized into seven chapters. The first chapter focuses on establishing a fundamental understanding on why it is critical to study the nano-scale chemically modified thin films characterization for CMP applications. Chapter 2 is an overview of the CMP process Development by initially describing the CMP process and detailing the functions of the three main component in CMP process; (i) the wafer surface to be polished, (ii) polishing pad and (iii) CMP slurries and their formulation summarizing the effects of slurry chemistry on CMP performance and chemically modified thin films. Mechanisms of dissolution and material removal rates on tungsten and germanium/silica CMP are also discussed in this chapter. Finally, the role of chemically modified thin films and their characterizations are summarized and discussed in terms of their functionalities in different CMP applications. Furthermore, new generation CMP applications are introduced.

Chapter 3 focuses on the metal oxide protective thin film characterization for metal CMP applications. Tungsten has been chosen in this part of the study since it has been the metal of choice to fill in the vias starting with the aluminum metallization and also remained to be the first layer fill metal for plugs even for the copper metallization. Hence it is the best studied metal film for the CMP applications and selected for the primary analyses in this study. The growth and material properties of the protective tungsten oxide thin films were studied as a function of the oxidizer concentration. Wettability as well as surface roughness behavior of the oxidized films were analyzed. The thicknesses of the formed oxide layers determined through XRR. Chapter 4 investigates the metal oxide protective nano-film based CMP applications on tungsten. The performances of the slurries were evaluated based on the material removal rate and surface quality analyses conducted on the polished wafers. Simultaneously, the changes

in slurry loading and concentration of H_2O_2 during polishing were demonstrated by introducing a mathematical model to estimate the CMP responses.

Chapter 5 discusses chemically modified thin film analysis on germanium CMP development. Germanium thin films were formed by an oxidizer as a function of concentration and pH. The wettability responses, dissolution rates, as well as the surface topography analyses were presented to characterize the chemically modified thin films in Ge CMP applications. It was observed that the selectivity of the germanium/silica system can be tuned as a function of the oxidizer concentration though the slurry stability was compromised resulting in defective surface finish. Chapter 6 concentrates on improving the Ge CMP performance through thin film modification in the presence of surface active agents to improve slurry stability and the surface defectivity. Slurry formulations were evaluated to enhance selectivity for germanium/silica planarization systems. Furthermore, since the slurry stability is necessary to prevent unacceptable levels of surface roughness and defects, the impact of adding surfactants on particle-particle interactions is investigated in this chapter. Finally, Chapter 7 summarizes the findings of the dissertation and gives an overview for the potential future work extensions of the study.

CHAPTER 2

AN OVERVIEW OF THE CHEMICAL MECHANICAL PLANARIZATION PROCESS AND EFFECT OF CHEMICALLY MODIFIED THIN FILMS IN CMP DEVELOPMENT

In this chapter, an overview of the CMP process is presented starting with outlining the CMP process and the impact of chemically modified nano-films on CMP development. The modern semiconductor manufacturing consists of a complex series of unit process steps which must be performed nearly flawlessly and thus microelectronic manufacturing can be defined as one of the most sophisticated volume production technologies practiced. The microelectronics fabrication steps are the production of silicon (Si) wafers, thermal oxidation, photolithography, etching, doping, film deposition and CMP. CMP is the process of smoothing and planarizing by the chemical and mechanical actions. There are three main components of the CMP process, namely; the surface to be polished, polishing pad, and the polishing slurry which is composed of surface active agents and nano-particles. These three functions as the main components of the CMP process are introduced in this chapter and the various integration schemes as well as the CMP performance criteria are based on the chemically modified thin films are discussed in detail.

Description of the Chemical Mechanical Planarization Process

CMP is a process which was developed for glass polishing primarily. It has been adopted as a microelectronic fabrication process by IBM in the 1980s for SiO_2 dielectric layer polishing. To achieve efficient planarization at miniaturized device dimensions,

there is a need for a better understanding of the physics, chemistry and the complex interplay of tribomechanical phenomena occurring at the interface of the pad and wafer in the presence of the slurry medium. CMP, due to its ability to achieve global planarization and thickness uniformity enables multilayer manufacturing. Furthermore, it has relative cost-effectiveness and hence it is the ideal planarizing medium for the interlayered dielectrics and metal films used in silicon integrated circuit fabrication. CMP is capable of achieving local planarization for features as far apart as 30-μm based on the deposition technique used for the layer to be planarized. The plasma enhanced chemical vapor deposited oxides have limited capability of gap filling and are restricted in their gap filling ability below patterns that have 0.3 μm feature size. High-density plasma (HDP) deposited oxides have acceptable gap filling capabilities; however, they produce variation in surface topography at local as well as global level. Even though spin on deposited (SOD) doped and undoped oxides and polymeric materials have acceptable ability for gap filling, CMP is the only technique, which produces excellent local and global planarity of these materials.

CMP process involves a wafer to be polished which is rotating on a polymeric pad as shown in Figure 2.1. Down force is applied on the wafer while the polishing slurry simultaneously flows in between the pad and the wafer surface. CMP slurries are liquid solutions which contain active chemicals, surface active agents, pH regulators and nano-size abrasive particles. The abrasive particles provide the mechanical action for the material removal and the chemical ingredients of the slurries aid in speeding up the process, achieving selectivity to improve planarization uniformity. Selectivity defines the tendency of the CMP slurry to remove certain materials over others, typically expressed in a ratio. For example an oxide-nitride selectivity ratio of 100:1 means the slurry will remove the oxide layer 100 times faster as compared to nitrides. This type of

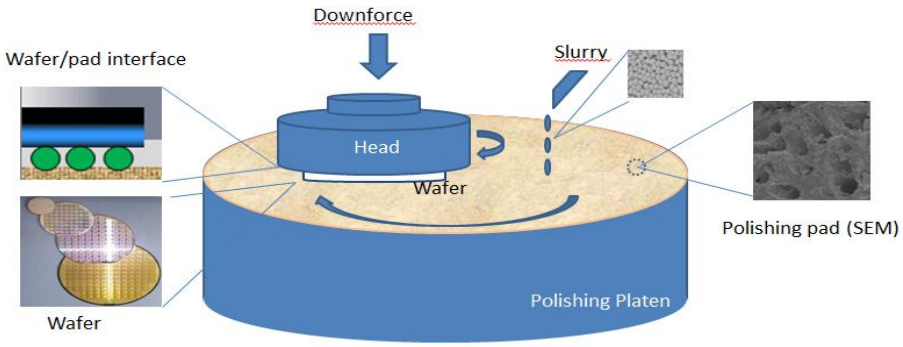

Figure 2.1. Typical Schematic of the CMP Process.

slurry would likely be used on an oxide layer or on an oxynitride layer where it is desired to remove oxides only. Often CMP applications will use multiple slurries with different selectivity in order to target the removal of different materials throughout the process. In general, both the platen and the carrier rotate at the same speed and direction to achieve a uniform relative velocity which is needed to get a uniform wafer thickness [Sad81]. For hard pads such as IC-1000, a diamond disk conditioner is used to regenerate the pad and to avoid glazing.

Advantages and disadvantages of the CMP Process:

The most important advantage of the CMP process is that it helps to achieve global planarization, which is essential for multilevel metallization. There are also several cost advantages of using CMP process. However, CMP process has also some disadvantages arise from the lack of optimization. Typically the process windows are narrow, requiring an increased level of wafer metrology to obtain the desired results. Moreover, there are several potential new defect modes created by CMP. For example, scratching due to the abrasive particles, residual abrasive particles remaining on the surface after cleaning, pressure related stress cracking and delamination at weak interfaces, corrosive attack from the slurry chemicals and across wafer thickness

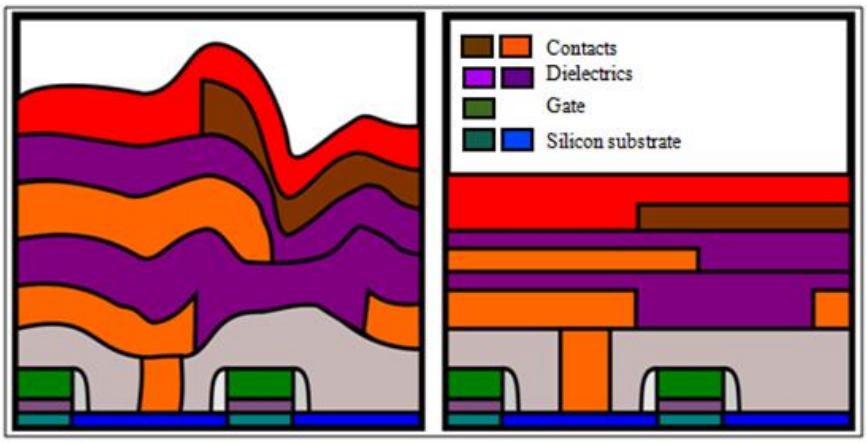

a. without CMP **b.** with CMP

Figure 2.2.a. Schematic of a without CMP and, b. with CMP MLM structure [Leu 14].

variations are all possible CMP-induced defects that must be controlled [Hla92]. Ultimately, CMP is a process that is continuously open to new development and introduction of new equipment on both processing as well as metrology. In order to lessen the process variability closed loop process control techniques have been introduced to measure wafer thickness during polishing via an end point system which was not available in earlier technologies [Jos04]. Need for planarization is increasing with the decreasing intermediate wiring pitch as the non-planarized surface topography results in several processing difficulties. The irregular surfaces cause a hindrance in conformal coating of the photoresist and efficient pattern transfer with contact lithography. The non-uniformity on the surface cause the variation of the thickness in fine line widths (sub 0.25 μm) depending upon photo resist thickness. Figure 2.2.a and b show a comparison between two multilayer metallization integrations without and with the implementation of the CMP planarization.

Main Components of the CMP Process

Wafer Surface:

Wafer surface and the relevant layer to be polished is the number one variable in the CMP processes defining the name of the CMP whether it is for oxides (silica or polysilicon), metals (tungsten, copper) etc'. Interconnects serve as the streets and highways of the integrated circuits (IC) connecting elements of the IC into a functioning transistor and to the outside world. Interconnect levels (or metal layers) vary in numbers depending on the complexity of the device. The first step of the interconnection starts with connecting the transistor to the first layer of metal by etching holes, called vias. Fabricating these intricate structures is one of the most process-intensive and cost-sensitive portions of chip manufacturing. The interconnect technology revolves around the growing number of metal layers in devices. Chemical mechanical planarization (CMP) applications have grown as the number of interconnect levels has increased. Each deposited layer must be polished to ensure a flat surface for subsequent lithography. Without it, the layers would become increasingly uneven and extend outside the depth of focus of available lithography, interfering with the ability to pattern (Figure 2.2). As each metal layer has to be surrounded with the dielectric insulators, CMP process typically starts with the shallow trench isolation which requires an oxide polish that ends at the nitride interface followed by tungsten plug CMP and oxide and metal CMP steps in the back end of the metallization. These steps will be further discussed in the following sections of this chapter.

Polishing Pad:

Polishing pads play a key role in CMP being one of the several consumables in the process. There is still research ongoing on how the pad's physical properties affect the

polishing performance. In the CMP process, polishing pad's main function is to transport the polishing slurry to the wafer surface and provide polishing as it interacts with the high level structures on the wafer. The surface structure and material properties of the polishing pads are important in determining the material removal and planarization ability of the CMP process. A polishing pad normally consists of a soft sub-pad adhered to a more rigid top pad. A Rodel IC1000 on top adhered to a Suba IV underneath, provides good conformability to the wafer surface on a global scale [Zst97]. The rigid top pad (IC1000) is manufactured from polyurethane, while the sub-pad (Suba IV) is polyester felt. Polyurethanes have the unique property of combining high strength with high hardness and modulus and high elongation at failure [Hep82]. A scanning electron micrograph of the pad cross-section is shown in Fig.2.4 [Mac01]. In addition, many of studies on CMP pads have investigated the pad surface qualities before and after CMP is performed.

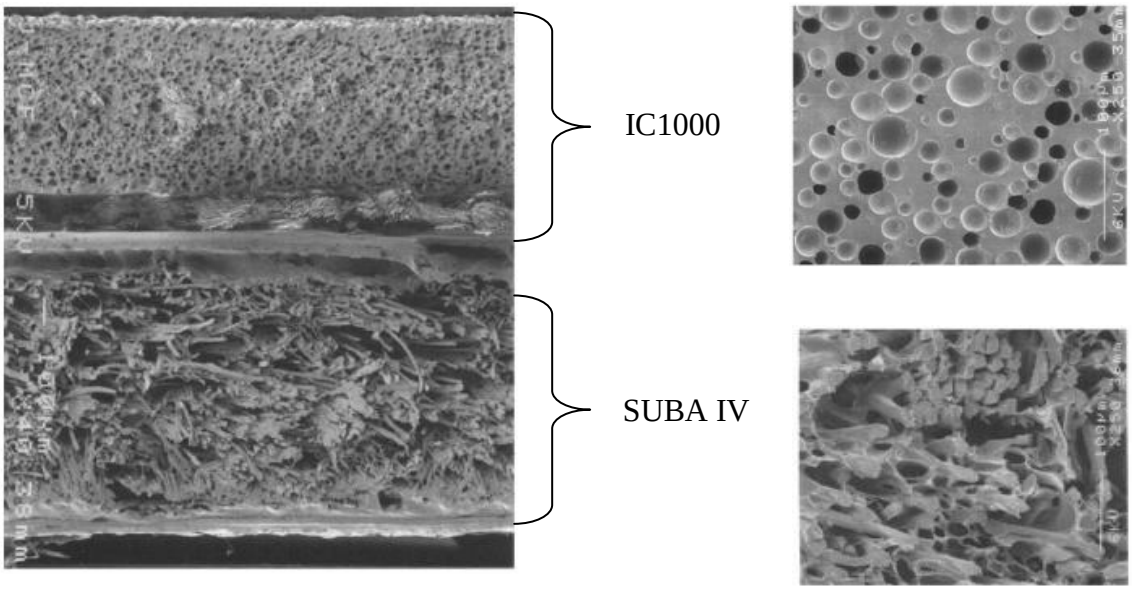

Figure 2.3. A cross-section SEM image of an IC1000 on a Suba IV stacked pad[Hlu02].

Scanning electron micrographs of a polishing pad surface (IC1000) shown in Fig.2.4 reveal the physical differences between new and old (used) pad surfaces, including changes in pore shape, size and depth together with the accumulation of debris as a result of CMP performance. The surface of a new IC1000 layer was shown to be undulating and debris free; but the surface of a used pad was flattened and exhibited elliptical pore geometry with the major pore-axes being parallel to the pad rotating direction. The pore volume of a used pad was decreased and filled with debris from residual slurry abrasive particle, wafer oxide material and/or the removed pad material. An accumulation of debris in the pores decreased the area available for slurry transport during polishing, thus, potentially modifying the nature of the polishing mechanism [Baj94]. Figure 2.4 showed that the pore shape on a new pad surface was circular, which changed as a result of the polishing time which induced an elliptical pore shape by deformation of the surface layer of the polymer. Measurements of the pore shapes were referenced as x parallel to the rotation direction of the pad and y perpendicular to the rotation direction.

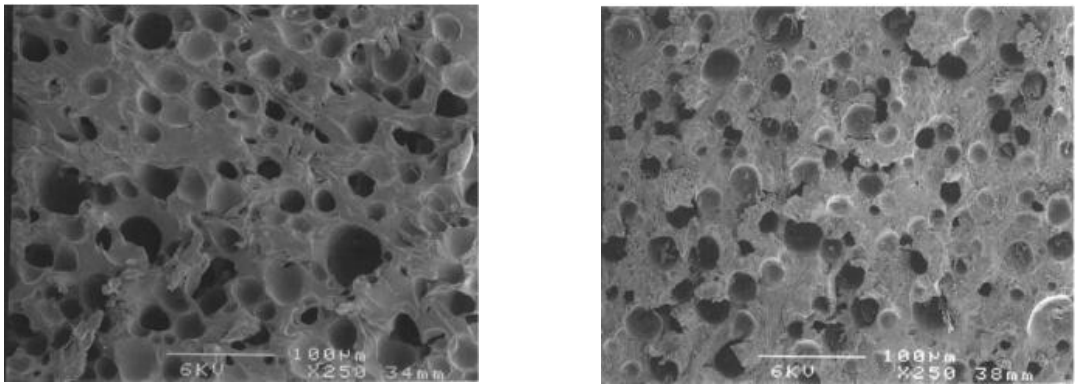

(a) (b)

Figure 2.4. SEM images of the polishing pad top surface (IC1000) : a. new pad and b. used pad [Mac01].

Polishing Slurries:

CMP slurries provide both the chemical action through the solution chemistry and the mechanical action through the abrasive particles during polishing. High polishing rates, planarity, selectivity, uniformity, post CMP cleaning efficiency (including environmental concerns), shelf-life, and dispersion ability are the factors which need to be considered to optimize the slurry performance. The dependence of the removal rate of a particular material to slurry chemistry can be explained through the chemical action of the slurry chemicals of the material, the mechanical abrasion of the abrasive particles on the polished materials, interplay of the different surface active agents, oxidizers and some corrosion inhibitors. The key to a good polishing step is the achievement of synergy between chemical etching and mechanical planarization. Figure 2.5 illustrates the pad-particle-wafer surface interactions with the formation of a passivation layer.

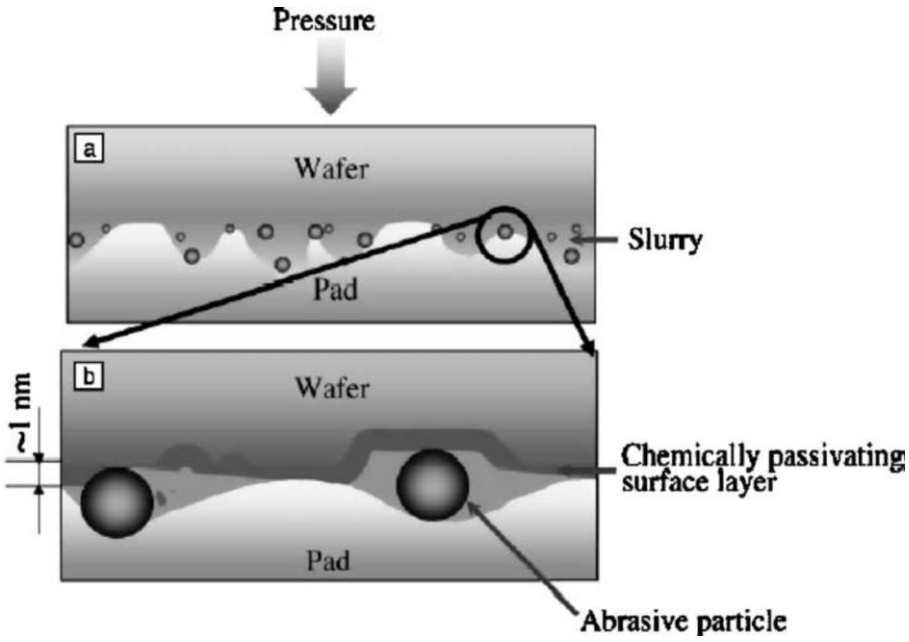

Figure 2.5. Schematic illustration of the micro-scale and nano-scale phenomena during CMP [Tht03].

Integration of CMP in Microelectronics Manufacturing

CMP process integration in microelectronic continuously being updated in all the three main integration levels of the semiconductor device manufacturing. The first level of integration is at the transistor device part which is known to be the front end of the line (FEOL), the contact metal (generally W) plug generation following the gate loop is defined as the middle of the line (MOL), and the interconnect part is called the back end of the line (BEOL). Figure 2.6 shows the cross-sectional images of the FEOL and BEOL integration levels. The most important FEOL CMP process is the shallow trench isolation (STI) CMP. MOL CMP is mainly tungsten contact level metal/liner polish and interlayer dielectric (ILD) polishing processes. Interconnect CMP for metallization is exclusively for Cu, TaN/Ta and other liner removal processes.

FEOL Integration of CMP Process:

CMP applications in FEOL are discussed in this chapter starting with the most important FEOL CMP process, shallow trench isolation (STI) CMP. Due to continuous

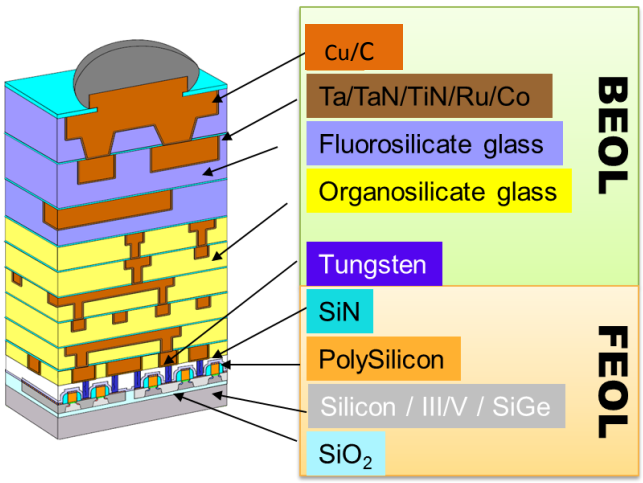

Figure 2.6. Cross-sectional images of the FEOL, MOL and BEOL structures.

shrinking of the transistor size, the gate length of a typical metal oxide field effect transistor (MOSFET) is becoming shorter and shorter bringing the source and the drain further closer to each other which reduces the ability of the gate electrode to control the potential distribution and current flow in the channel [Cro98]. To get rid of this type of short comings, transistors must have evolved from planar single gate devices to three-dimensional devices with multi gate structures. As another example of this type of transistors fin field effect transistor (FinFET) can be given which is another front end CMP application. Fabrication of FinFETs involves a poly-Si CMP step as shown in Figure 2.7. CMP slurry development is necessary which is selective to poly-Si and can stop on materials such as Si_3N_4 to enable planarization. Typically, these slurries consist of ceria or silica abrasive particles with chemical additives which selectively bind to SiO_2, Si_3N, yet do not affect the poly-Si material removal. In addition, new generation materials like germanium (Ge) and III-V semiconductors are replacing Si as the channel material in the future devices. These new generation materials also need CMP process for successful integration into the semiconductor manufacturing process. Shallow Trench Isolation: Shallow trench isolation (STI) structures were introduced at the 0.25 μm technology node to replace traditional LOCOS (local oxidation of silicon)

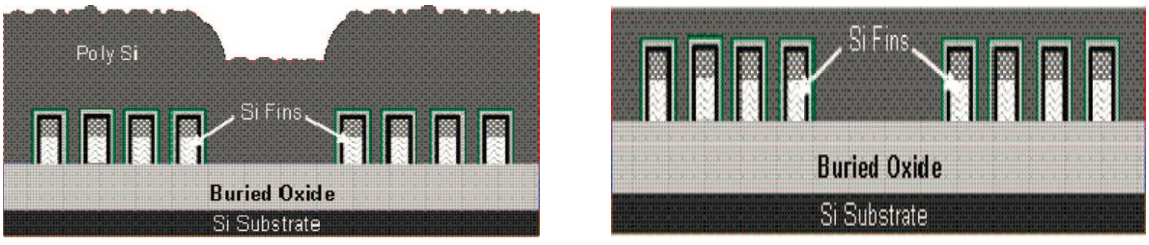

Before CMP After CMP

Figure 2.7. Schematic diagram of the poly-Si CMP process for FinFET before and after CMP Process [Mah09].

structures to provide better device isolation. STI enables improved trench profile control and vastly greater packing density. The schematic diagram of the STI CMP process along with the subsequent wet etch processes are described in Figure 2.8.

STI has become a key technology for device isolation in recent times. The importance and the need for shallow trench isolation have been discussed by Wolf [Swo91]. The method comprises of making a shallow trench on a silicon wafer, depositing SiO_2 on the wafer filling the trenches with an overcoat, and then planarizing with a chemical mechanical polishing step. A complicated reverse moat etch process had to be used in the absence of sufficiently selective slurries for SiO_2 to SiN polishing. Using an etch process, the high-density moat regions can be reduced to an acceptable level and therefore the chip or wafer level polishing uniformity can be greatly enhanced. If direct CMP without the reverse moat etch process was applied with conventional low

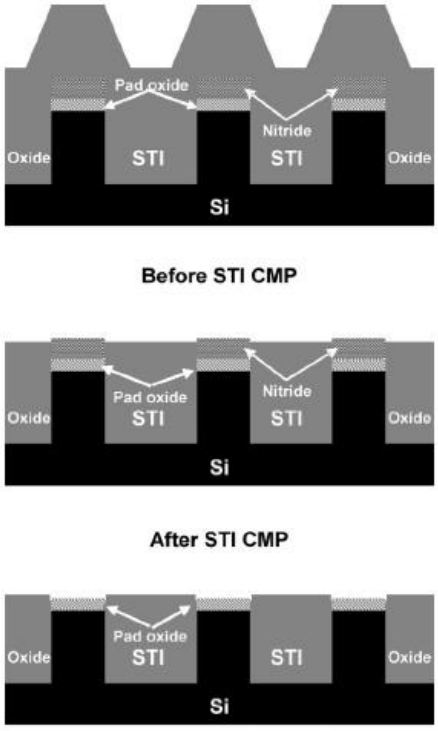

Figure 2.8. Schematic diagram of STI CMP process.

Selectivity slurries, damage might occur to active regions in the case of excessive CMP (overpolish), whereas, in the case of insufficient CMP, nitride residues might remain in the active regions after the nitride strip process due to oxide overburden [Psa98]. Currently, new materials like germanium (Ge) and III/V materials such as indium phosphide (InP), gallium arsenide (GaAs), etc. are replacing Si as the channel material in future transistor devices. These new materials also require CMP process for successful integration into future devices.

CMP of Germanium: The first bipolar transistors were made with germanium which is a semiconductor material. Although the photo response properties of germanium were determined earlier, [Eaf95] the large scale implementation of the germanium market, however, lagged behind the explosive growth in use of electronic devices of all kinds, since germanium was being supplanted in many ways by silicon. Silicon was cheaper as a material and, more importantly, lent itself much more readily to the new techniques developed for the manufacture of large-scale (LS) and very-large-scale (VLS) integrated circuits. Germanium was favored for certain high-frequency and high-power devices, but silicon had supplanted it in most microelectronic components by the end of the 1970s [Rep05]. Particularly, relaxed graded SiGe buffers have been used as substrates for the high electron mobility structures and for integration of III-V devices on silicon [Eaf91]. The high mobility structures in germanium (three times higher than in Si for electrons and four times for holes) can make it easier for the formation of higher-speed devices.

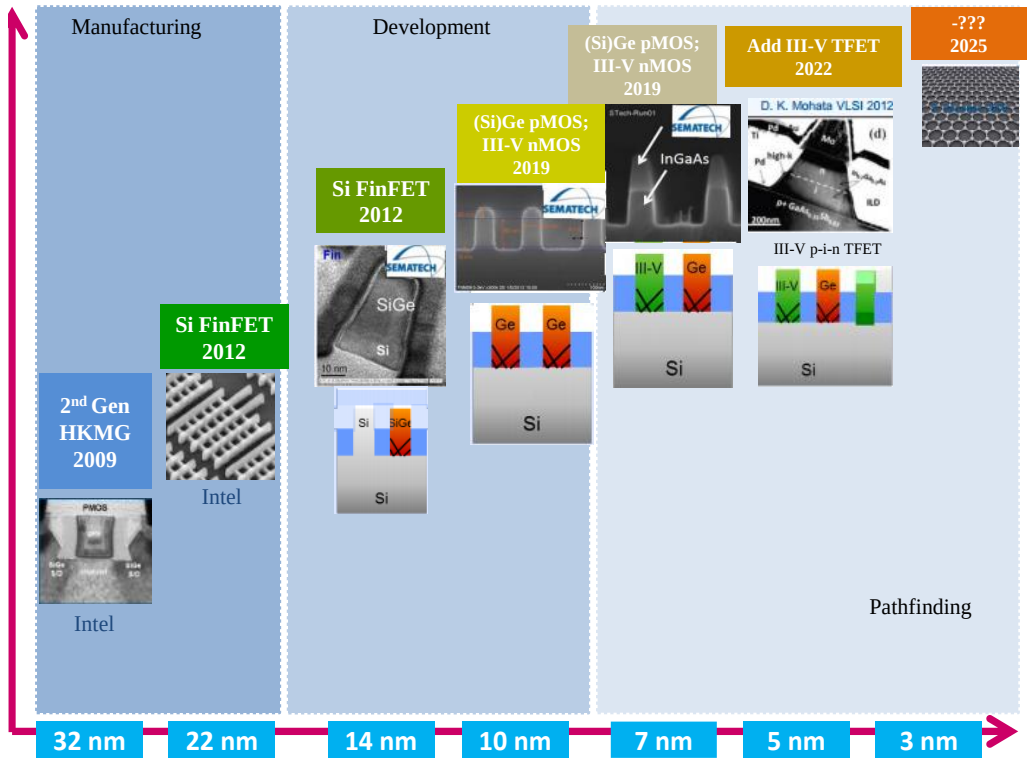

Figure 2.9. Possible logic technology roadmap [Rjw13].

CMP is a critical processing step for successful integration of germanium into the current manufacturing process. The improved performance for Ge-based pMOS devices has been demonstrated on a Si platform earlier [Jmi09]. Peddeti and coworkers used the colloidal silica and germanium surface for zeta potential measurements as a function of pH and concluded that the zeta potentials in the presence of H_2O_2 were also similar to J. B. Matovu's results [Ped12]. From the zeta potential measurements at pH 2.25, they selected a region where the silica surface was negatively charged and the Ge surface was positively charged, which was predicted to lead to electrostatic attraction and hence higher material removal rates (MRR). In contrast, at pH 6 and 10, both the Ge and silica particle surfaces were negatively charged leading to strong repulsion between the surfaces and thus required higher abrasive concentration to enhance the MRR. At pH 4

the Ge wafer surface was only slightly negative resulting in an intermediary position, where the repulsive forces were minimal and the MRRs were only slightly higher than at pH 6. On the other hand, while the attractive electrostatic interactions may lead to higher MRRs, the surface quality will be negatively impacted since the electrostatic attraction tends to result in particles sticking the germanium surface and result in post CMP defectivity. Moreover, Hydrick et al. used different additives (NaOCl, H_2O_2, and NH_4OH) in colloidal for improving Ge RR and one important result was reported that the high metal contamination determined on the samples when polished with NaOCl-based slurries was absent in the samples polished with H_2O_2 is the preferred oxidizer. When it comes to the expectations of Ge CMP performance criteria are similar to conventional STI CMP. In the literature it has been shown that a slightly recessed oxide profile is needed for better device performance (this means a slightly higher silica removal rate is preferred at the SiO_2/Ge interface. To enable material removal H_2O_2 is used as an oxidizer but higher concentrations of H_2O_2 result in pitting and very high Ge dissolution rate. It has also been shown that the use of CTAB (16 carbon standard) at 0.1 mM concentration and pH 8 can give a sufficient removal rate on Ge (~450 nm/min) with some selectivity.

MOL Integration of CMP Process

MOL is connecting layer which is between the devices in the FEOL to the interconnect layers in the BEOL. The material of choice for this connection (or plug) is tungsten (W), as it has superior electron migration properties along with being a good diffusion barrier for Cu (which is the interconnect material). Several process steps are involved in the fabrication of the W plug. A dielectric layer is deposited on the transistors developed at FEOL processing. CMP of this dielectric layer (also called as

the inter layer dielectric or ILD) removes the topography imprint of the underlying FEOL structures producing a uniform surface for further fabrication.

Tungsten CMP has been the foundation for contacts and vias, since tungsten is used for local wiring and for the contact level to the devices in microprocessors, ASICs (application-specific integrated circuit) and DRAMs (Dynamic random-access memory) [Wei09]. It also acts as a good diffusion barrier and prevents the diffusion of Al and Cu into the device structures at the thickness used in contact level metallurgy. The processing steps include deposition of tungsten by LPCVD (Low Pressure Chemical Vapor Deposition) over patterned trenches in dielectric and removal of the overburden to create inlaid metal via. LPCVD tungsten deposits have been conformal and have had good fill characteristics up to 90 nm technology node. Starting from 65 nm node, because of the high aspect ratio vias, seams in tungsten deposits have been observed. So far this has not affected the use of LPCVD tungsten for contact level metallization even though efforts are underway to find alternatives.

The W CMP process should provide excellent planarity since the first BEOL interconnect level will be adversely affected by the topography created by the contact via level polish. Thus dishing and erosion in W CMP could lead to serious shorting problems in the first interconnect metal level. This is worsened by the use of borophosphosilicate glass (BPSG) or borophosphorous tetraethyl orthosilicate (BPTEOS) as the dielectric material due to their softness as compared to oxide. In addition, the FEOL topography that is produced before the contact level is also significant. It is necessary to reduce the FEOL topography by using a CMP step after the BPSG dielectric deposition. This is known as the ILD polish. To improve the adhesion of tungsten to the dielectric, a Ti/TiN liner is used. This layer is also believed to act as a barrier layer for tungsten. The tungsten CMP process involves three steps:

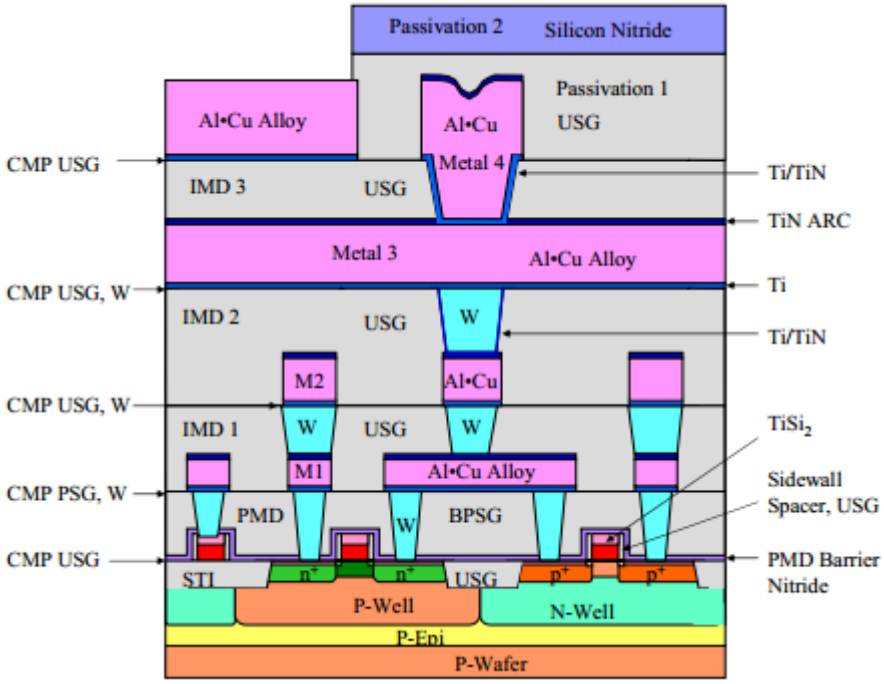

Figure 2.10. W integration structure on CMOS IC.

removal of tungsten and stopping in Ti/TiN liner, removal of the liner material, and stopping on the dielectric, followed by post- CMP cleaning.

BEOL Integration on CMP Process

The BEOL is the second part of IC fabrication where the individual devices such as transistors, capacitors, resistors, etc. get interconnects with wiring on the wafer. BEOL process generally begins when the first layer of metal is deposited on the wafer substrate. BEOL includes contacts, dielectrics, metal levels, and bonding parts for chip to package connections. After the last FEOL step, there is a wafer with isolated transistor. To improve performance of interconnects, Cu/low-k structure was introduced to reduce the parasitic resistance and capacitance in advanced CMOS technology. But when CMOS technology is scaling down to 16nm and beyond, Cu BEOL extension technology need to be developed to meet the chip performance requirements. In BEOL

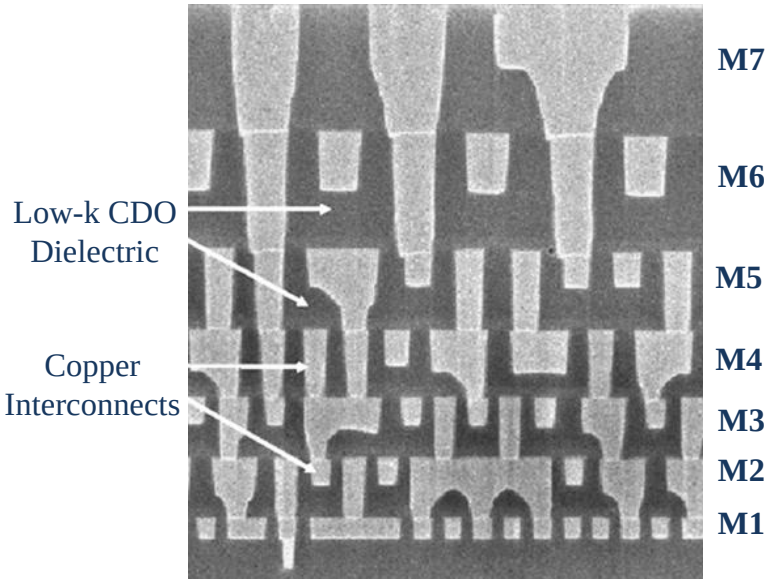

Figure 2.11. SEM cross section of a multilevel interconnect showing thin wire and fat wire levels.

part of fabrication stage contacts (pads), interconnect wires, vias and dielectric structures are formed. More than 10 metal layers can be added in the BEOL for modern IC process technology. Figure 2.11 shows the SEM cross-section of a modern multilevel interconnects structure with thin wire and fat wire levels.

The fabrication of copper interconnect lines is done through what are known as damascene and dual damascene processes as shown in figure 2.12 The deposition of a dielectric insulating layer is first step in these process SiO_2, fluorinated glass (SiOF), hydrogen silesquioxane (HSQ), porous methyl silesquioxane (MSQ), etc. are the alternatives. After deposition step, this layer is etched selectively to create trenches for interconnect materials (generally copper). Cu readily diffuses on these dielectric films and hence a thin conformal layer of a material which can act as a barrier to Cu diffusion and as an adhesion promoter is first deposited in the trenches. The most common materials for this aim are tantalum (Ta) and tantalum nitride (TaN), and most recently ruthenium (Ru) is being used.

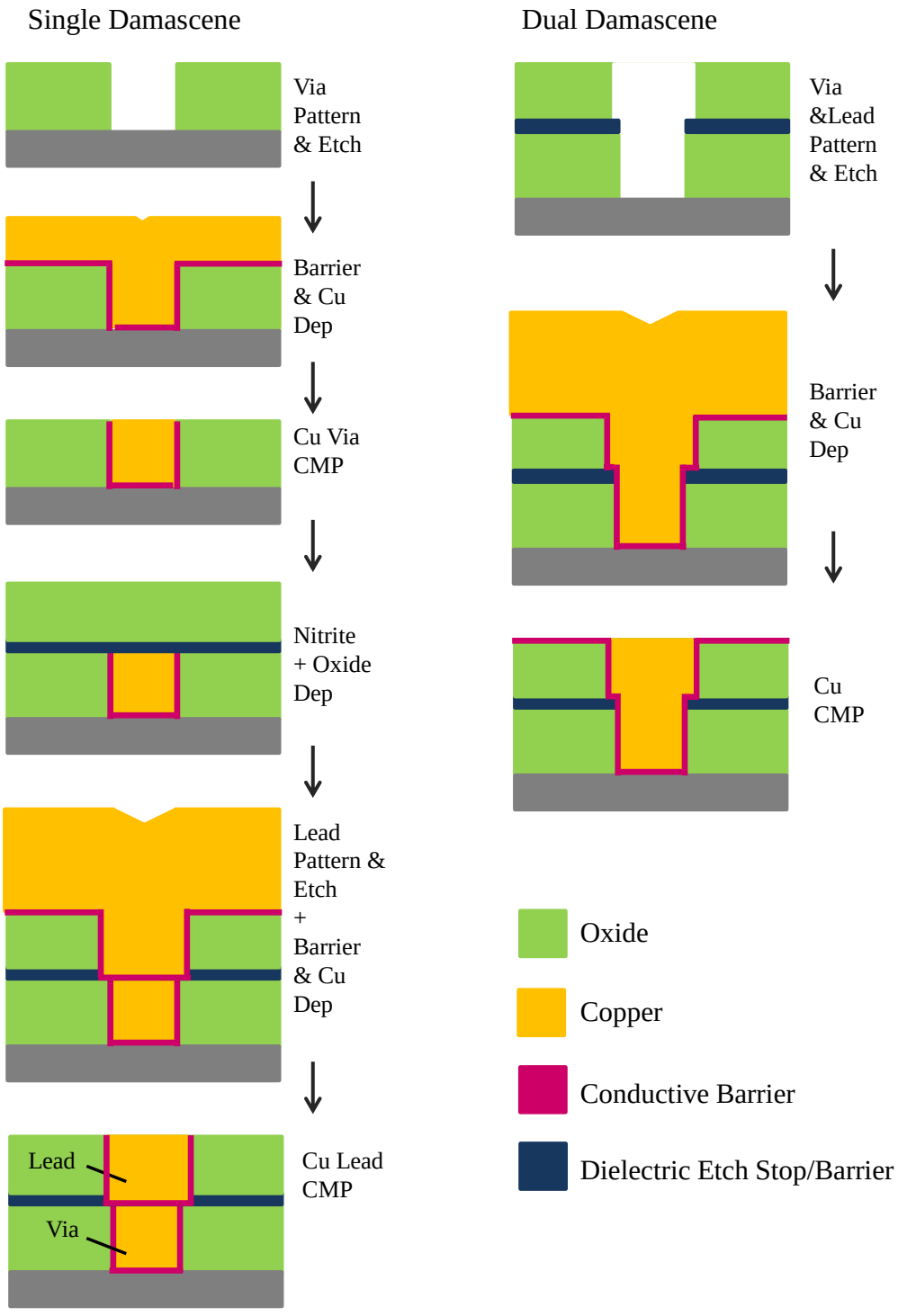

Figure.2.12. Fabrication process of Cu damascene.

The copper CMP process has two steps. The first step accomplishes the removal of Cu overburden and stops on TaN/Ta liner or slightly before the liner is exposed. The second step involves the removal of TaN/Ta liner, the hard or soft mask materials, and

then about 300-400 Å of the dielectric material as well. Complete removal of the liner and hard mask materials should be accomplished without significant loss of Cu line thickness and the dielectric removal target should be achieved without excessive thinning. These goals need to be achieved across all line widths, pattern densities, and feature sizes. Additional steps such as buffing and chemical rinsing may also be used to remove particulates and provide a protective layer on the Cu surface. The design and formulation of the slurries used in Cu and liner CMP processes are influenced by these stringent requirements. The major components of Cu CMP slurry are oxidizer, abrasive, adsorbate (inhibitor), surfactants, chelating agents, and polyelectrolytes. Several oxidizers such as HNO_3, H_2O_2, Fe $(NO_3)_3$, KIO_3, $KMnO_4$, and $K_2S_2O_8$ have been investigated. Most Cu slurries have alumina abrasive because of its high selectivity toward Cu and the ability to stop on Ta/TaN.

Effect of Chemically Modified Nano-Scale Thin Films on CMP Performance

In all the CMP processes a good balance must be achieved between the chemical and mechanical components of the CMP to provide optimum planarization. Fig. 2.13 shows the formation and the deformation mechanisms of the passivation layer formed by using the oxidizer contained in the slurry on a metal CMP process. If the mechanical component is too dominant, surface scratches and non-uniform polishing maybe observed. On the other hand, if the chemical component is too dominant during the process, local etching and over-polishing maybe observed which leads to severe surface topography imperfections. Mechanical abrasion depends on the size and concentration

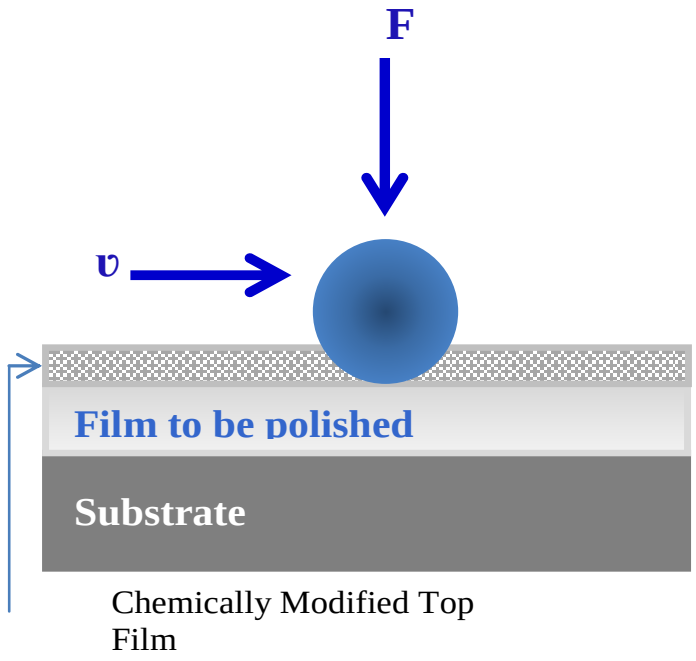

Figure 2.13. Illustration of chemically altered layer formation and material removal in CMP at single particle surface interaction level.

of the slurry particles, hardness and surface roughness of the pad, pad pressure, and the rotational speeds of the pad and the wafer. The chemical component is controlled by the chemistry, concentration, and pH of the slurry. In metal CMP process a protective oxide film forms in aqueous environment in the presence of surface active agents, corrosives, pH regulators etc' on the wafer surface. This film is utilized on the recessed layers to prevent further corrosion as the protruding structures are planarized through removal of this same chemically modified layer by mechanical interactions of the pad and particles.

This dissertation delineates the nature of growth of the chemically modified thin films for CMP and their optimized removal with minimal defectivity. The studies on the characterization of the chemically modified nano-films are also expected to have an impact on the nano-scale fabrications of future nanoelectronic applications and for many other fields where the characterization of the growth, internal stresses and

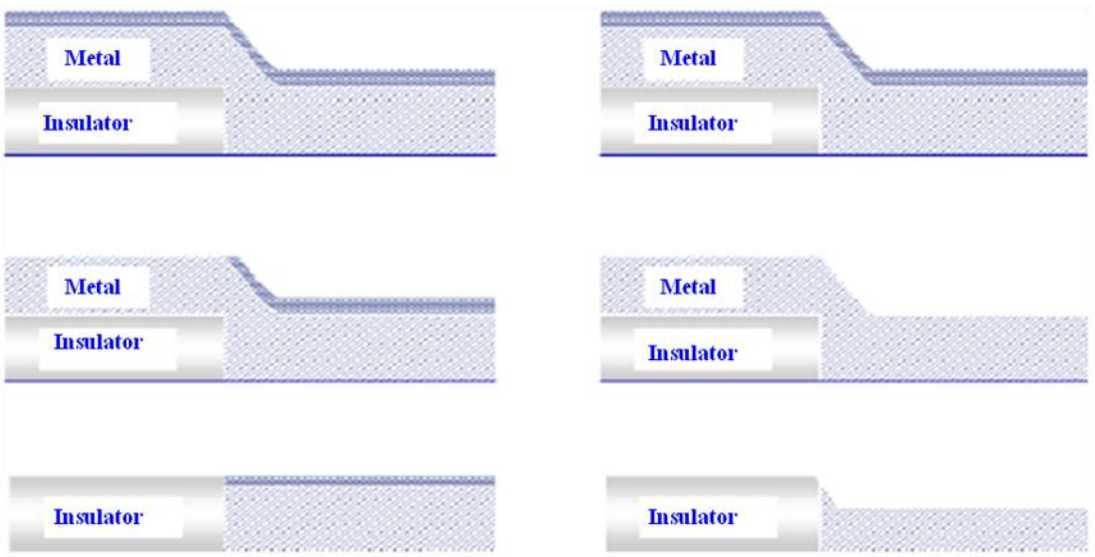

(Protective Film) (Non-Protective Film)

Figure 2.14. Self Protective films enable planarization in CMP

permeability of the thin films is critical. For example, in ferroelectric memory manufacturing a protective layer is needed to prevent hydrogen diffusion to the ferroelectric capacitor to stop degradation of the ferroelectric properties of the high-k material. Adhesion strength and hydrogen permeability of the protective film is critical for the proper functionality of the ferroelectric device within its life cycle [Hta00]. In chip packaging protective oxide films of the contact metals are promoted to reduce environmental attacks on the chip. It is also interesting to know that strain built in the thin films can be remedied by implantation and annealing of other chemical molecules. Therefore, chemical environment the film grows in is expected to affect the type of the stresses built-up at the interface.

Fig 2.14 shows the impact of self-protective oxide films in CMP enabling topographic selectivity. As a first step, a passive metal-oxide layer is chemically formed on both the recessed-areas as well as the protruding-areas of the metal film due

to the oxidation by the oxidizer solution. Secondly, the metal oxide film on the protruding areas is removed by the mechanical abrasion due to contact between the polishing pad and slurry abrasive particles. Since the polishing pad is hard enough to not conform into the recessed area, it is protected until the protruding areas are planarized to the level of the recessed regions. This action enables topographic selectivity.

Tendency of a film to protect the metal from further oxidation is related to the relative specific volumes of the oxide and metal. When an oxide film forms at the metal/oxide interface, the volume change due to the formation of oxide can be expressed with the Pilling-Bedworth ratio for metals, which is represented as in Equation [2.1],

$$\text{P-B Ratio} = \frac{\text{Volume of oxide}}{\text{Volume of metal}} = \frac{A_0 \rho_M}{A_M \rho_0} \qquad [2.1]$$

where , A_o is the molecular or formula weight of the oxide, A_M is the atomic weight of the metal, and ρ_O and ρ_M are the oxide and metal densities, respectively. It is generally accepted that when the P-B ratio < 1, which means that the volume of the oxide is less

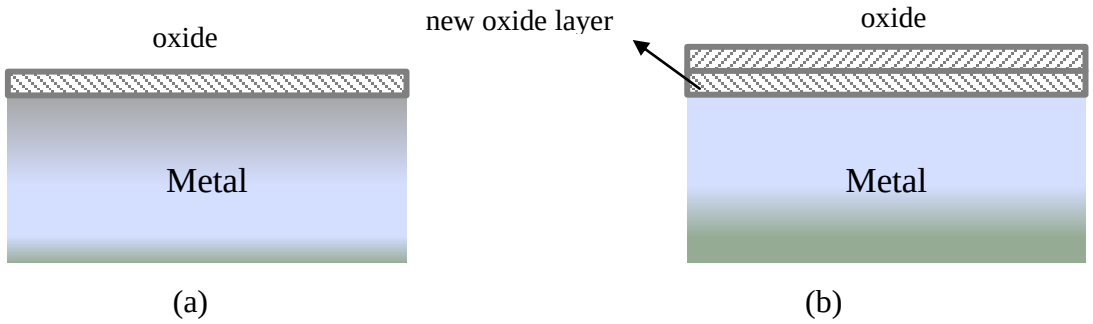

Figure 2.15. a. Native oxide layer before oxidation, and b. the new oxide layer at the oxide/metal interface after oxidation.

than the metal volume (or the lattice constant, a, of the oxide film is smaller than the metal), tensile stresses develop in the oxide film. As the thickness of the oxide layer increases, the oxide film starts to crack to relieve the strain and becomes porous. Consequently, for a subtractive application such as CMP, the underlying metal film will be etched locally and cannot be planarized uniformly. On the other hand, if the volume of the oxide is much greater than the metal (P-B ratio >> 1), compressive stresses will start to develop as the film grows.

Figure 2.15 schematically represents the regular oxidation process for a metal. When the oxide growth is controlled by the inward diffusion of anions, new oxide forms at the oxide/metal interface (Fig 2.15.b). This new oxide layer is forced by the substrate metal and the existing oxide layer resulting in stress generation. The stress generated in the scale is due to the fact that the specific volume of the oxide is rarely the same as the metal that is consumed. P-B ratio is therefore introduced to quantify the volume changes after oxidation [Chu00]. The oxide film releases the strain energy by breaking the bonds at the metal-oxide interface. An ideal protective oxide can be obtained when the P-B ratio is between 1 and 2. In this case, the oxide formed on the metal surface remains intact. Its growth is limited with diffusion of the metal ions through the oxide film. For a given metal undergoing oxidation, the P-B ratio provides a tool to predict the stresses developing in the film structure and the morphology of the formed oxide film. Furthermore, the stability of the oxide film on the metal surface depends on the strength of the bonds at the metal-oxide interface. As the film grows the stresses developed in the oxide film structure are balanced with the metal-oxide bond strength (σ_{bond}), which can be estimated by Equation [2.2], where E_{film} is the film elastic modulus, γ_O and γ_S are the surface energies at the site of the film and substrate, K_{Ic} is the fracture toughness of

the film substrate interface and d is the film thickness.

$$\sigma_{bond} = \left[\frac{E_{film}(\gamma_o + \gamma_s)}{d} \right]^{1/2} \left[\frac{K_{Ic}}{d^{1/2}} \right] \quad [2.2]$$

When a protective oxide film is formed, the internal stresses ($\sigma_{internal}$) induced by the oxide growth do not overcome the metal-oxide bond strength. But the oxide structure is under compression since P-B ratio is between 1 and 2. Within a given system external stresses ($\sigma_{external}$) the film is exposed to should also be considered to evaluate the oxide film stability. The stress balance in the metal-oxide interface can be given as in Equation 2.3 [Gbb13].

$$\sigma_{bond} = \sigma_{internal} + \sigma_{external} \quad [2.3]$$

When the total magnitude of the internal and external stresses exceeds the bond strength, the oxide film can be removed by breaking the metal-oxide bonds at the interface. Therefore, the optimal pressure level to break the metal-oxide bonds can be estimated by measuring the stresses at the interface and comparing them to the critical stress for the scale failure (σ_{bond}). This mechanism of material removal can give an atomically planarized surface due to the breakage of metal-oxide bonds at the interface for subtractive applications. If the film is grown for a permanent application, it needs to be intact for the process steps that will follow as the device is built. Yet, an affective film can be constructed by utilizing the given relationships.

For the applications of non-metal CMP, the chemically modified thin films are mainly the hydroxyl layers formed by the dissolution of the materials such as silicon, silica or germanium. As discussed in the previous chapter, the primary formation of the chemically modified thin films is based on the dissolution of the surface atoms to make

hydrated nano-layers in non-metal CMP. As explained, on silicon and silica, interactions are observed between the siloxane bonds (Si—O—Si) and water. Water breaks Si-O-Si bonds and a softer hydrated layer is formed, which is removed by the abrasive slurry nano-particles during polishing while simultaneously a new layer continue to grow. The reaction for the breakage of the network forming siloxane bonds with water to form a hydrated film on the surface through the attack of the solvated hydrogen ion ($H3O^{+}$) on the negative oxygen sites of silica [Bud61, Ile79]. This reaction is completed by first a water molecule from the environment attaching to the Si—O—Si bond by aligning itself due to the formation of a hydrogen bond between its hydrogen and the oxygen atom of the silica surface, and interaction of the lone pair orbitals of the oxygen in water structure with the Si atom. In the second step, a reaction occurs in which proton transfer from water hydrogen to the oxygen of silica is accomplished simultaneously with electron transfer from the oxygen of water to the silica atom. At the end of these reactions, two new bonds are formed by destroying the original bond between the silica and oxygen resulting in Si—O—H bonds on the surface. The rate of this reaction is believed to be controlled by the diffusion of water into silica structure [Dor73].

It is known that the Ge dissolution just like the silica is promoted at basic pH. The mechanism for the formation of the chemically modified layers on Ge is a two-step mechanism. In aqueous solutions of H_2O_2, dissociation of H_2O_2 occurs and when the O_2H^{-} ions diffuse into the germanium surface, they attach instantly to the surface Ge atoms forming surface complexes such as Ge $(OH)_2$ and $Ge(OH)_2^{++}$. Therefore, in the presence of H_2O_2 the mechanism of material removal is suggested to be the dissolution of the germanium predominantly. In the acidic and around the neutral pH ranges, the oxidation is lower as compared to the basic region resulting in minimal formation of the

soluble $Ge(OH)_2$. In both cases, Ge-Ge bonds, being weaker than Ge-O-Ge bonds, are ruptured during polishing. It is obvious that from the reaction equations, Ge removal mechanism is highly dependent on the oxidation of the Ge surface to GeO_2. Further details will be discussed on the chemically modified flms on germanium in Chapter 5.

CHAPTER 3

METAL OXIDE PROTECTIVE THIN FILMS CHRACTERIZATION FOR METAL CMP APPLICATIONS

Introduction

As detailed in the previous chapters, CMP is the process of choice for planarization of metal and dielectric surfaces to enable precise photolithography and multilevel metallization in microelectronics manufacturing [Mkr10]. Introduction of new automotive, medical and implantable devices challenge the needs to improve microelectronic device performances to meet aggressive targets on cost reduction, zero defectivity and enhanced reliability, which consecutively impact CMP process performance requirements [Jru06]. Although mainstream semiconductor engineering could involve tradeoffs between performance and reliability, these new applications enforce the assessment of new materials while dealing with limited margins requiring advances in processing, materials science and chemistry [Hiw09]. The main objective of this chapter is to characterize the self-protective oxide films grown on the metal surfaces in the presence of an oxidizing environment to be able to utilize them in advanced microelectronics manufacturing applications, predominantly focusing on CMP.

When characterizing the durability of thin film interfaces, a critical thickness is defined above which it is thermodynamically favorable for the film to partially or fully relax through misfit dislocations. Self-protective oxide films comply with the epitaxial stress requirements since the lattice constants match to the substrate (native metal of the oxidized film). Moreover, they are self-limiting in growth because the formation of the

protective oxide stops the progress of chemical reactions before a critical thickness is reached. They are continuous, pore free, adherent, non-volatile and non-reactive. Therefore, they are capable of preventing corrosion (such as formation of self-protective aluminum oxide on aluminum) [Nkd09]. Furthermore, it has been demonstrated that self-protective oxide films formed on the aluminum contacts during chip packaging reduced moisture driven corrosion significantly [Ysk97]. In this subtractive use of protective oxides, evaluation of the interfacial stresses between the metal and metal-oxide films and comparing them to the stresses provided by the abrasive particles is important to be able to enable material removal and simultaneously minimize the defectivity [Vac95].

Tendency of a film to protect the metal from further oxidation is related to the relative specific volumes of the oxide and metal. When an oxide film forms at the metal/oxide interface, the volume change due to the formation of oxide can be expressed with the Pilling-Bedworth ratio, which is represented as in Equation 3.1 [Chx00], where, A_o is the molecular or formula weight of the oxide, A_M is the atomic weight of the metal, and ρ_O and ρ_M are the oxide and metal densities, respectively.

$$PB - Ratio = \frac{A_0 \rho_M}{A_M \rho_0} \qquad [3.1]$$

It is generally accepted that when the P-B ratio < 1, which means that the volume of the oxide is less than the metal volume (or the lattice constant, a, of the oxide film is smaller than the metal), tensile stresses develop in the oxide film. As the thickness of the oxide layer increases, the oxide film starts to crack to relieve the strain and becomes porous. Consequently, for a subtractive metal oxide P-B Ratio < 1 (porous oxide) not protective thin film application, such as CMP, the underlying metal film will be etched

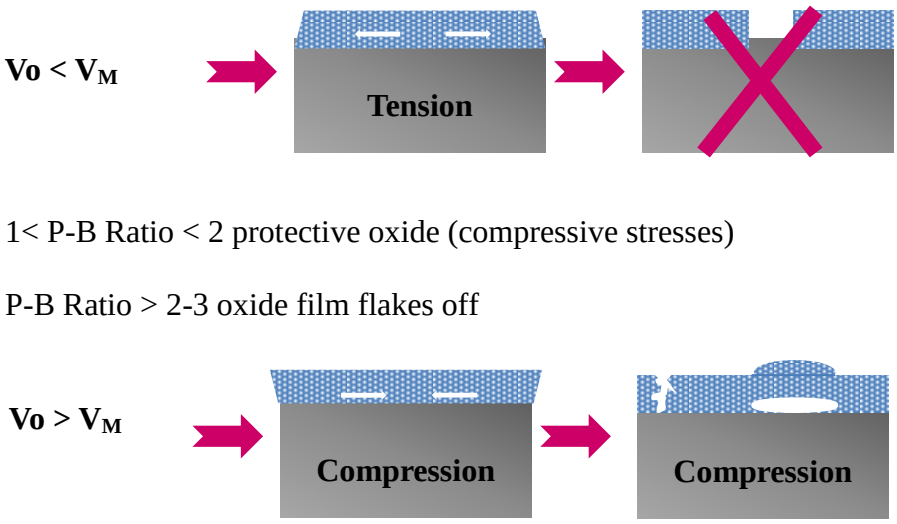

Figure 3.1. Stress formation in the self-protective oxide films as a function of P-B ratio.

film application, such as CMP, the underlying metal film will be etched locally and cannot be planarized uniformly. On the other hand, if the volume of the oxide is much greater than the metal (P-B ratio >> 1), compressive stresses will start to develop as the film grows. The oxide film releases the strain energy by breaking the bonds at the metal-oxide interface. An ideal protective oxide can be obtained when the P-B ratio is between 1 and 2. In this case, the oxide formed on the metal surface remains intact. Its growth is limited by the diffusion of the metal ions through the oxide film. For a given metal undergoing oxidation, the P-B ratio provides a tool to predict the stresses developing in the film structure and the morphology of the formed oxide film as summarized in Figure 3.1.

In the present study, tungsten was selected as a model system since it has been the metal of choice to fill in the vias starting with the aluminum metallization and remained to be the first layer-fill metal for plugs even for the copper metallization. Therefore, it is one of the best studied metal films for the CMP applications. Furthermore, tungsten has recently been adapted as inverted-T refractory metal gate

material where a relatively dense layer of chemical vapor deposition (CVD) tungsten is deposited on top of a thinner layer of less dense refractory metal, such as sputter deposition tungsten to promote adherence to a gate oxide layer grown on a silicon substrate [Fdo97, Mlo11]. Hence the characterization of tungsten oxide protective nano-films is important for both the subtractive and additive approaches in microelectronics manufacturing. Although it is known that the P-B ratio of tungsten is not protective in air (3.38 for WO_3) [Emc10] earlier CMP studies through electrochemical evaluations on tungsten demonstrated that it forms a protective oxide during the CMP applications [Fbk91, Rdw11, Mbi00]. In order to achieve stress-free, damage-free, atomically smooth and planar surfaces through CMP, it is necessary to understand the composition and the protective nature of these chemically modified films. In this study, we focused on growth and material properties of the protective metal oxide thin films on CVD deposited tungsten films pre and post polishing in the presence of an oxidizer. The material removal rates and surface roughness behavior, as well as the wettability and surface energy of the oxidized films were studied in addition to the calculation of the P-B ratio at the metal-oxide/metal interfaces based on the thickness and density values measured by advanced characterization techniques. This chapter takes an additional step into the characterization of the CMP process through analyzing the topographic nature of the metal oxide protective nano films and also follows a mathematical approach based on the minimization of the free energy during the formation of topography.

Materials and Methods

Tungsten oxide nano-film formation: Tungsten test wafers with ~10000 Å tungsten film deposited on a TiN/Ti adhesion layer were donated by Texas Instruments after a

standard CMP process was applied to induce homogeneous surface quality. These 8" size wafers were cut into smaller coupons (a minimum of 5 samples for each condition) and cleaned in high pH solutions prepared by KOH addition to remove any contaminated surface oxide and thoroughly rinsed with DI water and dried with nitrogen gas. Afterwards, the wafer coupons were dipped into H_2O_2 solutions for 5 minutes (pH 4.0) at concentrations of 0.05, 0.075, 0.1, 0.5 and 1 M (mol/L). Figure 3.2. shows a dipping procedure which is used in this study. All samples were kept in clean petri dishes in a desiccator pre and post formation of the surface oxides.

Surface topography analyses: Surface roughness values of the wafer coupons were measured by Nanomagnetics Instruments Atomic Force Microscope (AFM) on 5 μm by 5 μm scans using tapping mode to protect the naturally formed native oxide films from deformation during scanning. The averages of minimum three measurements were reported with standard deviations to verify the statistical significance of the observed values.

Surface wettability and surface energy calculations: All samples were characterized for contact angle responses through sessile drop method measurements using DI water droplets with a KSV ATTENSION Theta Lite Optic Contact Angle Goniometer. Five drops were measured at a room temperature of 25°C on each sample and the results were averaged. The drop images were stored by a camera and an image analysis system calculated the contact angle (Θ) from the shape of the drop. The contact angle measurements were also utilized to determine the surface energy values on the modified surfaces by using the acid-base technique as detailed in the literature [Sba09]. Polar and apolar probe liquids were selected as per standard procedures including ethylene glycol, formamide, glycerol, deionized water.

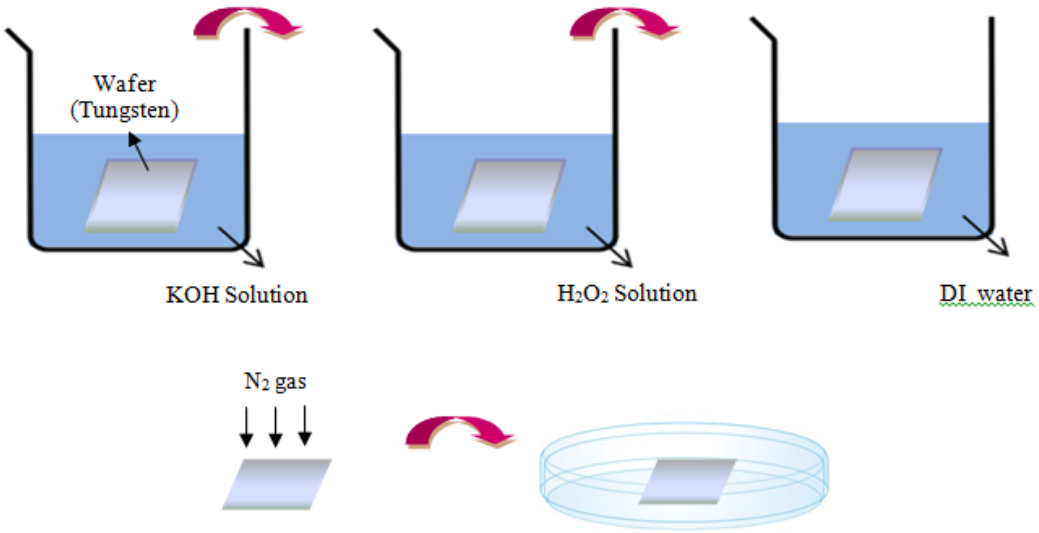

Figure 3.2. Dipping procedure which is used in this study.

Thickness and compositional evaluations of the metal oxide thin films: XRR analyses were conducted on the W wafers as a function of H_2O_2 concentration. Mass density and thickness of the oxidized layers were obtained from simulations of the x-ray reflectivity (XRR) curves acquired with a Analytical X'Pert MRD instrument operated at a voltage and current of 45 kV and 40 mA, respectively working in a parallel beam configuration, with a mirror and a (1/32)º slit on the incident beam side and a thin film collimator and a 0.1mm slit on the diffracted beam side. The same instrument was used for structural characterization by acquiring X-ray diffraction patterns both in symmetric and grazing incidence geometry (XRD and GIXD).

The chemical compositions of the films were investigated by X-ray photoelectron spectroscopy (XPS) in a Perkin-Elmer PHI 5100 ESCA system (300 W, 90°, 45°, or 20° take off angles, Mg K_α radiation). To obtain the bulk composition, measurements were collected after various time cycles of Ar ion sputtering (4 kV, 4 μA/cm^2, rastered over an area of 10 × 7 mm^2). XPS survey spectra (1 eV/step, 30 ms) were firstly acquired followed by high-resolution multiplex spectra (0.1 eV/step, 50 ms) for W 4f, C 1s, and

O 1 s regions. Binding energy calibration was based on adventitious C 1s at 284.6 eV.

Results and Discussion

Characterization of the thickness, density and composition of the tungsten oxide thin films in CMP solutions: Initial analyses conducted on the W wafers dipped into the oxidizer solutions at 0.0, 0.05, 0.075 and 0.1 M concentrations to investigate the nature of the formed tungsten oxide film. Table 1 summarizes the simulation results of the XRR data starting with the wafer only treated by the KOH solution at pH 4, followed by the measurements on the wafers treated with the increasing oxidizer concentrations after the KOH treatment. The results of the simulations of the XRR curves were performed by the commercially available software (WinGixa, Panalytical). This simulation program makes use of the Parratt formalism for reflectivity [Lgp54, Pff03]. The outcomes showed that a multilayer structure is present on the sample surface after the CMP treatment, with an extra layer in the upmost part of the structure labeled as Layer 0. The subsequent layers underneath are labeled as Layer 1, Layer 2 and the bulk substrate, based on the measured densities of each layer. T is the thickness in Å, D is the density in g/cm^3, and R/W is the roughness/width of the interface in Å. The top layer with 7-8 Å thicknesses has shown the lowest density among all the defined layers which was measured around 4.1-4.8 g/cm^3. This layer is believed to correspond to an oxyhydride compound since the hydrated tungsten compounds such as tungstite ($WO_3 \cdot H_2O$), meymacite ($WO_3 \cdot 2H_2O$) or hydrotungstite (H_2WO_4) have densities between 4.5 to 5.5 g/cm^3. The density of the layers increases from the surface towards the bulk; however, the values do not match the density of pure WO_3 (7.16 g/cm^3) or WO_2 (10.8 g/cm^3) [Pff03]. Furthermore, the measured density values at these layers were greater than 14 g/cm^3 indicating a mixed composition of tungsten oxides and

tungsten should present at this layer (density of the metallic tungsten layer was measured at ~17 g/cm^3) to average a density of 14 g/cm^3 and above.

The roughness/width ratios of the interfaces between adjacent layers are also relatively large indicative of intermixing/inter-diffusion between the adjacent layers. The density of the W substrate was also observed to gradually increase from the first sample (where the wafer surface was treated by KOH only) towards the later samples, which were treated by increasing concentrations of the oxidizer with the most pronounced difference in the first sample. Figure 3.3 illustrates the XRR curves collected on the sample with only KOH treatment versus the samples treated in the presence of the H_2O_2 highlighting the differences in the simulations. It is plausible that in the absence of an oxidizer, there might be some weak oxidation of the substrate on depths larger than 200 Å due to the absence of a protective oxide layer leading to the liquids to diffuse faster and deeper into the substrate and induce a partial oxidation. In order to analyze the composition of the formed layers, XRD and XPS analyses were performed. The GIXD and XRD results did not find any diffraction lines other than those belonging to metallic

Table 3.1. Thickness and density analyses of the oxidized tungsten films with XRR with 1 M KOH treatment and with 0.05, 0.075 and 0.1 M H2O2 addition after 1 M KOH treatment. W indicating that the formed oxide layers were amorphous. It is reported that the oxidation of tungsten results in formation of a mixture of WO2 and WO3 films [Gli06]. Furthermore, the tungsten and oxide phase diagram at room temperature also suggest the formation of WO2 and WO3 films [Haw89]. High resolution XPS scans of the W 4f region showed the presence of several peaks, partially overlapping. To find their areas and binding energies, the acquired spectra were fit with

Table 3.1. Thickness and density analyses of the oxidized tungsten films with XRR with 1 M KOH treatment and with 0.05, 0.075 and 0.1 M H_2O_2 addition after 1 M KOH treatment.

	1 M KOH			**0.05 M H_2O_2**			**0.075 M H_2O_2**			**0.10 M H_2O_2**		
	T	D	R/W	T	D	R/W	T	D	R/W	T	D	R/W
Layer 0	15	4.5	6	7	4.8	5	7	4.4	5	8	4.5	5
Layer 1	122	5.0	15	51	12.4	11	53	12.2	10	53	12.5	9
Layer2	20	14.7	24	43	14.5	12	40	15.6	18	42	15.8	17
W substrate		17.6	26		17.8	21		18.4	22		18.6	22

T: Thickness (Å)
D: Density (g/cm^3)
R/W: Roughness/width of the interface in Å

W 4f7/2 and 4f5/2 doublets (area ratios of 4:3 and doublet separation of 2.18 eV [Haw89]). Binding energy values for the W 4f7/2 peaks were located at 31.4 eV, 32.5 eV, and 35.9 eV, regardless of the oxidizer treatment, indicating the presence of metallic W, WO_2, and WO_3 [Nav05-Jdi10].There was a smaller 7^{th} peak, clearly visible in samples only after extended Ar ion sputtering and located at 5.5 eV higher that the first W peak and much broader, which was assigned to W 5p3/2 [Sma10]. The oxygen O1s peak was formed by two components, located at 531.9 eV and 530.4 eV, which could be assigned to chemical bonds in WO_3 and WO_2. The spectra acquired at 20° take-off angle also showed a small component at 533.3, most probably an oxy-hydrate component adsorbed on the surface. It has been suggested that O vacancies in WO_3 would results in a lower binding energy of around 0.5 eV for the W 4f peaks [Iri10-Sma10]. Since we did not observe significant changes in the position of the W4f peaks corresponding to WO_3 we could safely deduce that the formed oxides were quite stoichiometric. The relative intensities of W 4f peaks changed with the change of the

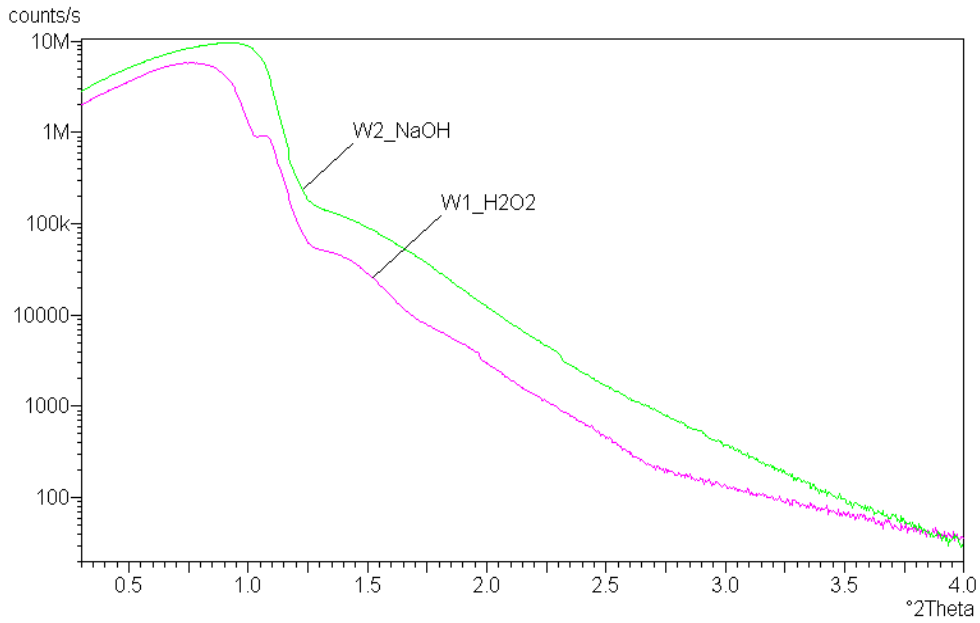

Figure 3.3. Changes in XRR profiles of the oxidized thin films on the tungsten surfaces between the pure KOH (1 M) treated surface versus the surface treated with 1 M H_2O_2 after the KOH treatment.

take-off angle. The relative increase of the peaks corresponding to WO_3 combined with the decrease of the intensities of the W metallic peaks showed that a thin oxide layer covered the samples. However, when plotting the logarithm of the intensities corresponding to the metallic substrate versus $1/\cos(\theta)$, where θ is the take-off angle, the decrease was much less pronounced than that expected for a metallic substrate covered by a uniform oxide layer as can be seen in very thin tungsten hydroxide layer. Figure 4. A similar behavior was noticed for W peaks assigned to WO_2. It appears that most of the oxide is actually mixed with the substrate and the oxidation front is not planar. It could be inferred that the oxidation proceeds much faster along the grain borders or defects than through the grains. The results suggest that at a certain depth beneath the surface there is a mixture of various oxides and metallic W. Furthermore, XPS spectra acquired on the first sample after more than 1000 s of Ar ion sputtering, which is expected to remove more than 200 Å still showed the presence of WO_2 and

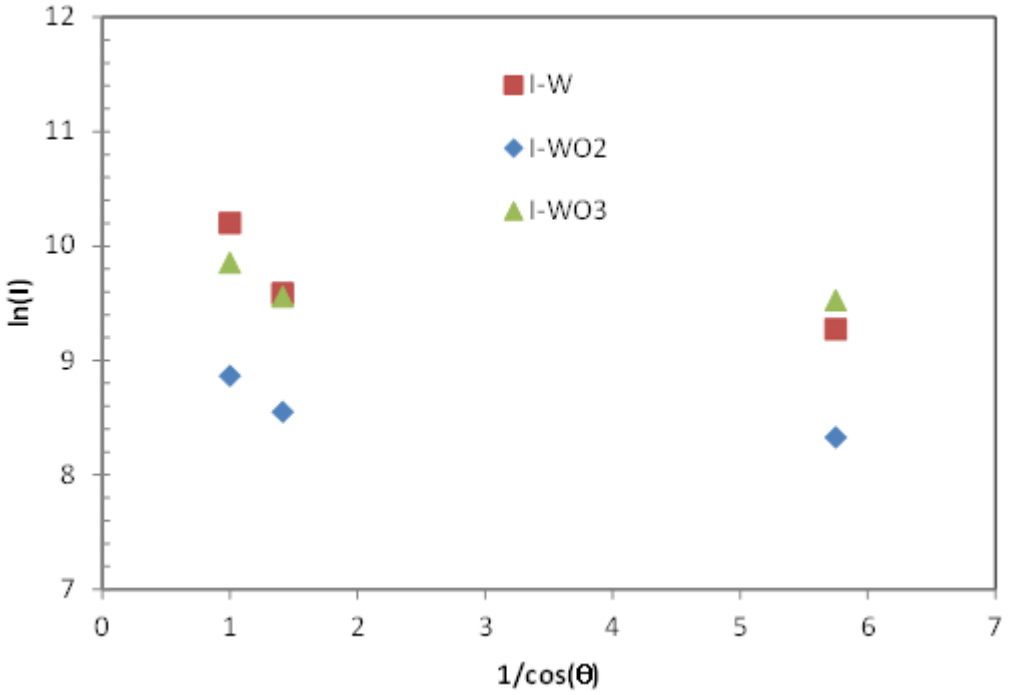

Figure 3.4. Plot of ln (Intensity) versus take-off angle of XPS data.

oxygen,consistent with the difference observed on the XRR curve of the first sample.

Overall, the results of the XPS investigations are corroborating the interpretation of the XRR simulation results in that after CMP treatment, a mixed composition layer, consisting of WO_2, WO_3 and metallic W is formed, covered by a thin WO_3 layer and a very thin tungsten hydroxide layer.

Characterization of the protective nature of the metal oxide thin films by P-B ratio calculations and interfacial stress evaluations: The thickness and the density results obtained from the simulations of the XRR curves summarized in Table 1 were used to calculate the P-B ratio values for the layered structure of the tungsten oxide nano-films based on Equation 1. As it was discussed earlier, the very top layer of oxide layer, Layer 0, was corresponding to a hydroxy tungsten as per the density measurements matching the hydroxy minerals of tungsten. The intermediate layers, Layer 1 and

Layer 2, on the other hand were determined to be a combination of the W and WO_3/WO_2 based on the compositional analyses conducted by XPS. From the reported density values, the estimated weight percent concentrations of metallic W and W-oxide of these intermediate layers were calculated by equating the measured density value to the sum of the density of pure oxide times the weight percent composition of the oxide and the density of metallic tungsten (measured as the bulk layer in the XRR analyses) and the concentration of metallic tungsten in the layer (1- concentration of the oxide). In order to come up with a range, the calculations were conducted by assuming either a pure WO_3 and metallic tungsten composition, or WO_2 and metallic tunsten composition, since the exact amounts of the type of oxide in a given layer is not known. Once the weight percent concentrations of the oxide to metallic tungsten were determined, these fractions were used to estimate the molecular weights of each layer. These values were than used to calculate the P-B ratios by using Equation 1. Table 3.2 summarizes the compositional contents and the calculated P-B ratios of each layer measured. The calculated tungsten to tungsten oxide fractions well matched the earlier literature data reported on tungsten after treating the surfacess with H_2O_2 at pH 2 and pH 4 [Eak96]. It can be seen that except for the very top hydroxy layer, the P-B ratios remain to be less than 2. As discussed previously, when the volume of the oxide is much greater than the metal (P-B ratio >> 1), compressive stresses start to develop in the growing film. The oxide film releases the strain energy by breaking the bonds at the metal-oxide interface. Hence the very top hydroxyl oxide layer (which is only 7-8 Å thick when the oxidizer is present in the solution) is not stable. This hydroxyl compound extends to a much deeper region (into Layer 1) in the absence of the oxidizer. Formation of two distinguishable layers at a total of ~130-140 Å thickness was observed, which retained a high P-B ratio. This result suggests that a protective layer does not form without the

oxidizer in the solution until a very thick oxide is formed. Beyond the 130-140 Å thickness, Layer 2/metallic tungsten interface shows a protective oxide layer formation with a P-B ratio of 1.28. However, since the top oxide film is expected to peel off continuously due to high interfacial stresses, the underlying layer will continue to corrode by getting exposed to the oxidizer in the solution. In the presence of oxidizer,

Table 3.2. Compositional analyses and P-B ratio calculations on the samples treated with 1 M KOH treatment and with 0.05, 0.075 and 0.1 M H_2O_2 addition after 1 M KOH treatment.

	KOH Treatment		**0.05 M H_2O_2**		**0.075 M H_2O_2**		**0.1 M H_2O_2**	
	Composition (% wt)	P-B Ratio	Composition (% wt)	P-B Ratio	Composition (% wt)	P-B Ratio	Composition (% wt)	P-B Ratio
Layer 0	W-OH: 100	1.28	W-OH: 100	3.05	W-OH: 100	3.53	W-OH: 100	3.64
			on WO_3/W	3.32	on WO_3/W	3.54	on WO_3/W	3.64
			on WO_2/W		on WO_2/W		on WO_2/W	
Layer 1	W-OH: 100	3.06	WO_3/W 51/49	1.23	WO_3/W 55/45	1.37	WO_3/W 53/47	1.35
	on WO_3/W	3.48	WO_2/W 77/33	1.33	WO_2/W 81/19	1.37	WO_2/W 78/22	1.35
	on WO_2/W							
Layer 2	WO_3/W 28/72	1.28	WO_3/W 31/69	1.33	WO_3/W 25/75	1.26	WO_3/W 25/75	1.25
	WO_2/W 42/58	1.28	WO_2/W 47/53	1.33	WO_2/W 37/63	1.25	WO_2/W 35/65	1.25
W substrate	W: ~100		W: 100		W: 100		W: 100	

on the other hand, the unprotective hydroxyl compound of tungsten is only 7-8 Å, while the underlying layers have P-B ratios within 1.25 to 1.37 ranges. An ideal protective oxide can be obtained when the P-B ratio is between 1 and 2. In this case, the oxide formed on the metal surface remains intact and its growth is limited by the diffusion of the metal ions through the oxide film. As it can be seen from the values reported in Table 2, all the P-B ratios calculated between the composite layers Layer 1/Layer 2 and Layer 2/metallic tungsten substrate remained between 1 and 2 suggesting the formation of protective oxide layer in the presence of H_2O_2 in the solution. In summary, it is observed that the inner tungsten and oxide composite layers remain stable after oxidation yet the very top pure oxide film with a 7-8 Å thickness is not protective. The fact that the measured density of the metallic tungsten layer increased by the increasing oxidizer concentration from 17.6 g/cm^3 in the absence of the oxidizer to17.8, 18.4 and 18.6 g/cm^3 with the addition of 0.05, 0.075 and 0.1 M oxidizer solution is another indicator of the formation of a protective oxide film that can stop the oxygen diffusion in the presence of the oxidizer. It is obvious that the higher the oxidizer concentration, the more protective the metal oxide thin films formed leading to less of a diffusion of the oxygen towards the metallic substrate through imperfections, such as vacancies or grain boundaries as it was also discussed through the results of the XRR analyses.

Characterization of the surface roughness and surface energy of the metal oxide thin films in CMP solutions and their impact on surface quality response: Figure 3.5 illustrates the surface topography of the tungsten wafers (a minimum of 5 samples for each condition) dipped into the H_2O_2 solutions at 0.0, 0.05, 0.075, 0.1, 0.5 and 1 M concentrations for 5 minutes after the surfaces were cleaned in 1 M KOH solution.

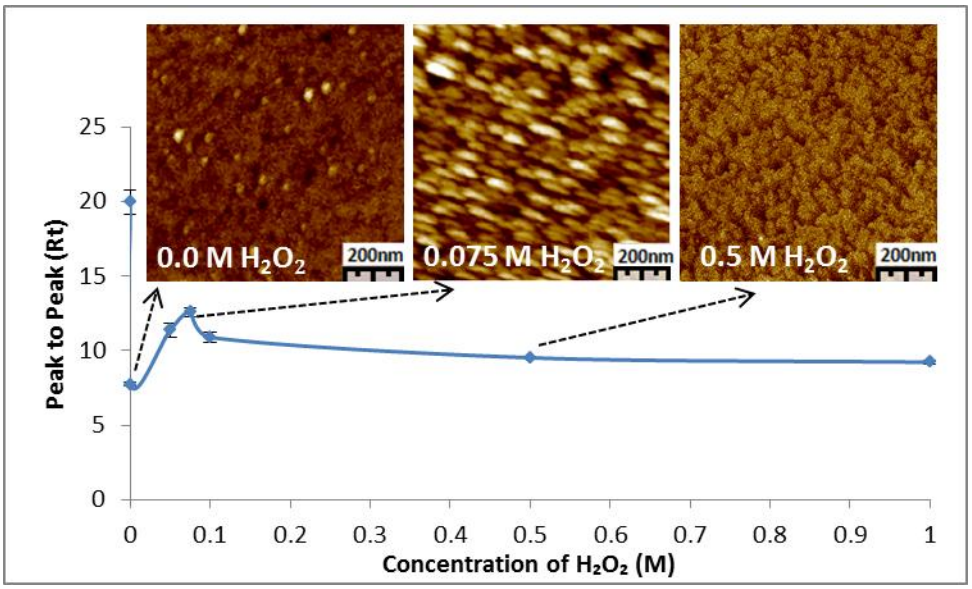

Figure 3.5. Characterization of the tungsten oxide protective thin films for surface by AFM surface roughness measurements.

Surface roughness analyses were conducted by AFM surface scans at 5 x 5 μm for at least 3 different locations on each wafer. It was observed that the wafers before the KOH treatment had high root mean square (RMS) surface roughness values (~10 nm) although they were polished prior to the surface treatment by dipping into the oxidizer solutions. Treating the surfaces with 1 M KOH solution reduced the surface roughness value to 3 nm. This can be attributed to the removal of the surface oxide at this very high pH solution. When the samples were treated with increasing concentrations of the oxidizer after the KOH treatment, there was a change in the roughness values with a peak observed at the 0.075 M concentration. From the micrographs, it can be observed that there is oxidation taking place on the wafer surfaces in the presence of the oxidizer. It appears that up to a 0.075 M oxidizer concentration, the surface oxide tends to form through nucleation and growth and above this concentration, the hillocks formed by the nucleation reach a critical size among which diffusion mechanism take over and a transition through a granular surface topography is observed starting at 0.1 M H_2O_2

concentration. The further increase in the oxidizer concentration from 0.1 to 1 M, however, did not show a difference in the surface roughness measurements due to consistent formation of columnar oxide structures on the substrate surface. This is believed to be due to Ostwald ripening of the tungsten oxide crystals at the elevated oxidizer concentrations [Pff03, Scj78]. The changes in the surface structure of the tungsten as a function of the oxidizer type during the CMP operations was investigated also in the earlier literature. Experiments conducted on tungsten wafers with addition of hydrogen peroxide and ferric nitride as oxidizers at a fixed concentration indicated changes in the surface topography similar to our observations [Gli06].

Summary

It is important to understand the chemical and mechanical nature of the CMP process to better control the process and design processes for the CMP of new generation materials. This study summarized our findings on the chemically formed metal oxide thin films of tungsten wafers in the CMP slurry environment. The characterization of the nature of the surface films has shown a layered oxide formation and the calculation of the P-B ratios suggested that the very top oxide film is a hydroxyl compound of tungsten and it is prone to delamination due to very high P-B ratio. However, the subsequent layers have shown stability with P-B rations calculated in between 1 and 2 in the presence of the oxidizer in the solution. Furthermore, we have demonstrated that the surface topography of the tungsten wafers tend to change as a function of the oxidizer concentration.

In summary, the presented study proposes a new methodology to characterize the metal oxide thin films for new generation materials introduced to the semiconductor industry. Fundamental understanding of the conducted research is also expected to be

important in many other fields such as in biological systems, thin film coatings, chip packaging and applications where the interface and thin film properties affect the product performance.

CHAPTER 4

METAL OXIDE PROTECTIVE NANO-FILM BASED CMP APPLICATIONS ON TUNGSTEN

Introduction

In chapter 3, characterization of the chemically modified metal oxide thin films formed on tungsten wafers as a model system has been performed. Tungsten is widely used as the plug material to connect the transistors to the interlayer metallization. Tungsten CMP has been the foundation for the contact and via level metallization, since tungsten is used for local wiring enabling contact to the transistor in the microprocessors [Wei09]. As described in the previous chapter the CMP slurry plays an important role in the formation of the chemically modified layers in CMP process. Figure 4.1 shows the interaction of abrasive particles and wafer surface to be polished during the CMP process. Removal of tungsten is driven by formation of a nano-scale protective oxide film that is continuously removed by abrasive nano-particles.

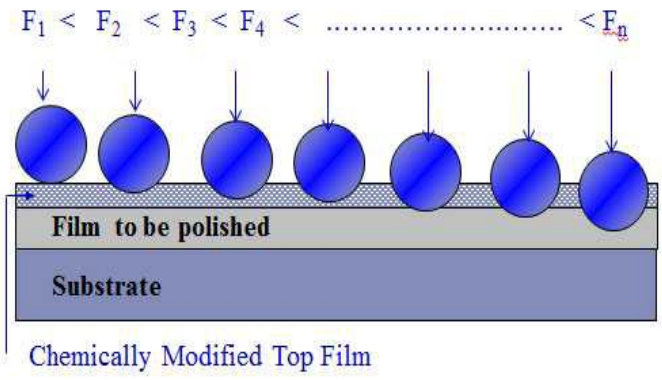

Figure 4.1. Chemical and mechanical interaction during CMP process at a single-particle level.

Moreover, we have also demonstrated that the surface topography of the tungsten wafers tend to change as a function of the oxidizer concentration. The observed changes in the surface topography were also found to affect the wettability, of the wafers. Hence, it is obvious that the protective nature this thin films, as well as the surface nano-topography of the metal oxide thin films need to be studied to assess the CMP performance. An optimal CMP process for metallic layers require the, formation of the protective metal oxide films. These films should be self-limiting and once formed they must protect the underlying metal from the further attack of the slurry chemicals as demonstrated in Figure 2.9. This is necessary to polish the higher level metal while protecting the lower levels, in other words, to achieve topographic selectivity and hence provide planarization [Fbk91].

In order to conduct a stress-free, damagefree, atomically smooth and planar surface through CMP, it is necessary to understand the composition and the protective nature of the chemically modified films. When there is a balance between the chemical and the mechanical action of the CMP process, the resulting interface can be controlled for the defect prevention and an optimal material removal rate. Figure 4.3 illustrates the competitive action of the chemical and mechanical interactions at a single particle surface interaction level for metal CMP schematically [Gbb11]. It is obvious that when the applied pressure levels calculated at a single particle level are larger as compared to the chemical action on the surface, the defect formation cannot be prevented. CMP process employs slurries that involve an aggressive chemistry to alter the properties of the film to be polished and this film is removed by the mechanical actions of the abrasive nano-particles in the suspension. Wei at al.,reported that the slurry used in the W-CMP introduces chemical interaction and dissolves W to form passivation layer, WO_3. Simultaneously, the mechanical interaction occurs when the slurry nano particles

Figure 4.2. Desk-top chemical mechanical planarization tool in operation.

interact with this WO_3 layer and remove the WO_3 locally and globally [Wei09]. Figure 4.2. shows a photograph of the bench-top CMP tool used in this study.

In this chapter, chemical mechanical polishing performance of the tungsten is studied with slurries composed of 50 nm alumina particles at pH 4 as a function of slurry solids loading and oxidizer concentration. The CMP performance was of evaluated through the material removal rate and surface quality analyses, conducted on the polished wafers. It has been demonstrated in chapter 3 that a protective oxide film forms on tungsten (W) substrate. Tungsten is the metal of choice for the modeling studies since its CMP is very well established. Other than the CMP process, the tungsten oxide films are also being used as the gate oxide for the new generation thin film transistors (TNT) [Lor11]. In order to explain the change in the surface roughness and the nano-scale topographic nature of the tungsten oxide thin films, a mathematical approach was utilized by assuming a constant temperature and conservation of metal oxide thin film volume. Since the metal oxide films of tungsten formed during the CMP

process have been shown to be self-protective and the oxide formation takes place at room temperature, these assumptions are valid. The topographic nature of the tungsten oxide nano films were evaluated by atomic force microscopy (AFM) characterization and compared to the theoretical predictions. The two stages of the changes observed in the topography of the tungsten oxide films were distinguished as, nucleation occurs an second, the nucleated grains reach a critical size to grow further through diffusion. Then larger particles grow at the expense of the smaller ones, which is a form of competitive growth called the Ostwald ripening [Jai78-Hga03]. The growth of the surface structures as a function of the slurry oxidizer concentration is modeled by the Cahn-Hilliard equation (CHE) [Tku94]. We also investigated the transition from the classical nucleation theory that explains the growth of surface structures with a sharp interface between the growing particle and the surrounding medium, to a softer transition definition by the CHE approach. The topographical changes on the surface of the tungsten metal in CMP slurries may also be affecting the removal rates, surface energy and defectivity during the CMP applications. Hence, it is expected that the findings presented in this paper are applicable to many other fields of microelectronics manufacturing where the modeling of the nano-scale metal oxide films can be critical. It is believed that the presented findings will help in characterizing the next generation materials for microelectronics manufacturing and additional applications where metal oxide thin films play an important role.

Materials and Methods

Preparation of Slurries: CMP slurries were prepared by ultrasonicating used alumina (Al_2O_3) particles with 50 nm size at % 3 wt concentration in DI water . The pH of the slurry was adjusted with HCl and KOH solutions.

CMP Experiments: CMP experiments were conducted on a desktop Tegrapol-31 polisher by using SUBAIV-IC1000 stacked polishing pad (The pad is made of polyurethane). The down force was 70 N on the 1.6 × 1.6 mm wafer coupons with 150 rpm rotational velocity and 100 ml/min slurry flow rate. CMP responses were obtained in terms of MRR (Å/min) and surface roughness measurements. The material removal rates were determined from the difference in the weights of the wafer coupons before and after polishing measured by a high precision balance with five digits after zero.

Surface Roughness Measurement: Surface roughness analysis were performed by contact mode with Nanomagnetics Instruments Atomic Force Microscope (AFM) before and after polishing. Three measurements were done per sample at the center of the wafer coupons by 2.5 µm × 2.5 µm scans. The reported roughness is the root mean.

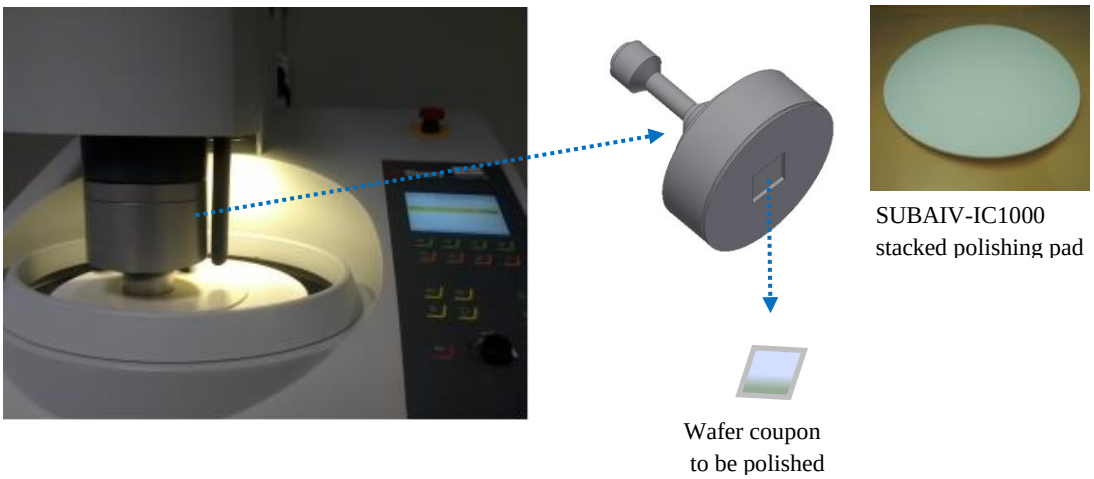

Figure 4.3. Desk-top chemical mechanical planarization tool in operation in the CMP process.

Film Thickness Analysis: The sheet resistance of tungsten thin films were measured by using a 4-point probe (Cascade CPS-0.5 Four Point Probe Station) for calculation of removal rates. A four point probe is a simple tool for measuring the resistivity of semiconductor samples. By passing a current through two outer probes and measuring the voltage through the inner probes allows the measurement of the substrate resistivity.

Surface energy and work of adhesion calculations: All samples were characterized for contact angle responses through sessile drop method measurements using DI water droplets with a KSV ATTENSION Theta Lite Optic Contact Angle Goniometer. Five drops were measured at a room temperature of 25°C on each sample and the results were averaged. The contact angle measurements were also utilized to determine the surface energy and work of adhesion on the modified surfaces by using the acid-base technique as detailed in the literature [Bar09]. Polar and apolar probe liquids were selected as per standard liquids including ethylene glycol, formamide, glycerol, deionized water. In polar systems, solid surface free energies (γ_s^{tot}) involve both Lifthitz-van der Waals (LW) and polar acid base (AB) interactions as

$$\gamma_s^{tot} = \gamma_s^{LW} + \gamma_s^{AB}$$

where acid base component of the surface free energy is the geometric mean of two important polar parameters, γ_s^- and γ_s^+ components given by

$$\gamma_s^{AB} = 2(\sqrt{\gamma_s^- \gamma_s^+})$$

The dispersive component of the surface energy, γ_s^{LW} was calculated using

$$\gamma_s^{LW} = \gamma_l \frac{(1+\text{Cos}\Theta)^2}{4}$$

where γ_l is the liquid surface tension. The polar γ_s^- and γ_s^+ components were calculated using the McCafferty linear plot method [Fdo97]. A linear plot of $\left(\frac{(1+\cos\theta)}{2}\gamma_l - \sqrt{\gamma_s^{LW}\gamma_l^{LW}}\right)/\sqrt{\gamma_l^+}$ versus $\sqrt{\gamma_l^-/\gamma_l^+}$ produce a straight line, where $\sqrt{\gamma_s^+}$ is

given by the slope and $\sqrt{\gamma_s^-}$ is the intercept. Based on the total surface energy calculation, the work of adhesion, W_a, which is the work required to separate two surfaces from contact, is considered to be the surface free energy density in this paper. Given the γ_l is the liquid surface tension and considering these three components of the surface free energy, W_a becomes

$$W_a = 2\left(\sqrt{\gamma_s^{LW}\gamma_l^{LW}} + \sqrt{\gamma_s^+\gamma_l^-} + \sqrt{\gamma_s^-\gamma_l^+}\right).$$

Results and Discussion

In order to quantify the surface roughness of the polished surfaces, AFM analyses were conducted using contact mode scans on 5 x 5 µm micrographs. Figure 4.4.a shows th AFM micrographs of the before polishing tungsten coupon and 4.4.b shows the micrograph of the surface after CMP conducted with used alumina (Al_2O_3) particles with 50 nm size at 3 wt % concentration in DI water in the presence of 0.075 M H_2O_2 as an oxidizer. As it can be seen, the surface roughness reduced significantly after CMP from ~20 nm RMS value on the original sample to ~4 nm RMS value post CMP. In order to evaluate the impact of the changes in surface topography on CMP performance, CMP tests were conducted by 10 wt % alumina slurries at pH 4 using 0.05 µm size

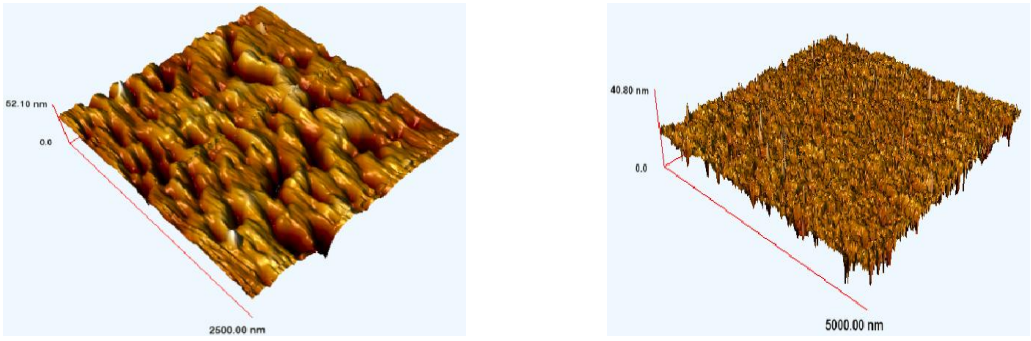

(a) (b)

Figure 4.4. The AFM surface topography of the tungsten coupon samples, a. before polishing and b. after polishing.

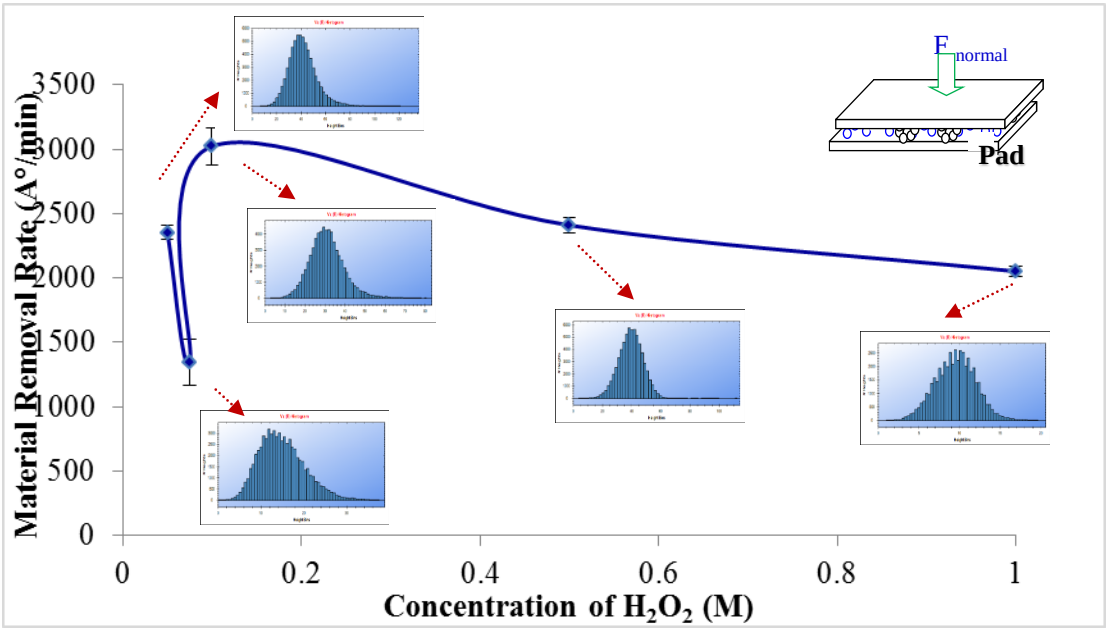

Figure 4.5. Material removal rate evaluations for W surfaces polished with 10 wt % 50 nm Al_2O_3 at pH 4.

particles. It can be seen in Figure 4.5 that there was again a minimum in the material removal rate (MRR) response obtained in the presence of 0.075 M H_2O_2 concentration in the CMP Slurry. Additionally, Figure 4.6 illustrates the surface roughness response on the tungsten wafers polished in the presence of the H_2O_2 at 0, 0.05, 0.075, 0.1, 0.5 and 1 M concentrations. The highest surface roughness is obtained once again at the 0.075 M concentration indicating that the material removal takes place more predominantly by mechanical abrasions, which further suggest that the elastic modulus of the formed oxide layer is higher.

Effect of particle size and solids loading on surface finishes: The impact of the chemical nature of the oxide film on the material removal mechanisms can be further discussed based on Figures 4.7.a, and 4.7.b, where the MRR responses and the surface roughness values are demonstrated as a function of the oxidizer concentration at increasing slurry solids loadings. From Figure 4.7.a, it is seen that the MRR tungsten increases by the

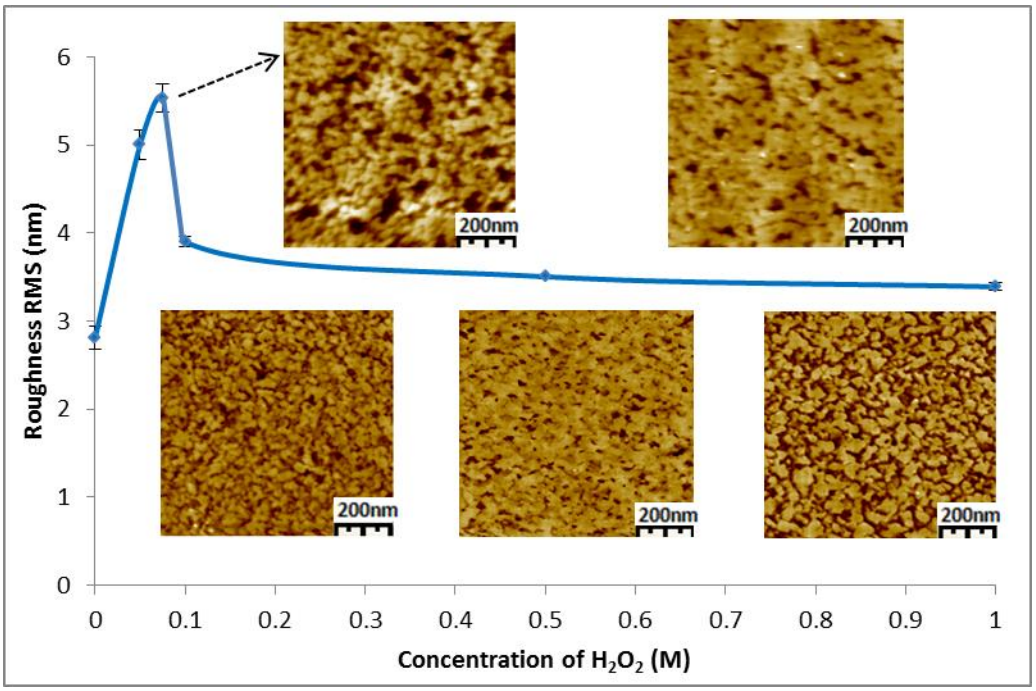

Figure 4.6. Characterization of the tungsten wafers after CMP with slurries containing H_2O_2 oxidizer at increasing concentrations for surface roughness responses.

increasing slurry oxidizer concentration except for the irregularity observed at 0.075 M concentration. The trend of increasing removal rates can be attributed to the increased chemical reaction rate of the oxidation by the increasing slurry oxidizer concentration. The irregularity observed at the 0.075 M H_2O_2 concentration is consistently observed in this two figure as well, delineating the change in total surface energy and oxidation mechanism at this critical concentration. Even though the chemically modified tungsten oxide thin films are protective in the presence of an oxidizer at the recessed locations of the patterned wafer, the mechanical abrasion of the slurry particles continuously expose fresh tungsten metal to oxidation at the protruding locations. Yet, a plateau is reached at each slurry solids loading after ~5–10 wt % concentration of particles indicating that a saturation occurs in the abrasion frequency as it was also observed for tungsten CMP in the previous literature as a function of the particle size [Mbi00]. Therefore, the particles

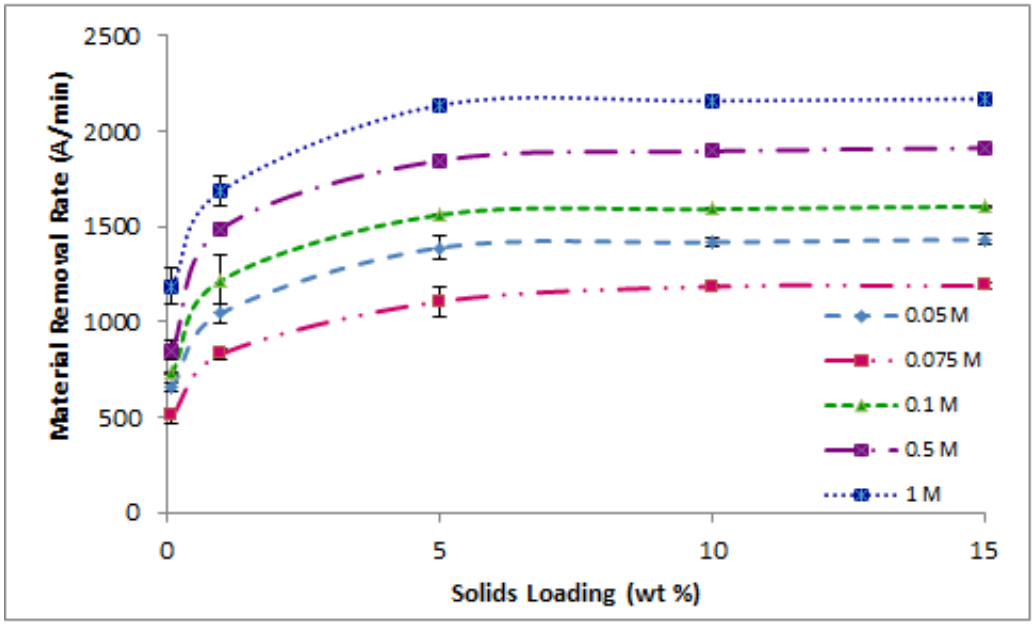

Figure 4.7.a. Material removal rate response as a function of slurry solids loading at increasing oxidizer concentartions.

can be assumed to adopt a hexagonal closed packed formation within the pad-wafer interface similar to the results demonstrated on the silica-silica CMP system [Gbb03] Based on the hexagonal closed packing, the frequency of the particle abrasion on given

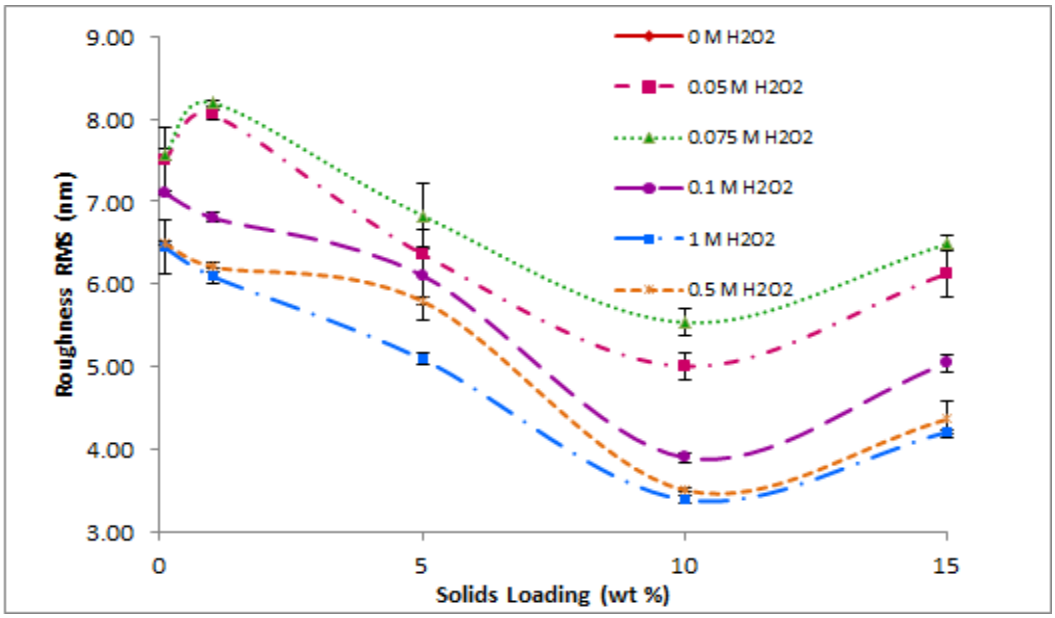

Figure 4.7.b. Surface roughness response as a function of slurry solids loading at increasing oxidizer concentrations.

spot of the wafer surface has to be equivalent to the particle diameter divided by the rotational velocity as demonstrated in Figure 4.8. Figure 4.8. Schematical demonstration of the time per abrasion calculations during CMP. By taking into account that only 0.33 % of the pad surface is in contact with the wafer surface [Gbb03], it is predicted that there is 1 abrasion taking place per every 9.24 × 104 seconds when 50 nm abrasive particles are used. At this frequency of abrasion, if it is assumed that every single particle can result in material removal, we can calculate the approximate removal thickness per particle by dividing the experimentally observed material removal rates to the abrasion rate per particle. In the given system, the removal rates are 1100 Å/min at 0.075 M H_2O_2 concentration and ~2200 Å/min at 1 M H_2O_2 concentration, respectively. Hence the material removal per particle is calculated to be in the range of

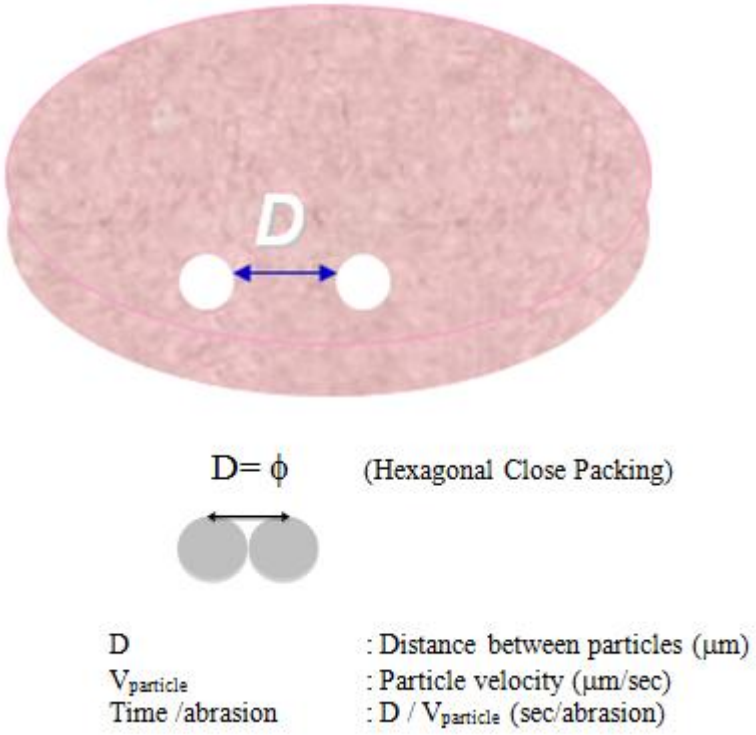

Figure 4.8. Schematical demonstration of the time per abrasion calculations during CMP.

0.2×10^{-3} to 0.4×10^{-4} Å/abrasion. Since this value is even smaller than a single tungsten oxide lattice dimension (7–10 Å), it can be concluded that only 1 in a 1000 to 10000 of the slurry particles contacting the surface can results in material removal. Hence we can conclude that the CMP process is limited by the chemical reaction rates rather than the rates of the mechanical interactions. Moreover, it can be suggested that only the protruded oxide hillocks can be removed by the abrasive particles during the CMP process. Since the increased oxidizer concentration results in formation of columnar oxide structures on the surface the removal rates tend to get elevated with the increased oxidizer concentration. Yet, the observation of the lowered removal rates with the increased surface roughness at the 0.075 M concentration of the oxidizer also suggest that the mechanical properties of the surface structure also tend to influence the removal mechanisms. In order to evaluate the impact of surface topography on the CMP, we have initially evaluated the wettability response of the tungsten oxide surfaces by using contact angle goniometer with sessile drop method after dipping the wafers

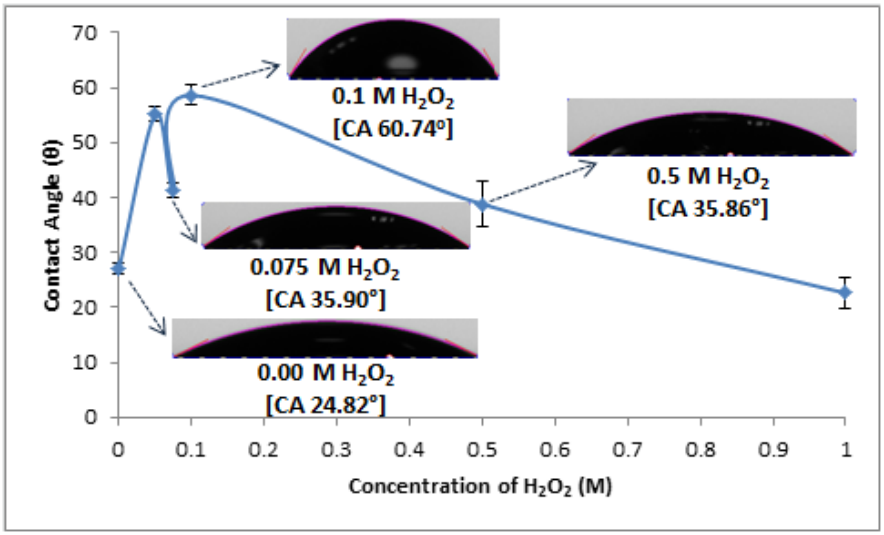

Figure 4.9. Contact angle measurements of polished W surfaces treated for 5 minutes with H_2O_2 at increasing concentrations.

into solutions at different oxidizer concentrations. Initially, DI water was used to measure the wettability responses as a function of the changing surface topography of the substrates. Figure 4.9 illustrates the contact angle responses of the tungsten oxide surfaces including the pictures of the droplets. It can be seen that, the minimum contact angle measurement was taken at 0.075 M H_2O_2 concentration, where a maximum was obtained in the surface roughness [Gbb12].

It appears that the surface topography tends to affect the wettability responses of the surfaces, which is directly related to the changes in the surface energy. In order to evaluate the surface energy responses, we measured the contact angles on the sample surfaces with polar and non-polar liquids (ethylene glycol, formamide, glycerol and DI-water) and calculated the total surface energy by acid-base method as detailed in the literature [Hiw09]. Figure 4.10 illustrates the calculated total surface energy values, which also demonstrates that the minimum total surface energy was obtained at 0.075 M concentration. Hence, it is expected that the surface nature of the metal oxide

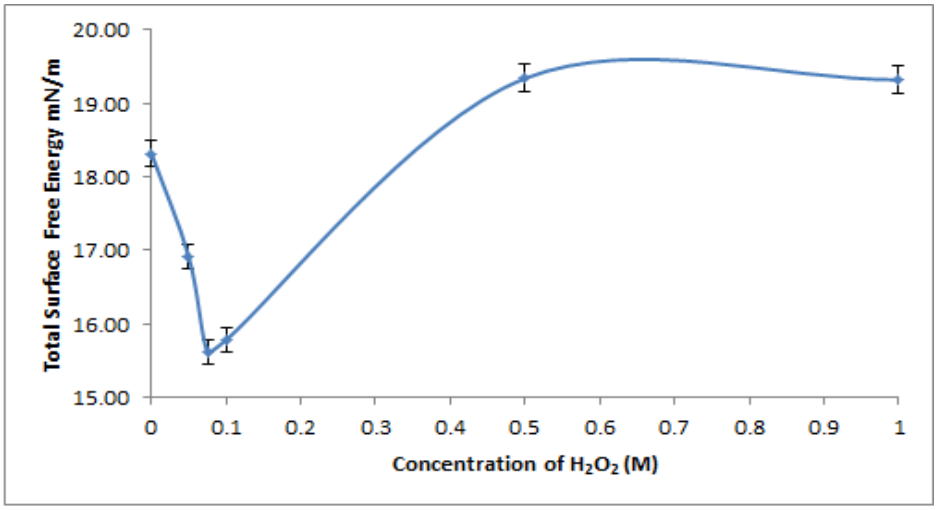

Figure 4.10. Calculated surface energy values for W surfaces treated for 5 minutes with H_2O_2 at increasing concentrations based on measuring with polar and apolar liquids.

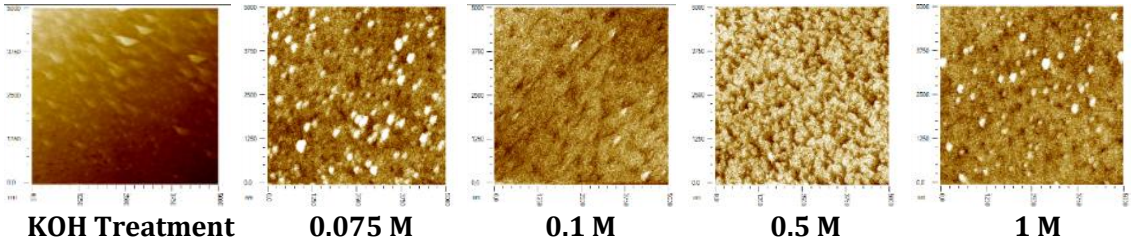

Figure 4.11. AFM surface micrographs of the tungsten wafers dipped into the various concentrations of H_2O_2 solutions for 5 minutes.

thin films may also be important in evaluating the CMP performance. This result correlated very well with the observations in Figures 4.9 through 4.10. In summary, the minimum in the contact angle measurement with DI water, the minimum in the total surface energy and the maximum in the surface roughness value obtained at 0.075 M oxidizer concentration. One of the main significance of this finding is that, the very simple and bulk level measurement of wettability through contact angle is a good predictor of the surface roughness and total surface energy of the metal oxide thin films. Figure 4.10 consistently illustrates decreasing surface roughness values with the increasing oxidizer concentrations. The irregularity observed at the 0.075 M H_2O_2 concentration is consistently observed in these two figures as well, delineating the change in total surface energy and oxidation mechanism at this critical concentration.

Even though the chemically modified tungsten oxide thin films are protective in the presence of an oxidizer at the recessed locations of the patterned wafer, the mechanical abrasion of the slurry particles continuously expose fresh tungsten metal to oxidation at the protruding locations. Tungsten forms a protective oxide film in the CMP applications as it was shown in Figure 4.10. However, it was observed that the surface nano topography change as a function of the oxidizer as illustrated in

Figure 4.11 and also in Figure 4.12 SEM migrographs which illustrate variation in the nature of the surfave with varying H_2O_2 concentration.

The W wafer had some oxide formation pre-treatment, which was cleaned in high pH KOH solution. When the wafers were dipped in the increasing concentrations of the oxidizer, the oxide formation started to take place as it can be seen in the AFM micrographs. Detailed analyses conducted in earlier studies have shown that the surface tungsten oxide film formed gradually as a composite of W and WO_x mixture and reached a depth of approximately 10 nm in total [Mlo11]. In addition, the surface roughness and contact angle analyses conducted on the tungsten surface as a function of dipped oxidizer concentration (0, 0.05, 0.075, 0.1, 0.5 and 1 M) have shown a critical point in surface topography at 0.075 M concentration. It appears that up to a 0.075 M oxidizer, concentration, the surface oxide tends to form through nucleation and growth and above this concentration, the hillocks formed by the nucleation reach a critical size among which diffusion mechanism take over and a transition through a granular surface topography is observed. This is believed to be due to Ostwald ripening of the tungsten oxide crystals at the elevated oxidizer concentrations. Hence we have evaluated the total surface energy and W_a data as listed in Table I. It can be seen that the minimum surface energy is obtained at 0.075 M H_2O_2 concentration, which supports the change in the nature of oxide growth. However, it can also be seen that the W_a is not a minimum at this concentration which further supports the tendency of the system to transition onto a diffusion based oxide growth mechanism that enables the continuity in the observed trend.

Comparison with the mathematical model: The dynamics of phase separation in a binary system was modeled by Cahn and Hilliard [Jwc58, Jwc61, Jwc65] by incorporating the interfacial energy captured between two phases. We follow their approach to investigate

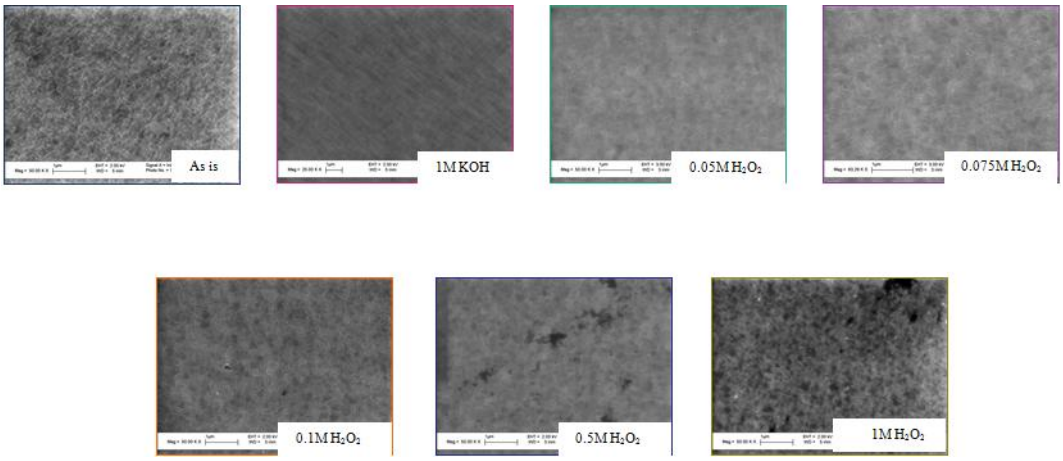

Figure 4.12. SEM micrographs illustrate variation in the nature of the surface with varying H_2O_2 concentration.

the interface between WO_2 and H_2O_2 in the CMP process. This requires introduction of a gradient term in the free energy which leads to the consideration of the energy functional where $c(x,t)$ is the concentration, f is the free energy density and κ is the

$$E(t) = \int_{\Omega} \left(f(c) + \frac{\kappa}{2} |\nabla c|^2 \right) dx,$$

positive parameter to be chosen depending on the material. Looking at the first variation of the energy functional we obtain the so-called Cahn-Hilliard equation

$$c_t = \Delta(f'(c) - \kappa \Delta c), \qquad (x,t) \in \Omega \times \mathbb{R}^+.$$

It is worth mentioning that $E(t)$ is a Lyapunov functional for the above equation, that is, $E(t)$ is non-increasing along its solutions. We couple this nonlinear differential equation with the mass conservation law

$$\frac{1}{|\Omega|} \int_{\Omega} c(x,t)\, dx = \text{constant}.$$

A common choice for f is the double-well potential as seen in Figure 4.13.(a). Interpreting the free energy density as the work of adhesion in the system, one can see clearly from Figure 4.13 (b) that the energy is not minimized when the composition of

Table 4.1. Surface roughness, contact angle, surface energy and Wa data obtained on the samples treated with different concentrations of the H_2O_2 as an oxidizer.

Concentration of H_2O_2 [M]	Surface Roughness RMS (nm)	Contact Angle (θ)	Surface Energy (J/m^2)	Wa (J/m^2)
0	2.81	24.82	18.3	812
0.05	3.00	57.42	16.9	660
0.075	3.79	35.90	15.6	670
0.1	2.93	60.74	15.8	612
0.5	3.26	35.86	19.3	812
1	2.94	25.32	19.3	813

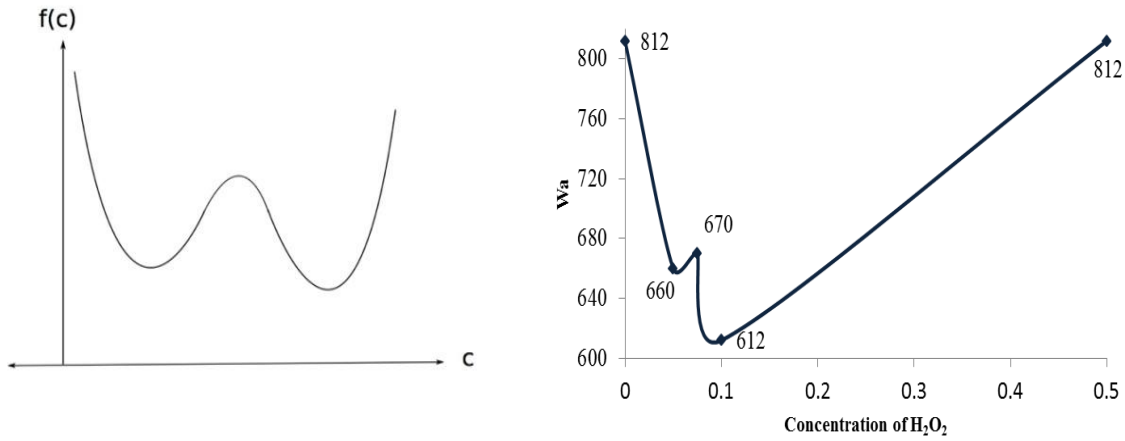

Figure 4.13. Double-well potential predicted by energy minimization compared to Wa measurements.

H_2O_2 is 0.075 M, which we think of as the critical concentration in the process. However, the surface energy is minimum at this concentration as listed in Table 4.1. This suggests that the interplay between the interfacial surface energy and the free energy is crucial supporting the Cahn-Hilliard theory.

Summary

CMP process of tungsten coupons were performed to improve surface morphology and removal rate by alumina slurries with an addition of H_2O_2 oxidizer at

pH 4which was widely used as an oxidizer in metal CMP process. The removal rate of tungsten was high around 1100 Å/min at 0.075 M H_2O_2 concentration and ~2200 Å/min at 1 M H_2O_2 concentration. In addition, as the result of AFM analyses, we confirmed that the surface morphology and the RMS roughness were improved. After CMP the surface roughness of tungsten coupon reduced significantly from ~20 nm RMS value on the original sample to ~4 nm RMS. It is suggested also that this approach will be useful for understanding the mechanism of CMP and thin film formation during CMP process development.

The observed changes in the surface topography were also found to affect the wettability and total surface energy. Hence it is obvious that the protective nature, as well as the surface nano-topography of the metal oxide thin films need to be studied to assess the CMP performance. Changes in the surface roughness and topography with the oxidizer concentration were explained through a mathematical approach using Cahn-Hilliard theory. Therefore, mathematical approach using Cahn-Hillard theory on CMP performance will be worked as a part of future work for modeling new CMP slurry optimization.

CHAPTER 5

CHEMICALLY MODIFIED THIN FILM ANALYSES ON GERMANIUM CHEMICAL MECHANICAL PLANARIZATION DEVELOPMENT

Introduction

This chapter focuses on improving the Ge CMP through analysis of chemically modified thin films with a focus on improving germanium/silica selectivity. In the previous chapters, the preliminary studies were conducted on the effect of chemically modified thin films on tungsten wafer surfaces. There is an increased focus on germanium (Ge) and III–V semiconductors as potential channel materials for sub-22 nm devices since both electron and hole mobilities in Ge are higher than those in silicon (Si). Particularly, beyond the 14nm technology the development needs made it a must to introduce high mobility channel materials such as Ge. CMP is an enabler for integration of these new materials into future devices.

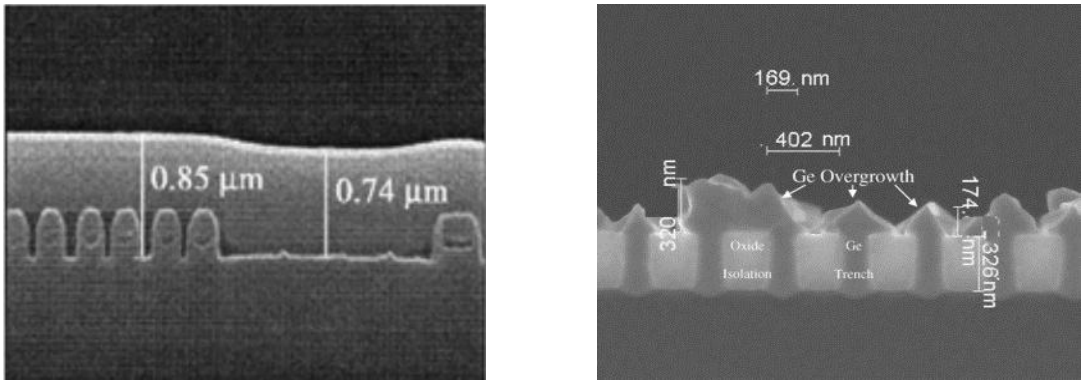

(a) (b)

Figure 5.1.a. Cross sectional SEM image of conventional STI CMP and **b.** 160 nm trenches of germanium STI structures before CMP [Shi12].

In the conventional STI CMP, standard consumable sets (pads and slurries) are used to obtain silica/nitride selectivity to produce isolation trenches between the transistors. Germanium (Ge) has higher charge mobility (electrons: ≤3900 cm^2 $V^{-1}s^{-1}$ and holes: ≤1900 cm^2 $V^{-1}s^{-1}$) as compared to silicon (electrons: ≤ 1400cm^2 $V^{-1}s^{-1}$ and holes: 450≤ cm^2 $V^{-1}s^{-1}$) and hence it is a possible replacement for future MOSFET manufacturing [Wbc11]. In Ge STI integration, Ge is epitaxially grown on Si in SiO_2 trenches after standard STI is formed. As a result of this process integration, germanium surface becomes much rougher as compared to the oxide deposition that needs to be process through CMP in the standard STI application. Figure 5.1.a. illustrates conventional STI CMP integration while 5.1.b. represents a typical cross sectional view of the 160 nm Ge STI structure before the CMP is performed. The height of the roughened Ge overburden at its highest point is around ~175 nm from the oxide surface. Oxide layer has ~325 nm thickness which is also the depth of the filled Ge trenches remaining after the CMP is completed. A successful CMP process of Ge requires effectively controlled material removal selectivity between Ge and SiO_2 [Jsp09]. Simultaneously, slurry particle stability has to be maintained for minimal surface defectivity to produce functional devices. Therefore, advanced slurry formulations are needed for Ge CMP applications for an optimized planarization performance.

Recent investigations on Ge CMP have outlined some of the fundamental aspects of the process requirements [Spe12]. It has been shown that slurries containing colloidal and fumed silica particles along with hydrogen peroxide (H_2O_2) were effective in polishing Ge and the material removal rates (MRRs) and dissolution rates (DRs) in the basic pH region (greater than pH 9) were higher than those in the acidic pH regions [Spe11]. Furthermore, Ge dissolution rates also got promoted chemically by the

increasing oxidizer concentration resulting in very high removal rates [Jbm11]. The uncontrolled dissolution rates at high pH and oxidizer concentrations made it harder to control the process variability, in addition to pitting observed on the Ge surfaces. Peddeti and coworkers used the colloidal silica and germanium surface for zeta potential measurements as a function of pH and concluded that the zeta potentials in the presence of H_2O_2 were also similar to J. B. Matovu's results [Vak10]. From the device performance standpoint, a slightly recessed oxide profile was proposed to be needed for better performance suggesting that a slightly higher silica removal rate is preferred at the SiO_2/Ge interface once the excess of the deposited Ge is removed.

Nano-scale wear rate analyses are applicable to CMP process to understand the interactions at a single particle-surface interaction level by comparing wear rates of the materials at the interfaces that necessitate critical selectivity at nano-scale [Iuv10-Iuv12]. AFM is the main instrument utilized to investigate nano-scale friction and wear to predict the system level interactions. Through employing the lateral force mode of the AFM either with a nano-scale bare tip or with a micrometer-scale colloid probe with a spherical particle glued on the top of the cantilever, various surface modifications can be easily evaluated. Namely; (i) the affect of slurry ionic strength [Iuv10], (ii) pH dependence of frictional interactions between the particles and the surface [Eta06] and (iii) the properties of the chemically modified top layers which drive the chemical component of the CMP performance [Iuv12]. However, most of the earlier studies were performed on silica/nitride interfaces based on the needs of conventional STI processing. Typically, a bare AFM tip is preferred to study CMP process at nano-scale due to the colloidal particle being very large as compared to the point contact that can be achieved by the sharp AFM tip. Briefly, this chapter shows that the lateral interactions between an AFM tip and the germanium and silica surfaces as a function of

the solution conditions, such as pH and surfactant concentration [Bcd06]. Furthermore, the knowledge base on the wear rate testing is adopted to the germanium/silica system in an attempt to define a suitable slurry formulation with sufficient selectivity and removal rates while preserving a defect free surface finish.

In the previous two chapters were focused on the findings on the chemically formed metal oxide thin films on metal CMP applications. In chapter 5, chemically modified thin film characterization on the nonmetal CMP applications were evaluated on Ge/HDP SiO_2 wafers. The chemically modified thin films are mainly the hydroxyl layers formed by the dissolution of the materials such as silicon, silica or germanium in front end applications of the CMP so this chapter is started dissolution rate analyses. Then, wear rate analyses are evaluated on germanium/HDP SiO_2 wafer surface as a preliminary predictive approach through CMP material removal rate analysis. AFM wear rates are a good indicator of the polish rate response in the various CMP slurry medium. The wear rate experimentation cannot be done in the presence of the oxidizer due to bubbling and the corrosion of the AFM tip. Therefore, we have started our testing by evaluating the effect of oxidizer concentration on material removal rate. It can be seen from the MRR plots that the best selectivity is achieved in the absence of the oxidizer, however, the removal rates need to be higher for the CMP operations for which some amount of H_2O_2 addition is required. CMP performances of Ge and SiO_2 wafers were evaluated in terms of material removal rates, and surface quality. The surface roughness of the post-CMP finish is studied based on the polishing conditions such as slurry design. Additionally, on Ge/HDPSiO_2 the chemically modified thin film characteristics were studied through contact angle and ATR/FTIR analyses.

Materials and Methods

Dissolution Rates: Ge and HDP SiO_2 wafer coupons dissolution rates were measured in a glass beaker containing 100 mL of the etchant solution. Ge wafer coupons (10 x 10 mm^2, diced from N type Germanium wafers with 2" diameter and 400 μm Ge thickness obtained from University Wafer and 6000 Å thick HDP SiO_2 wafers) were used as the samples. These wafers had a 30 nm SiO_2 layer deposited on top of the epitaxially grown Ge to prevent the formation of native oxides. The SiO_2 layer was etched out just before the experiments were performed. Each coupon was initially weighed on an PRECISA 360 ES scientific balance (0.01 mg accuracy). The solution was stirred using a magnetic stirrer at 300 rpm rotational speed at room temperature. The coupon was removed, washed repeatedly with deionized (DI) water, dried in a nitrogen stream, and reweighed. The weight loss was used to calculate the dissolution rate and the reported rates were obtained by averaging over three experiments, each spanning at least 1 min.

Contact Angle Measurements: The contact angle is the angle, conventionally measured through the liquid, where a liquid/vapor interface meets a solid surface. It quantifies the wettability of a solid surface by a liquid via Young Eguation. In this chapter, contact angle measurements were performed by sessile-drop contact angle measurement technique on Ge/HDP SiO_2 surfaces with a KSV ATTENSION Theta Lite Optic Contact Angle Goniometer. Three bubbles were measured on each sample. The bubble image stored by a camera and an image analysis system calculated the contact angle (Θ) from the shape of the bubble.

AFM Wear Experiments: AFM wear experiments on Ge/HDP SiO_2 system were conducted using a rectangular cantilevers, K_N = 4.5 N/m (NSC35/Si_3N_4, MikroMasch). AFM tip was made to continuously scan over a fixed position on the substrate surface

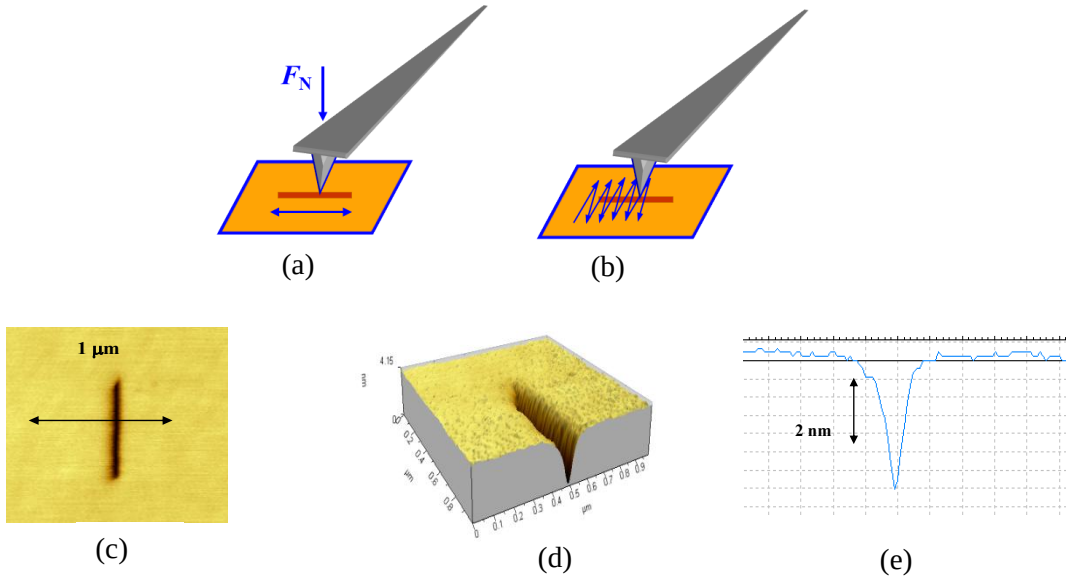

Figure 5.2. Schematics of the wear test experiment: (a) the AFM tip makes continuous lateral scans over a fixed position on the substrate surface using applied load FN, (b) the scan direction is changed to image the wear trace applying a minimum load (c) used to estimate the wear depth. (d) Three dimensional cross-section of the same scratch (e) Cross section of the image at the line indicated on.

laterally using an applied load F_N. Scan direction was changed to image the wear trace applying a minimum load. AFM image and cross sections were used to estimate the wear depth. The cantilevers were chosen to have an integrated etched silicon conical tip of 25-30 µm height and cone angle of 40°C and coated with about 10 nm thick layer of silicon nitride (coated tips radius of about 20 nm). In a standard test scan size of 1 µm, scan rate of 8.4 Hz, scan time of 51 seconds (420 scan cycles) and applied load of about 720 nN (4 Volts deflection of 4.5 N/m cantilever) were used. Experiment set up illustrated in Figure 5.2.

Material Removal Rate Analysis: Material removal rate analysis were conducted on a desktop Tegrapol-31 polisher by using SUBAIV-IC1000 stacked polishing pad. The down force was 70 N on the 1.0 × 1.0 cm wafer coupons with 150 rpm rotational

velocity and 100 ml/min slurry flow rate. CMP responses were obtained in terms of MRR (Å/min) and surface roughness measurements. The material removal rates were determined from the difference in the weights of the wafer coupons before and after polishing measured by a high precision balance with five digits after zero.

FTIR/ATR Measurements: FTIR/ATR analyses were conducted on the unpolished Ge and SiO_2 wafers as a function of H_2O_2 concentration. Wafers were cut into small coupons and dipped into H_2O_2 solutions at different concentrations for 5 minutes as a function of pH. Before dipping the wafers into the oxidizer solution, a pre-clean procedure was applied by dipping the wafers into a 1 M KOH solution to remove the excessive surface oxide followed by a rinse with deionized water and drying with nitrogen gas. Wafer coupons were tightly clamped over the measurement crystal of the ATR accessory of a Bruker Equinox 55 model FTIR spectrophotometer. Sixtyfour scans were averaged and corrected using the rubber-band correction mode (70 points) of the Bruker OPUSV 3.1 software.

Surface Quality Analyses: Surface roughness values of the wafer coupons were measured by Nanomagnetics Instruments Atomic Force Microscope (AFM) on 2.5 μm by 2.5 μm scans using tapping mode to protect the naturally formed oxide films from deformation during scanning. The averages of minimum tree measurements were reported with standard deviations to verify the statistical significance of the observed values.

Results and Discussion

The dissolution rates of Ge/ HDP SiO_2 wafer coupons, measured in a solution of 0.1 M H_2O_2 and in DI water as a function of pH at room temperature (~25ºC), is shown

in Figure 5.3. There was no detectable dissolution of Ge or HDP SiO_2 in the pure DI water system. However, in the presence of 0.1 M H_2O_2 which is add as an oxidizer, dissolution was observed on both Ge and HDP-SiO_2 wafer coupons (Figure 5.3). The germanium dissolution rate was ~81 Å/min in acidic and neutral pH regions and increased to ~242 Å/min in the basic region at pH 11. It is known that the Ge dissolution is promoted at basic pH for which a two-step mechanism is proposed. In aqueous solutions of H_2O_2, as suggested by Schumb *et al.** the dissociation of H_2O_2 occurs as in the reaction given in Equation [5.1]

$$2H_2O_2 \longrightarrow 2H_2O_2^{+} + O_2H^{-} \qquad [5.1]$$

When the O_2H^- ions diffuse into the germanium surface, they attach instantly to surface Ge atoms forming surface complexes suc as $Ge(OH)_2$ and $Ge(OH)_2^{++}$, by the reaction shown in Equation [5.2]. Therefore, in the presence of H_2O_2 the mechanism of material removal is suggested to be the dissolution of the germanium predominantly.

$$Ge + O_2H^- + H_2O + 2e^+ \longrightarrow Ge(OH)_2^{++} + OH^- \qquad [5.2]$$

In the acidic and around the neutral pH ranges, the oxidation is lower as compared to the basic region resulting in minimal formation of the soluble $Ge(OH)_2$. Figure 5.4. is proposed Ge removal mechanism in H_2O_2 aqueous solution, the negatively charge on Ge surface decrease the attack by OH- and *OH (negative charge on Ge screens OH- and *OH due the negative charge and the negative inductive effect OH- and in *OH since oxygen is more electronegative than hydrogen, recpectively). In both cases, Ge-Ge

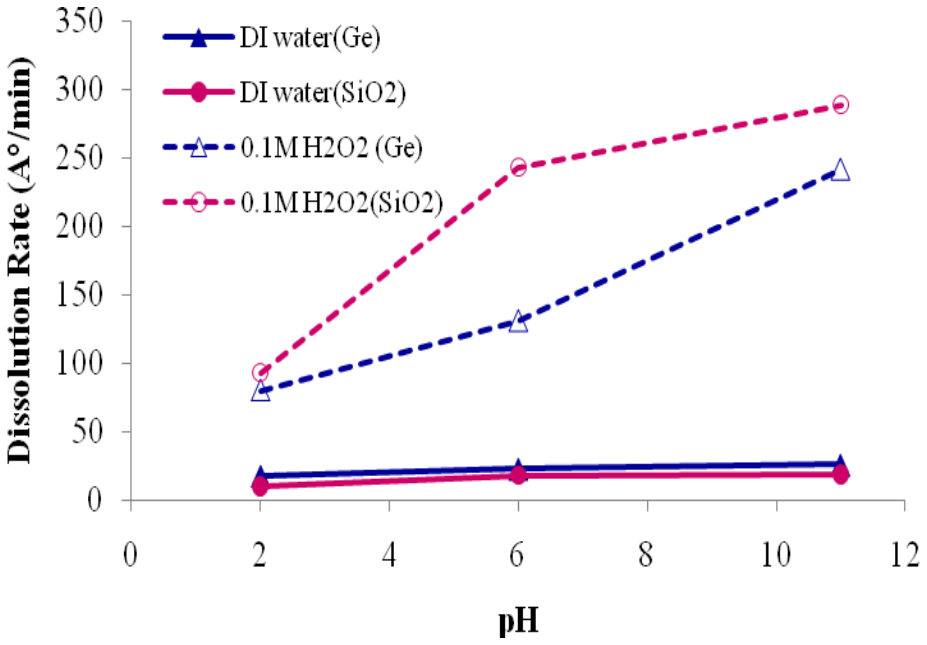

Figure 5.3. Ge/HDP SiO_2 wafer coupons dissolution rate in a.Ge wafer coupon in pH adjusted DI water at 25°C, b. HDP SiO_2 wafer coupon in pH adjusted DI water at 25°C, c. Ge wafer coupon in 0.1 M H_2O_2 at 25°C, d. HDP SiO_2 wafer coupons dissolution rate in 0.1 M H_2O_2 at 25°C.

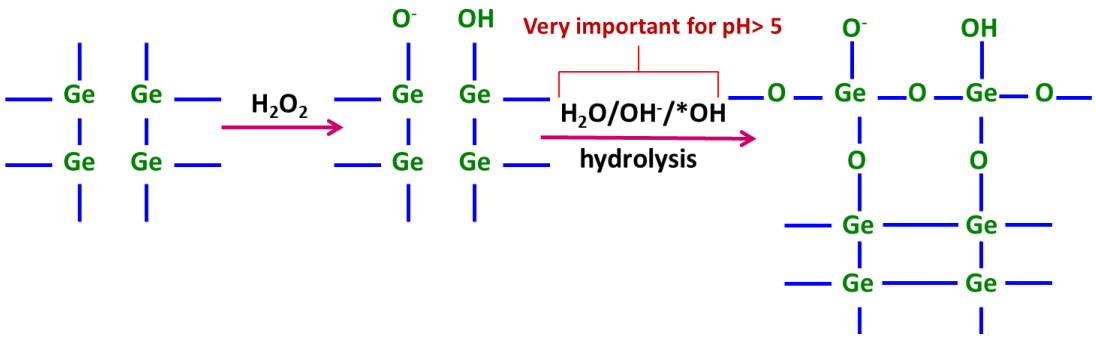

Figure 5.4. Mechanism of H_2O_2 diffusion on Ge surface.

bonds, being weaker than Ge-O-Ge bonds, are ruptured during polishing. It is obvious that from the reaction equations, Ge removal mechanism is highly dependent on the oxidation of the Ge surface to GeO_2.

Ge dissolution is promoted at basic pH. Therefore, we analyzed the wear rate as a function of pH from asidic pH region to basic pH region, the AFM wear rate responses

were as expectedly increasing with the increasing pH values. Figure 5.5.a illustrates the results of the wear rate responses of the germanium versus silica wear rates as a function of pH in DI water. It is clearly seen that the silica wear rate increases significantly with the increasing pH values, which is consistent with the earlier literature findings [Jdr87]. However, the wear rates of Ge did not increase at the same magnitude although a similar trend was observed on Ge as well showing an increase in the wear rate as a function of pH. Since in the presence of the oxidizer bubbling is observed and the AFM tip is corroded, the wear rate experimentation cannot be done in the presence of H_2O_2. However, in the high volüme manufacturing envoirenment of the CMP operations it is necessary to add some oxidizer (typically H_2O_2) to increase the material removal rates to speed up the manufacturing. Therefore, the effect of oxidizer concentration was studied on the removal rates of the Ge and silica as can be seen in Figure 5.5.a.

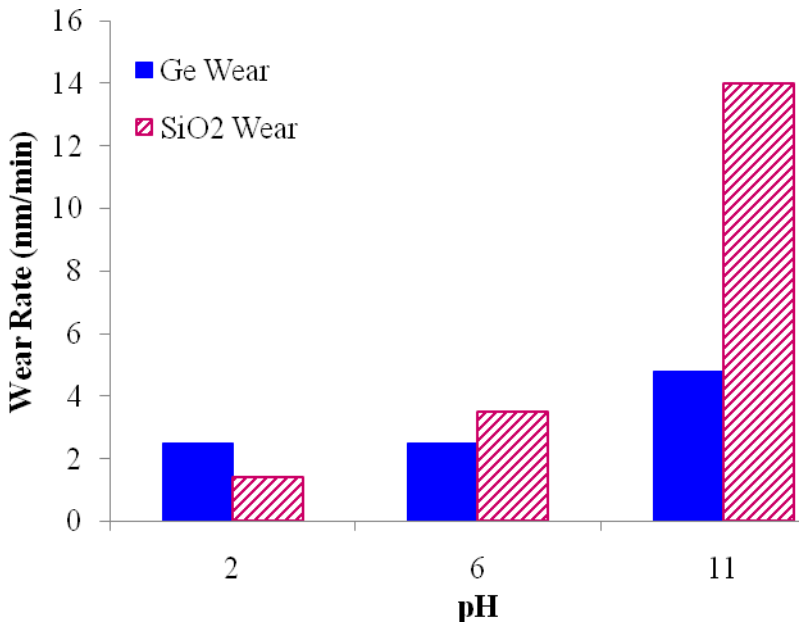

Figure 5.5.a. Wear rates response in pH adjusted DI water.

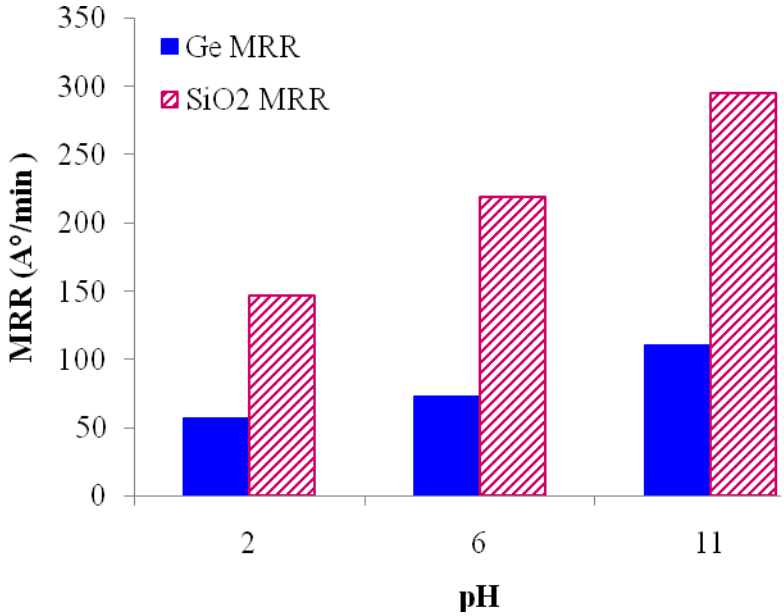

Figure 5.5.b. Material removal rate responses on Ge/SiO_2 as a function of pH.

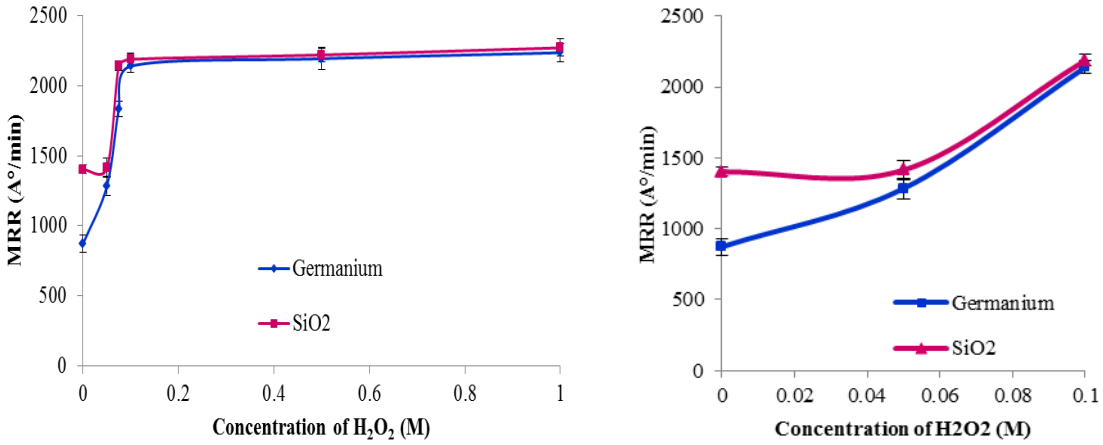

(a) (b)

Figure 5.6.a. Effect of H_2O_2 concentration on selectivity **b.** selectivity response magnified up to 0.1 M H_2O_2 concentration.

It was observed that H_2O_2 as a function of concentration can enable reduction in Ge CMP rates with higher oxide removal rate. Hence H_2O_2 concentration was kept at the minimum level where a plateau is reached in the material removal rates and the

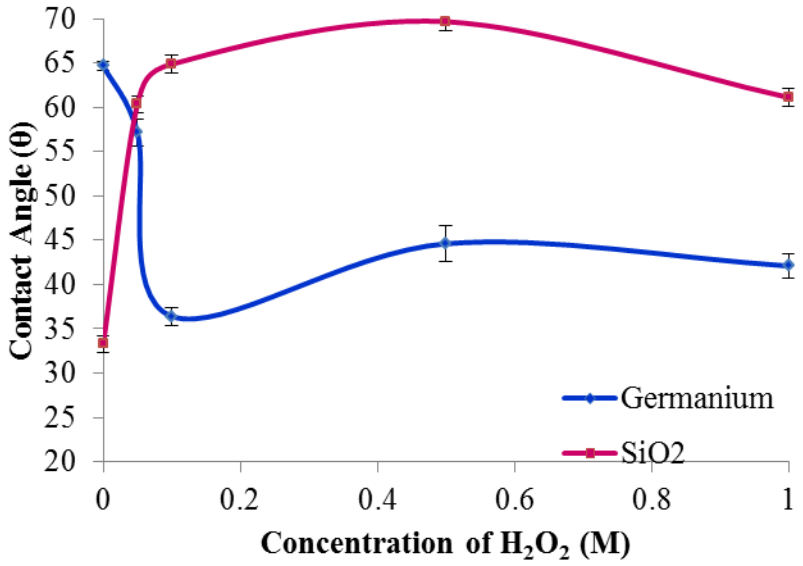

Figure 5.7. Contact angle on Ge and SiO2 by H2O2 concentration at pH 6.

Values stabilize (0.1 M H_2O_2). In addition, wettability of the Ge/HDP SiO_2 surface was investigated by measuring the contact angle values through sessile drop method. Ge is a naturally hydrophobic mineral below pH 4, and based on the knowledge from the froth flotation testing, it can be altered hydrophobic in the presence of surfactants even above pH 4 [Drz87]. Yet, the addition of H_2O_2 creates an oxide layer on the surface of the germanium rendering it more hydrophobic while resulting in more OH groups forming on the silica surfaces, which is suggested to be the reason for the silica surface to get more hydrophobic which is shown that in figure 5.7.

Effect of slurry pH on surface finishes: The effect of H_2O_2 as an oxidizer on surface quality after CMP process can be further discussed based on Figure 5.8.a and 5.8.b, where the surface roughness responses are demonstrated as a function of the oxidizer concentration at 3 wt % solids loadings. From Figure 5.8 consistently illustrates decreasing surface roughness values with % 3 wt fumed silica at increasing pH for surface roughness responses on germanium wafers after CMP. The highest surface roughness is obtained at acidic pH 2.

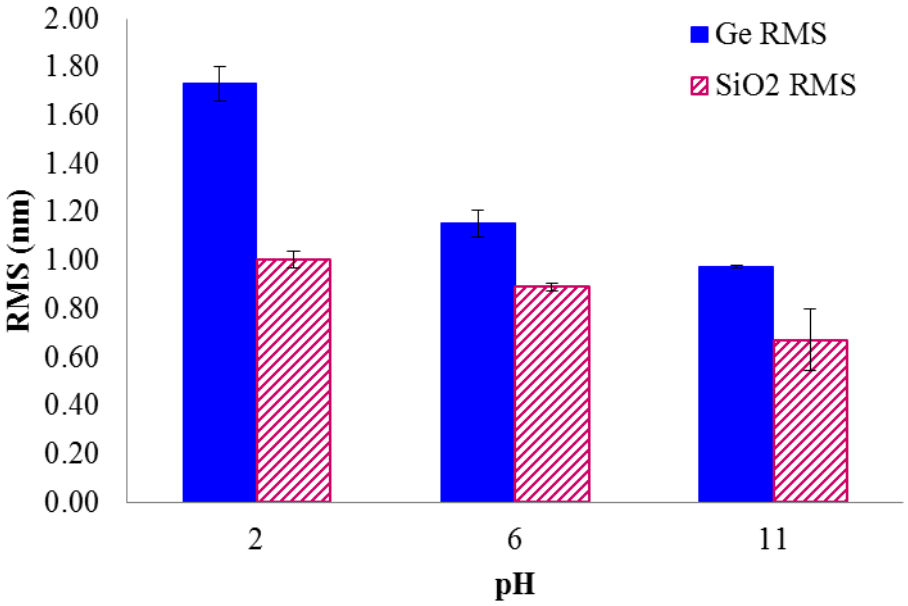

Figure 5.8. Surface roughness responses on Ge/HDP SiO2 wafers after CMP with 3 wt % fumed silica at increasing pH.

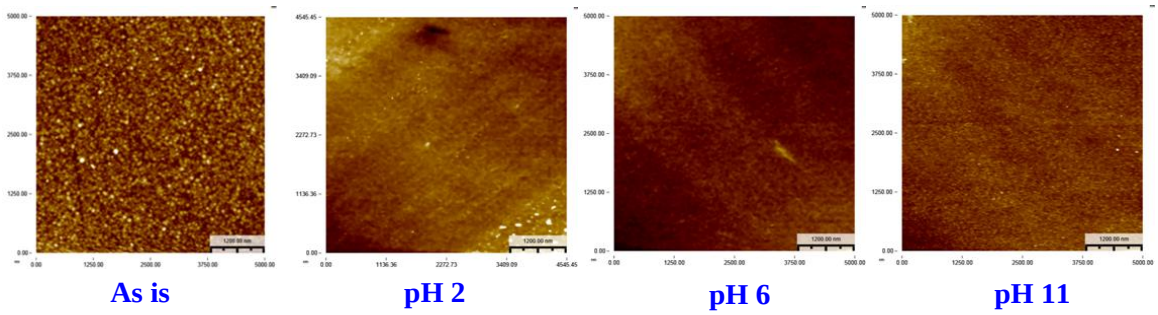

Figure 5.9.a. Characterization of the germanium wafers after CMP with 3 wt % fumed silica at increasing pH for surface roughness responses.

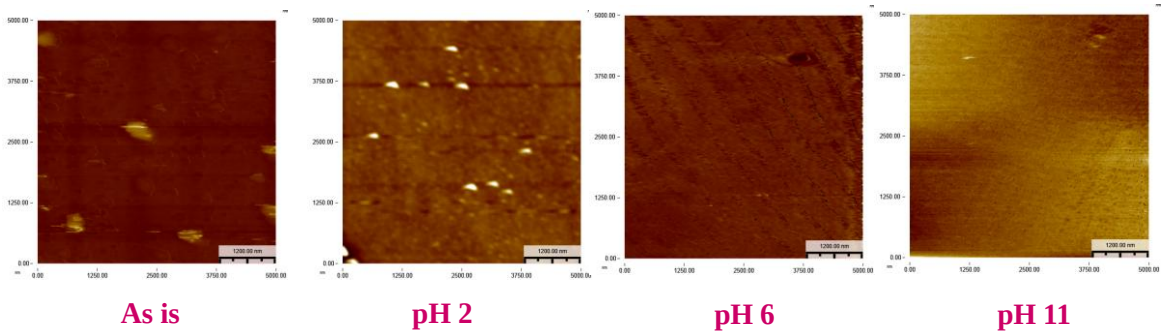

Figure 5.9.b. Characterization of the HDP SiO_2 wafers after CMP with 3 wt % fumed silica at increasing pH for surface roughness responses.

Surface roughness values are signaficantly decreasing as a function of pH. However, surface quality results do not seem well as it is shown that in figure 5.8.a for germanium wafer surfaces and in figure 5.9.b for HDP SiO_2 wafer surfaces. The surface quality analyses have conducted in a slurry which has no more additives such as oxidizers and surface active agents. These results also show that the slurry of fumed silica is not stable without any additives, and abrasive particles are attached on the wafer surface as it is shown from AFM images obviously. Therefore in the next chapter, slurry stability was improved with self-assembled surfactant structures.

Summary

AFM wear rates are good indicator of the polish rate analysis. Wear rate results are higher at pH 11 as compared to pH 6 and pH 2 as expected. Germanium wear rate at pH 11 is also higher than pH 6 wear but not that dramatically increased as in the silica case. Based on wear rate results, pH 6 is a good region where both SiO_2 and Ge removal can be achieved. The Ge/HDP SiO_2 wafers were also polished with fumed silica particles as a function of pH to determine the correlation to MRR. In addition, the results of this study have shown that in the presence of hydrogen peroxide in the slurry, removal rates are mainly affected by the oxidizer. Germanium dissolution is negligible and post polish surface quality is not good with 3 wt % fumed silica in the presence of 0.1 M H_2O_2 as an oxidizer because slurry is not stable and abrasive particles remain on the wafer surfaces. Therefore, in the next chapter cationic and anionic surface active agents were used for improving slurry stability for after CMP surface quality and simultaneously improve the selectivity responses.

CHAPTER 6

IMPROVING THE GERMANIUM CHEMICAL MECHANICAL PLANARIZATION PERFORMANCE THROUGH THIN FILM MODIFICATION WITH SURFACE ACTIVE AGENTS

Introduction

In chapter 6, slurry formulations are evaluated to enhance selectivity for germanium/silica planarization systems. Initial, selectivity analyses were conducted by wear rate responses measured at a single particle-surface level through atomic force microscopy (AFM) as described in the previous chapter. Furthermore the effects of using both anionic (sodium dodecyl sulfate-SDS) and cationic (cetyl trimethyl ammonium bromide-C_{12}TAB) surfactants at their sub-micelle and above critical micelle concentrations (CMC) were demonstrated. CMP performances of Ge and HDP SiO_2 wafers were evaluated in terms of material removal rates, selectivity and surface quality. The surfactant adsorption characteristics were studied through surface wettability and streaming potential measurements. In addition, since the slurry stability is necessary to prevent unacceptable levels of surface roughness and defects, the impact of adding surfactants on particle-particle interactions is investigated in the study.

In this part of dissertation, it is aimed to extend the current knowledge base in the use of surfactant systems established on the standart STI CMP to the Ge STI CMP. The results are reported on CMP experiments conducted by using fumed silica particles at 3wt% loading and 200-300 nm particle size in the presence of the twelve carbon chain cationic and anionic surfactants. The oxidizer, H_2O_2, concentartion was kept at 0.1 M

as per the outcomes of the previous chapter, where the preliminary analyses were conducted by evaluating the effect of oxidizer concentration on selectivity. It was observed that the best selectivity is achieved in the absence of the oxidizer, however, the removal rates need to be higher for the CMP process for which some amount of H_2O_2 addition is required. Therefore, concentration of H_2O_2 was kept at 0.1 M at the minimum level where a plateau is reached in the material removal rates. Depending on this experimental set-up, contact angle measurements, zeta potential and AFM wear experiments were evalueted on the Ge/HDP SiO_2 system in the presence of 0.1 M H_2O_2, and C_{12}TAB, SDS surfactants as function of critical micalle concentration (CMC) values.

Based on the findings on the surfactant mediation on the slurry selectivity, a design of experiment (DOE) methodology was implemented in order to understand the optimized CMP slurry parameters such as optimal concentration of surface active agent (sodium dodecyl sulfate-SDS), concentration of abrasive particles and pH from the viewpoint of high removal rate and selectivity while maintaining a defect free surface finish. The responses examined were particle size distribution (slurry stability), zeta potential, material removal rate (MRR) and the surface defectivity as a function of the selected design variables. The impact of particle solids loadings, oxidizer (H_2O_2) concentration, SDS surfactant concentration and pH were analyzed on Ge/silica selectivity through material removal rate (MRR) surface roughness and defectivity analyses. DOE methodology has been only studied in the presence of SDS because of the poor surface quality responses obtained with C_{12}TAB surfactant due to agglomeration.

Materials and Methods

AFM Wear Experiments: Wear tests were done using a rectangular cantilevers, K_N = 4.5 N/m (NSC35/Si_3N_4, MikroMasch). The cantilevers have an integrated etched silicon conical tip of 25-30 μm height and cone angle of 40°, coated with about 10 nm thick layer of silicon nitride (coated tips radius of about 20 nm). In a standard test we used the following scan parameters: scan size of 1 μm; scan rate of 8.4 Hz; scan time of 51 seconds (420 scan cycles), applied load of about 720 nN (4 Volts deflection of 4.5 N/m cantilever) as it explained in previous chapter.

Chemical Mechanical Polishing : The polishing slurries were prepared using 0.2-0.3 μm average size silica, fumed powder (Sigma) and DI water. All slurries were set up at pH 2, 6 and 11 through the addition of KOH or HCl had a solids loading of 3 wt %. The slurries were mechanically dispersed through sonication in pH 9 DI water. C_{12}TAB surfactants was used to impart slurry stability. To monitor the monodispersion and stability of the slurries, particle size analysis measurements were performed via light scattering technique using a LS-13-320 Laser Diffraction Particle Size Analyzer (Beckman Coulter ALM-aqueous Liquid Module) instrument. The background water used to run the size analysis experiments was prepared to have the same pH.

CMP experiments were conducted on bare N type Germanium wafers with 2" diameter and 400 μm Ge thickness obtained from University Wafer and 6000 Å thick HDP SiO_2 wafers which were cut into 16x16mm^2 coupons on a desktop Tegrapol-31 polisher by using SUBAIV-IC1000 stacked polishing pad (Table 6.1). Slurries were prepared using fumed silica particles at 3% wt concentration and H_2O_2 as an oxidizer. C_{12}TAB surfactant was added to CMP slurries at 2 x CMC (critical micelle concentration) after the slurry pH was adjusted to 2,6,11. The pH of the slurries was adjusted using HCl or KOH, as there was no detectable removal of Ge when polished

Table 6.1. Polishing Conditions

	Desktop Tegrapol-31 Polisher at Ozyegin University
Substrate	1.6 x 1.6 mm^2 Ge and HDPSiO_2 wafer coupons
Abrassive Particles	3 wt % fume silica particles
Rotational Speed (rpm)	150
Pad	SUBAIV-IC1000 stacked polishing pad
Applied Pressure (psi)	~ 16.4
Slurry Flow Rate (ml/min)	100
Conditioning	2 min after each polish

with DI water whose pH was adjusted using these chemicals. CMP tests were conducted at 30 N downforce (~16.4 psi downforce) on the used sample size at 150 rpm rotational velocity and 100ml/min slurry flow rate. Ge and HDP SiO_2 material removal rates (MRR), averaged over 3 experiments, were determined from the change in weight after polishing the Ge and HDP SiO_2 wafer coupons and drying it in an N_2 stream. An analytical balance with a precision of 0.01 mg was used to measure the Ge and HDP SiO_2 wafer coupons mass before and after polishing.

Surface Roughness: Surface roughness analysis were performed by tapping mode with Nanomagnetics Instruments Atomic Force Microscope (AFM) before and after polishing. Three measurements were done per sample at the center of the wafer coupons by 2.5 μm × 2.5 μm scans. The reported roughness is the root mean square (RMS) value of each of the measurements.

Contact Angle Measurements: Contact angle measurements were performed by sessile-drop contact angle measurement technique on Ge/HDP SiO_2 surfaces with a KSV

ATTENSION Theta Lite Optic Contact Angle Goniometer. Three bubbles were measured on each sample. The images of bubbles were captured by a camera and an image analysis system used to calculate the contact angle (Θ) from the shape of the bubbles.

Particle Size Measurements: The particle size of the abrasives in the slurry was measured using a LS 13 320 Laser Diffraction Particle Size Analyzer (Beckman Coulter ALM-aqueous Liquid Module) with C_{12}TAB and without C_{12}TAB as a function of pH. The pH of the solutions were adjusted using KOH or HCl as needed.

Zeta Potential(ζ) Measurements: The zeta potentials of 3 wt % fumed silica particles were measured as a function of pH before and after surfactant addition at Malvern ZS Zetasizer. An electrokinetic analyzer (SurPASS, Anton Paar GmbH) was used to measure the zeta potential of the germanium and HDP SiO_2 surfaces as a function of surfactant concentration. In brief, an adjustable-gap cell for circular discs with a diameter of 10 x 10 cm was used and the variable separation between the two wafer surfaces was set to approximately 100 μm. Flow was induced in the measurement cell by ramping the differential pressure from 0 to 400 mbar in both flow directions. The zeta potential was determined from the Smoluchowski equation by measuring the change in streaming current versus the applied differential pressure. A 1 mM KCl solution was used as electrolyte.

Design of Experiments: A response surface design was conducted to optimize the selectivity performance based on the slurry solids loading, pH and SDS surfactant concentration. The central composite design has the advantage of analyzing three factors at five levels with a relatively small number of observations, that are enough to estimate the second order effects of the response surface [Mas89]. It is also suitable for process optimization. Figure 6.1 shows the three-factor layout for the rotatable central

composite design. On this layout, the high and low levels of the design are coded as -1 and +1 and the factorial portion is represented with the circles, which are forming a box. The star (α) points are the axial points, and they are located 1.68 coded units away from the center ($\alpha = [2k]^{1/4}$, for k=3 α= 1.68), making the design rotatable. A rotatable design provides equally good predictions at points of equal distance away from the center. Design Expert software (by Stat-Ease Inc.) was utilized to create the response surface design and to analyze the experimental results. The design required 20 experimental runs including 6 repeat tests at the center point, which provided an estimate of the uncontrolled experimental error variation. The studied design and the obtained responses are given in the appendix with the mathematical equations showing the dependence of the selected factors to the experimental variables. Polishing slurries were prepared using fumed silica powders obtained from Sigma-Aldrich by following the procedure described in Chapter 5. Table 6.2 summarizes the selected design levels determined based on the industrially used values.

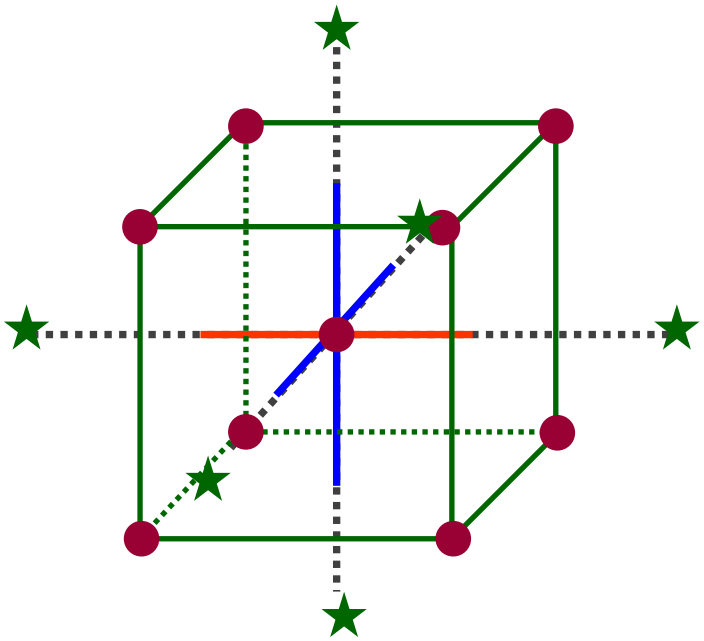

Figure 6.1. Central composite design for three factors.

Table 6.2. Selected design levels for the three-factor rotatable central composite design.

	-1.68	-1.0	0	+1.0	+1.68
Concentration of SDS (mM)	0	0.8	2	3.2	4.0
Solid loading (% wt)	0.1	1.2	3	4.8	6.0
pH	3	4.2	6	7.8	9

Polishing tests were performed on Ge and HDP SiO_2 wafer coupons (10 x 10 mm^2, diced from N type Germanium wafers with 2" diameter and 400 µm Ge thickness obtained from University Wafer and 6000 Å thick HDP SiO_2 wafers donated by Texas Instruments Inc.). Struers desktop Tegrapol-31 polisher and SUBAIV-IC1000 stacked polishing pad were used for polishing as outlined in Chapter 4.

Results and Discussions

Figure 6.2 illustrates Ge/HDP SiO_2 wear rates in the presence of 32 mM C_{12}TAB (2 x CMC) as a function of pH. When the C_{12}TAB surfactant was added at twice the CMC concentration, the wear rates decreased significantly both for silica and germanium wafers, becoming almost negligible except for the pH 6. At pH 6 both SiO_2 and Ge wear could be achieved at a low rate. Hence we decided to continue the preliminary analyses at pH 6. The pH dependencies of the zeta potentials of the germanium and HDP SiO_2 surfaces are shown in Figure 6.3. From the zeta potential measurements, the germanium and HDP SiO_2 wafer surfaces are both negatively charged at pH 6 with Ge has a surface charge of -20 mV and silica -55 mV. Therefore, the expected mechanism of surfactant adsorption on the wafer surfaces should favor the adsorption of the cationic surfactant while limiting the adsorption of the anionic

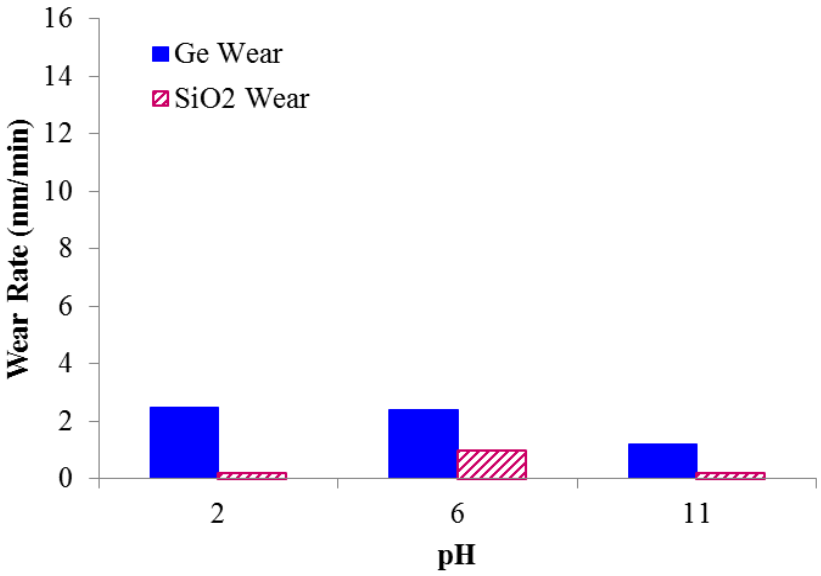

Figure 6.2. Wear rates in the presence of 32 mM C_{12}TAB as a function of pH.

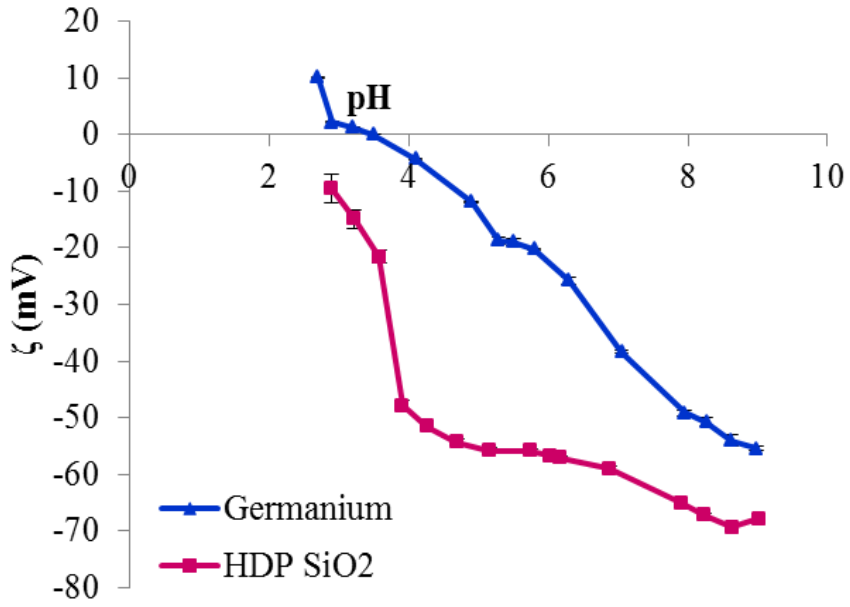

Figure 6.3. Zeta potentials of Ge and HDP SiO_2 wafer surface as a function of pH.

surfactant. As it is illustrated in Figure 6.4, it is expected expect that at pH 6, silica should attract more cationic surfactant structures on the surface resulting increased lubrication and hence much lover material removal rates. When the negatively charged surfactant, SDS, is used instead of C_{12}TAB, however, the degree of surfactant adsorption in between the silica and Ge surfaces is reversed which should help achieving the desired selectivity.

When we conducted the zeta potential measurements on the fumed silica nanoparticles as a function of surface active agents at pH 6, surface charge of the fumed silica changed from -32 mV to around ~ +16 mV as a function of C_{12}TAB concentration. In the presence of SDS, however, the surface charge of silica nanoparticles changed to become more negatively charged as a funtion of concentartion. Figure 6.5 illustrates the surface charge on silica nanoparticles as a funtion of surface active agents. The same analyses were also conducted on germanium and silica surfaces by Surpass streaming potential measurement.

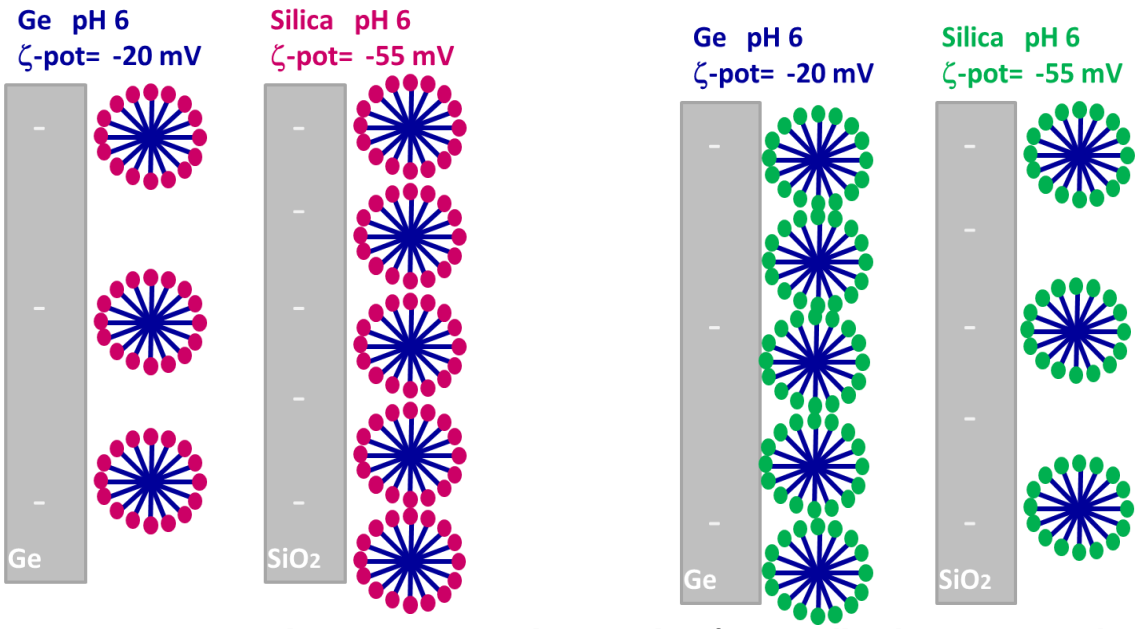

Figure 6.4. ζ-potential measurements and expected surface micelle adsorption **a.** with C_{12}TAB (2 x CMC = 32 mM) and, **b.** with SDS (2 x CMC = 16 mM).

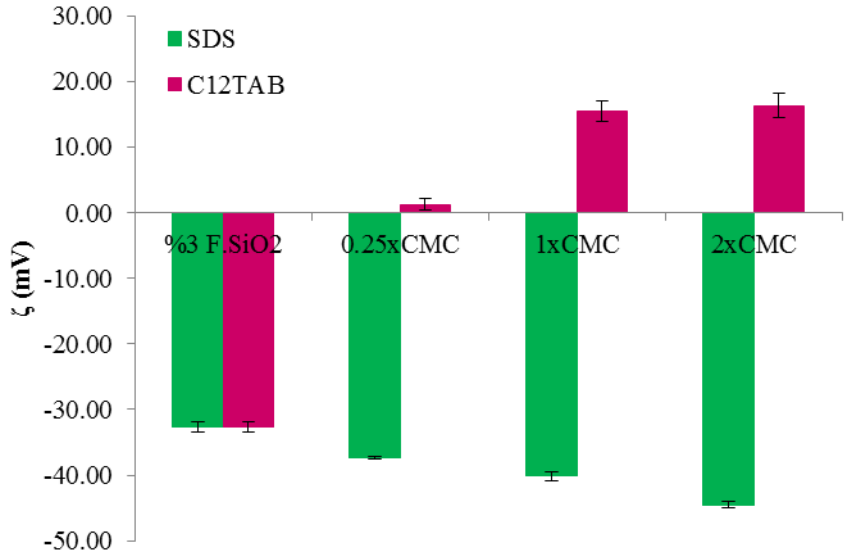

Figure 6.5. ζ-potential of CMP slurry a. with C12TAB (2 x CMC = 32 mM) and b. with SDS (2 x CMC = 16 mM).

Effects of surfactant Concentration on Adsorption: As shown in Figure 6.6.a, the surface charge of germanium is around -20mV without any surface active agent, addition of C_{12}TAB changed the germanium wafer surface more positively charged, and addition of SDS made the germanium surface more negatively charged. The same trends were observed on the silica surfaces as well with relatively more negative charge induced as compared to germanium as shown in Figure 6.6.b. The adsorption model illustrated on Figure 6.4 is partially justified at the 2 x CMC concentration as the micelles tend to be driven towards the surface at this very high concentration. Yet, the wear rate responses obtained at 0.25 x CMC concentrations of the SDS surfactant resulted in 2.2 nm on germanium and 3.3 nm on silica validating the schematic model represented in Figure 6.4.

Material Removal Rate Responses: When we conducted the CMP experiments at H_2O_2 concentration of 0.1 M and selected surfactant concentrations both with the cationic and the anionic surfactants, we observed that both systems were able to provide selectivity

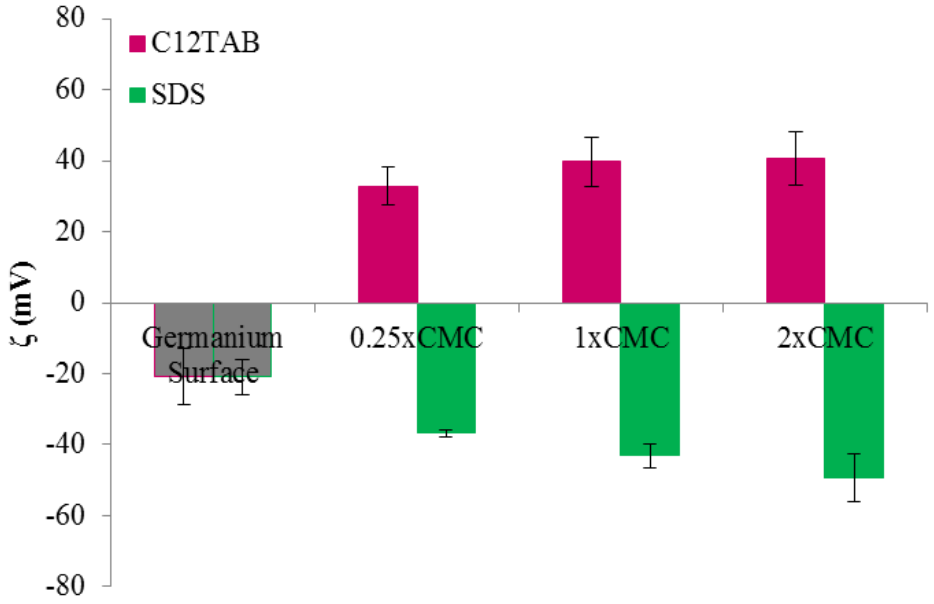

Figure 6.6.a. Zeta potential (ζ) values of a Germanium surface measured in 1 mM KCl solution as a function of surfactant concentration at pH 6.

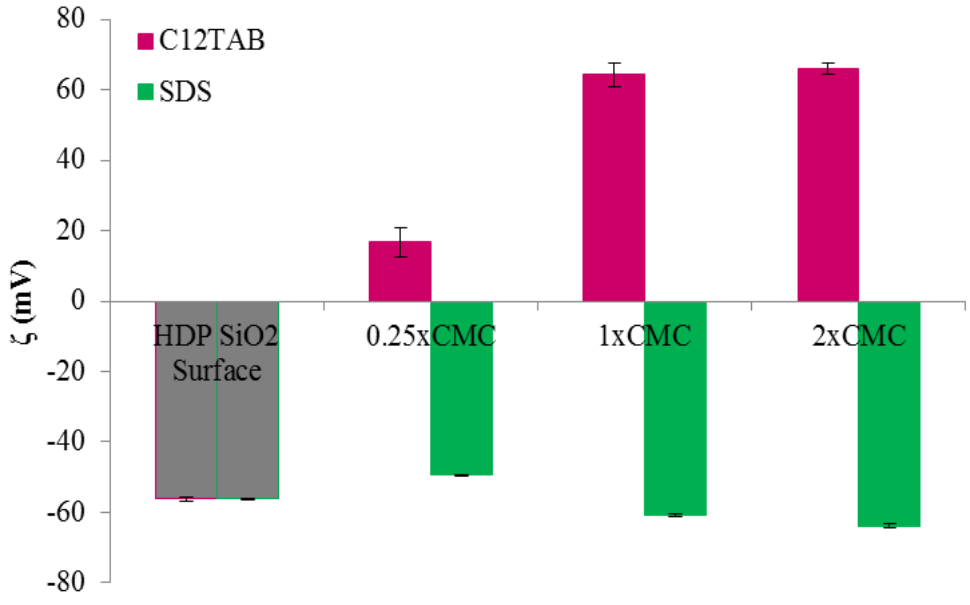

Figure 6.6.b. Zeta potential (ζ) values of a HDP SiO_2 surface measured in a 1 mM KCl solution as a function of surfactant concentration at pH6.

Table 6.3. MRR on SiO_2 vs Ge by C_{12}TAB Concentration

C_{12}TAB	4 mM (0.25xCMC)	16 mM (1xCMC)	32 mM (2xCMC)
Germanium	787	1605	1196
HDP SiO_2	3718	2158	1237
SiO_2/Ge Selectivity	4.7	1.3	~1.0

Table 6.4. MRR on SiO_2 vs Ge by SDS Concentration

SDS	2mM (0.25xCMC)	8 mM (1xCMC)	16mM (2xCMC)
Germanium	873	997	1221
HDP SiO_2	3120	1435	1474
SiO_2/Ge Selectivity	3.6	1.4	~1.2

as required having a higher removal rate on silica as compared to germanium. The measured material removal rates on germanium and HDP SiO2 as a function of C12TAB and SDS concentrations are shown in Table 6.3 and Table 6.4, respectively. From these results, we observed that both systems were able to provide selectivity as required having a higher removal rate of silica as compared to the germanium. These results are suggesting once again that the dissolution reaction is more predominant in Ge CMP and can be inhibited in the presence of surfactants. However, when we evaluated the surface quality responses for both systems, C12TAB was observed to result in a very poor surface as it is shown in figure 6.7 due to poor stability of the slurry system. Furthermore, the attraction in between the negatively charged surface and positively charged particles due to cationic surfactant addition resulted in sticking of the particles on the surface leading to pooor surface roughness measurements. Figure 6.8 shows the surface roughness values of the Ge/HDP SiO2 system as a function of surfactant concentration at pH 6. In addition, it is probable that the C12TAB complexes in the presence of H2O2 as can be seen from the agglomeration of the slurries when C12TAB is added. This complexation can also be the reason for the high selectivity obtained in the

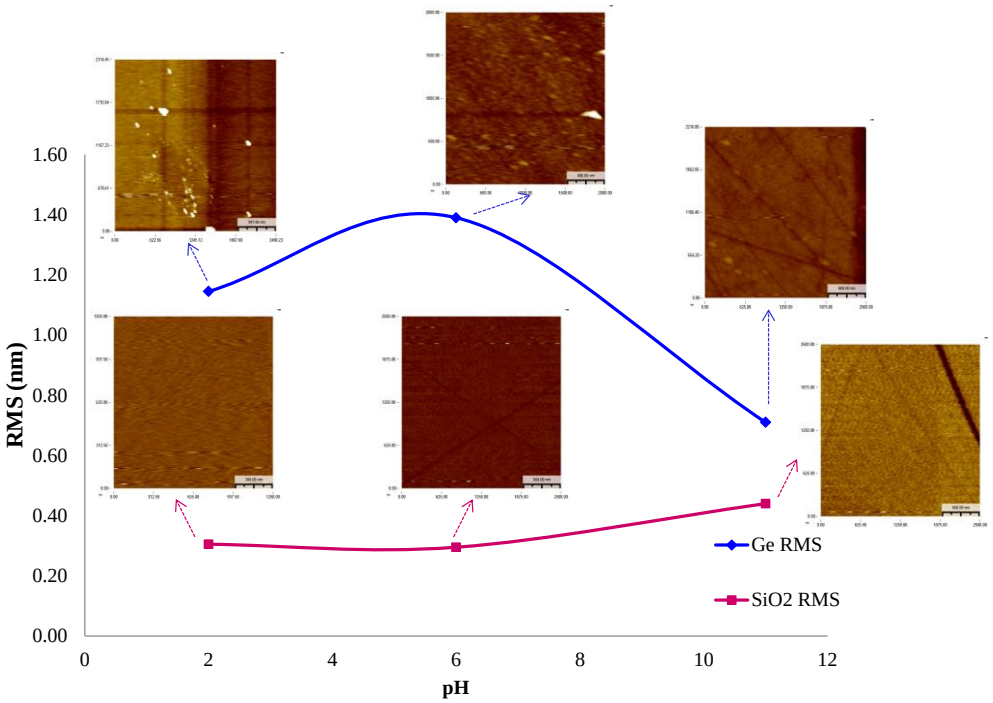

Figure 6.7. Characterization of the Germanium/ HDP SiO_2 wafers after CMP with 32 mM C_{12}TAB at increasing pH for surface roughness responses

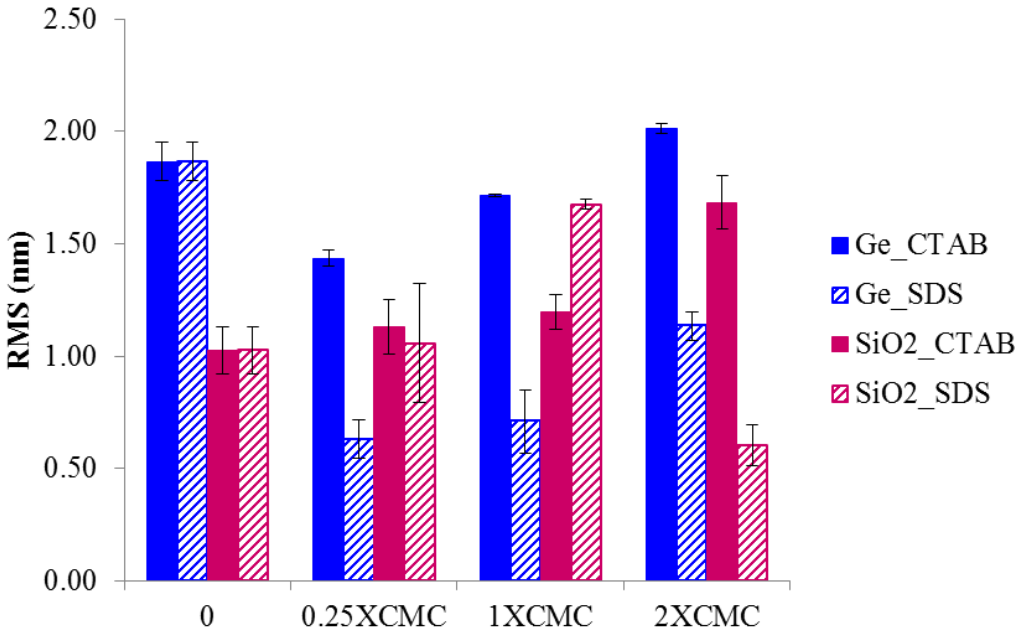

Figure 6.8. Surface Roughness values of a Ge/HDP SiO_2 surface as a function of surfactant concentration at pH 6.

presence of C_{12}TAB although our initial hypothesis does not suggest this system to

provide observed selectivity.(In an aqueous environment, monolayer and bilayer structures of C_{12}TAB aggregates on silica have been confirmed in the literature but the surfactant aggregates are not evenly distributed on the surface) [Liu 13]. Hence it appears that C_{12}TAB is not the correct choice to obtain the desired selectivity. A much exceptable surface quality was obtained with SDS at 2 mM concentration and therefore we continued rest of the study with the SDS surfactant.

DOE Evaluations_Material Removal Rate Response: Statistical analysis showed that the slurry solids loadings and SDS concentration had a significant effect on the material removal rate response within 90 % confidence interval as summarized in the appendix. The three-dimensional surface response plot the silica based CMP slurry is illustrated in Figure 6.9.a for germanium surface and in figure 6.9.b for HDP SiO_2 surface. It is observed from these figures that, increasing the SDS concentration resuls in a decrease in both the material removal rate values on both silica and germanium. Increasing the solids concentration of the slurries, on the other hand, resulted in an increase in the material removal rates. In Figure 6.10 selectivity responses are shown as a function of the SDS concentration and solid loadings. According to these analyses, selectivity is achieved on both the systems. However, it is observed that the optimal polishing is achieved at medium solid loading and 2 x CMC concentration of SDS. Furthermore, the surface quality responses summarized in the earlier sections are also indicating that the best performances on the germanium and the silica surfaces can be obtained in the presence of the SDS surfactant. Hence the use of SDS at 0.25 CMC concentration is the most optimal solution for selectivity with the maximum selectivity obtained simultaneoulsy providing the best surface response and high removal rates.

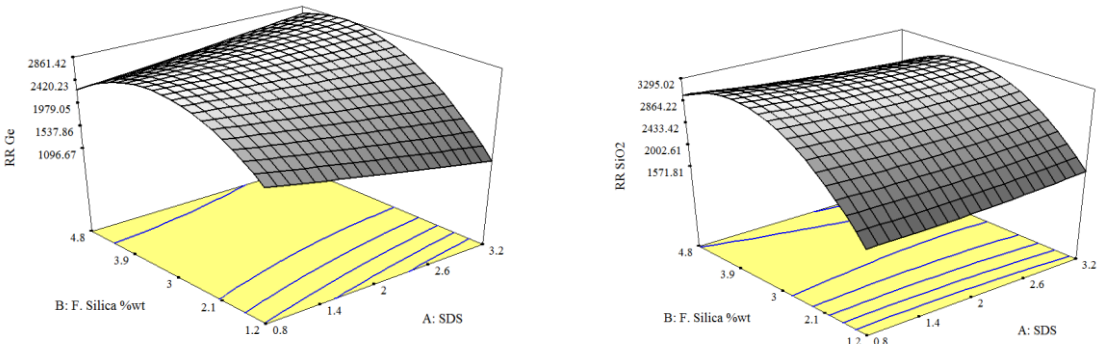

(a) (b)

Figure 6.9. Material Removal Rate response with CMP slurry particle size slurry a. Ge and b. HDP SiO_2

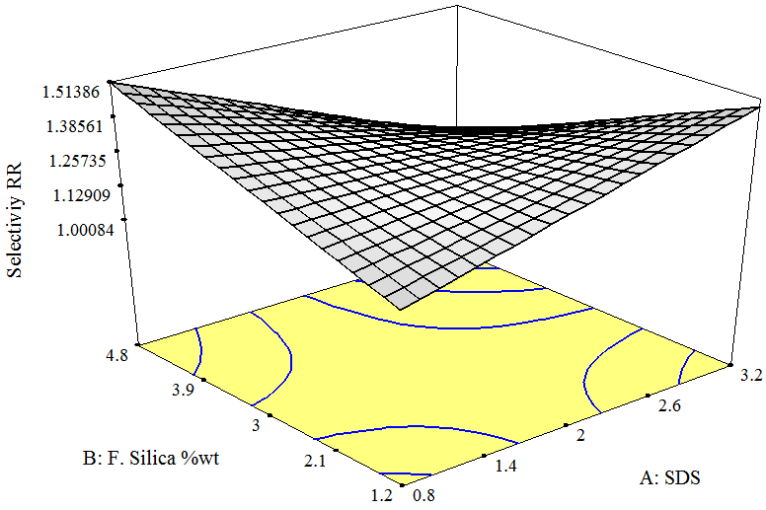

Figure 6.10. Selectivity response as a function of solid loading and SDS Concentration at pH 6.

Summary

It was determined that strong or loose self-assembled surfactant structures can help obtain selectivity on the silica/germanium systems. In addition, good defectivity control with a sufficient material removal rate values were obtained. However, the surface charge of the wafer and the hydrophobic nature of the germanium surface add to the complex surface assembly of the surfactant systems. In summary it was shown that

the use of 2 mM SDS at pH 6 and 0.1 M oxidizer concentration can enable reduction in Ge CMP rates with higher oxide removal rate. AFM wear tests were once again proven to be an easy way of comparing the removal rate responses in the presence of surface active agents. Furthermore, the design of experiments provide an optimal level of slury solids loadings and surfactant concentration that is in agreement with the experimental results obtained in the preliminary studies.

CHAPTER 7

SUMMARY AND SUGGESTIONS FOR FUTURE WORK

Summary

Chemical mechanical planarization (CMP) was adopted by semiconductor industry in 1980s to achieve global planarization of the wafer surfaces for enabling multilevel metallization [Ste04]. As the demand for the processing power of the microelectronic devices increase, more complicated CMP processes are being introduced due to the utilization of advanced materials such as polymeric dielectrics and metal interconnects like Cu and Ge for applications like photovoltaic's, automobiles, RF where efficiency and frequency becomes important. Traditional CMP process involves slurries made of sub-micron size abrasive particles stabilized in an aggressive chemistry which provides a chemical modification on the surface to be polished. The surface film modified by the slurry chemicals is in nanometer scale, and it is removed by the mechanical action provided by the nano nanometer sized particles suspended in the slurry [Kri10].

In this dissertation, focus is on the characterization of the chemically modified thin films which form during the CMP process through the exposure of the surface to be polished to the slurry chemicals to optimize the process performance at a nano-scale. The studies are branched into two main sections. In the first section, the chemically formed metal oxide thin films on metal CMP applications are characterized and in the second section the chemically modified thin film characterization is studied on the nonmetal CMP applications.

The first concentartion of the dissertation on metal CMP applications, the characterization and the nature of the chemically modified surface films have shown a layered oxide formation and the calculation of the P-B ratios suggested that the very top oxide film is a hydroxyl compound of tungsten. However, the subsequent layers have shown stability with P-B ratios calculated in between 1 and 2 in the presence of the oxidizer in the solution. Furthermore, we have investigated that the surface topography of the tungsten wafers tend to change as a function of the oxidizer concentration with a maxima at the 0.075 M concentartion of the oxidizer. The removal rate evaluations by CMP tests also followed the surface roughness response of tungsten showing a minium at this particular concentration. Hence it appears that the investigation at the nano-scale surface topographical changes are important to understand the deviations in the CMP porocess. Furthermore, the observed changes in the surface topography were also found to affect the wettability and total surface energy. Hence it is obvious that the protective nature, as well as the surface nano-topography of the metal oxide thin films need to be studied to assess the CMP performance. Changes in the surface roughness and topography with the oxidizer concentration were explained through a mathematical approach using Cahn-Hilliard theory. The mathematical approach using Cahn-Hillard theory on CMP performance is suggested as a future work for modeling new CMP slurry optimization schemes.

In the second concebtartion of the dissertation, slurry formulations were investigated to characterize the chemically modified thin films to enhance selectivity for germanium/silica (Ge/SiO_2) CMP systems. According to the analysis the impact of chemically modified thin films of the Ge/SiO_2 system, it was observed to be necessary to modify these chemically modified films with oxidizers and surface active agents (surfactants) to achieve optimal removal rate selectivity. Therefore, initially selectivity

analyses were conducted by wear rate responses measured at a single particle-surface interaction level through Atomic Force Microscopy (AFM) with and without the use of surfactants. Both anionic (sodium dodecyl sulfate-SDS) and cationic (cetyl trimethyl ammonium bromide-C_{12}TAB) surfactants were evaluated at their sub-micelle and above critical micelle concentrations (CMC) as a function of pH and oxidizer concentrations. CMP performances of Ge and SiO_2 wafers were evaluated in terms of material removal rates, selectivity and surface quality. It was shown that use of 2 mM SDS at pH 6 and 0.1 M oxidizer concentration can enable reduction in Ge CMP rates with higher oxide removal rates as the selectivity requires. AFM wear tests were observed to correlate to the System level CMP tests and can be utilized as an easy way of evaluating the removal rate responses in the presence of surface active agents. Contact angle measurements have also shown to be a good method to determine the relative selectivity of the surfaces to slurry modifications. In addition, design of experiment (DOE) has also been presnted presented as a function of pH and oxidizer concentration on Ge/SiO_2 selectivity in the optimal conditions for CMP slurry formulations.

CMP process has many problems such as mechanical stress and aggressive chemical action during polishing process. The polishing pressure and the elastic deformation of the pad are viewed as the source of excessive dishing and erosion. Scratching and other mechanical damages have been imputed on the extremely high localized mechanical stress created by the abrasive particles under high pressure. Some of the chemicals, oxidizers are required to obtain high removal rate. In addition to the above, the fragile nature of low-*k* interconnects has prompted the development of alternative CMP processes such as abrasive-free polish [Kon00, Mat03]. Early formulations were called “abrasive-less” simply because they had less abrasive particle concentrations than before. New generation formulations appear to be free of abrasive

particles and contain only surface active agents, bindings, oxidizers, and inhibitor. Matsuda et al.[Mat03] have shown that abrasive-free formulations containing heteropolyacids, surfactants such as poly(ethylene glycol), water-soluble polymers, and other additives. These are called micelle slurries, and polish rates up to 4000 Å have been achieved at down force as low as~1 psi. It appears that abrasive-free CMP processes may have potential benefits in terms of defectivity; however significant process development efforts may be necessary before these new processes become viable options for a manufacturable planarization process for future process.

Suggestions for Future Work

The findings reported in this study can be further expanded to investigate several other issues which are critical to increased performance of the CMP process and chracterization of the chemically modified thin films which form during the CMP process.

One of the main challenges faced in CMP is the development of effective predictive methodologies which can lead to better control of CMP by enabling selection of effective operational and slurry properties. The predictive methodologies must account for the pad-particle-substrate interactions rather than the operational variables alone, as has been the common practice so far. In addition, the chemical effects must be taken into account to develop effective predictive methodologies enabling the formation of a chemically altered layer on the wafer surface during polishing. The mechanical properties of the chemically modified surface are believed to be very different than the substrate material to be polished. Therefore, unless these properties are investigated, the modeling efforts will be incomplete. The most effective technique to measure the mechanical properties of the chemically modified layers is nano-indentation analysis.

However, they cannot provide the required sensitivity for the very thin films formed during CMP. The new techniques, such as ultrasonic force microscopy, introduced for the measurement of the mechanical properties of the ultra-thin films are more promising as they provide highly sensitive and nondestructive methodologies [Cro00, Yar00].

It has been verified in this investigation that the frictional forces play an important role on material removal during the CMP applications. Addition of surfactants, surfactant chain length, change in slurry ionic strength and valency of the added salt were observed to alter the lateral (frictional) interactions in polishing. Although a correlation was detected between the material removal rate and the measured frictional forces, the entire relationship is not known. Therefore, it is also required to model the impact of frictional interactions during the CMP applications. Furthermore, manipulation of the frictional forces during polishing by controlling surfactant adsorption/desorption can be used to design material selective slurries. Enabling the selective adsorption of surfactant molecules to a selected material while the other materials on the substrate remains uncoated, particle-substrate engagement could be achieved for the bare material leading to its polishing, whereas the coated material cannot be removed due to the presence of the lubricating layer. Naturally, these slurries must be tested with the patterned wafers to confirm the degree of selectivity they will provide during polishing.

LIST OF REFERENCES

Baj94 Bajaj R, Desai M, Jairath R, Stell M, Tolles R. Effect of polishing pad material properties on chemical mechanical polishing (CMP) processes. Mater Res Soc Symp Proc;337:637,(1994).

Bar09 S. Bargir, S. Dunn, B. Jefferson, J. Macadam, and S. Parsons, The use of contact angle measurements to estimate the adhesion propensity of calcium carbonate to solid substrates in water, Applied Surface Science, 255(9), 4873 (2009).

Bcd06 B.C. Donose, E. Taran, I.U. Vakarelski, H. Shinto, K. Higashitani, J. Colloid Interface Sci. 299, p.233-237 (2006).

Bro92 Brown, K. H.; Grose, D. A.; Lange, R. C.; Ning, T. H.; Totta, P. A. IBM J. Res. DeV., 36, 821,(1992).

Bud61 S. M. Budd, Phys. Chem. Glasses, 2, 111 (1961).

Chu00 Chunhua Xu · Wei Gao, Pilling-Bedworth ratio for oxidation of alloys, Mat Res Innovat, 3:231–235,(2000).

Chx00 C. H. Xu and W. Gao, Pilling-Bedworth ratio for oxidation of alloys, Materials Research Innovations, **3**(4), 231 (2000).

Cro98 C. Rogers, J. Coppeta, L. Racz, A. Philipossian, F. B. Kaufman and D. Bramon, Journal of Electronic Materials, **27** (10), 1082-1087 (1998).

Dor73 R. Doremus, Glass Science, Wiley, New York, NY (1973).

Dub05 M. Dubash, Techworld.com, April (2005).

Eaf92 E. A. Fitzgerald, Y.-H. Xie, D. Monroe, P. J. Silverman, J. M. Kuo, A. R. Kortan, F. A. Thiel, and B. E. Weir, J. Vac. Sci. Technol. B 10, 1807 (1992).

Eaf95 E. A. Fitzgerald, Annu. Rev. Mater. Sci. 25, 417 ~(1995).

Eak96 E. A. Kneer, C. Taghunath, and S. Raghavan, Electrochemistry of Chemical Vapor Deposited Tungsten Films with Relevance to Chemical Mechanical Polishing, Journal of the Electrochemical Society, 143(12), (1996).

Eal09 E.Alaca, International Materials Reviews, forthcoming, (2009).

Eta06 E. Taran, B.C. Donose, I.U. Vakarelski, K. Higashitani, Colloid and Interface Science, 297, p. 199-203 (2006).

Emc10 E. McCaffery, Introduction to corrosion science, Springer 2010, New York 235,(2010).

Fbk91 F. B. Kaufmann, D. B. Thomson, R. E. Broadie, M. A. Jaso, W. L. Guthrie, M. B. Pearson, and M. B. Small, Chemical-Mechanical polishing for fabricating Patterned W metal features as chip interconnects, Journal of Electrochemical Society, 138(11), 3460 (1991).

Fdo97 F. Dorleans, CMOS transistor with two layer inverse T tungsten gate US patent no: 5633522A (1997).

Gbb03 G. B. Basim, I. U. Vakarelski, and B. M. Moudgil, Role of interaction forces in controlling the stability and polishing performance of CMP slurries, Journal of Colloid and Interface Science, 263, 506 (2003).

Gbb11 G.B. Basim. In Engineered Particulate Systems for Chemical Mechanical Planarization, Lambert Academic Publishing, Saarbrucken, Germany (2011).

Gbb12 G. B. Basim, A. Karagoz, and Z. Ozdemir, Advanced Slurry Formulations for New Generation Chemical Mechanical Planarization (CMP) Applications, MRS Proceedings, 1428, mrss12-1428-c07-08 (2012).

Gbb13 Basim, G.B., Karagoz, A., Ozdemir, Z., ECS Trans. 50 (39), p. 3-7 (2013).

Gli06 G. Lim, J-H. Lee, J-W. Son, H-W. Lee, and K. Kim, Journal of the Electrochemical Society, 153(5), B169 (2006).

Haw06 H. A. Wriedt, The O-W (Oxygen-Tungsten) System, Bulletin of Alloy Phase Diagrams, 10(4), 368 (1989).

Hga03 H. Garcke, B. Niethammer, M. Rumpf, U. Weikard, Acta Mater. 51, p. 2823-2830 (2003).

Hen08 C.Henderson, Semitracs Inc., (2008).

Hep82 Hepburn C. Polyurethane elastomers. London: Applied Science; (1982).

Hiw09 H. Iwai, Roadmap for 22 nm and beyond, Microelectronic Engineering, 86(7–9),1520 (2009).

Hla92 H.Landis, P.Burke, W. Cote, W.Hill, C.Hoffman, C.Kaanta, C.Koburger, W.Lange, and S.Luce, Thin Solid Films, 220,1 (1992).

Hlu02 H. Lua, B. Fookesa, Y. Obengb, S. Machinskia, K.A. Richardsona, Quantitative analysis of physical and chemical changes in CMP polyurethane pad surfaces, Materials Characterization 49,35 – 44,(2002).

Hta00 H. Takasu, Journal of Electroceramics, V.4, (2000).

Hyi06 H.Y. Erbil, Solid and Liquid Interfaces, Blackwell Publishing, (2006).

Ile79 R. Iler, The Chemistry of Silica: Solubility, Polymerization, Colloid and Surface Properties, and Biochemistry, Wiley, New York, NY (1979).

Iuv10 I.U. Vakarelski, S.C. Brown, G.B. Basim, Y.I. Rabinovich, B.M. Moudgil, ACS Applied Materials & Interfaces, Vol. 2, No 4, pp. 1228-1235, (2010).

Iuv12 I.U. Vakarelski, N. Teramoto, C.E. McNamee, J.O. Marston, K. Higashitani. Langmuir, 28 (46), p.16072 (2012).

Iri10 I. Riech, M. Acosta, J. L. Pena, and P. Bartolo-Perez, Effects of working pressure on physical properties of tungsten oxide thin films sputtered from oxide target, Journal of Vacuum Science & Technology, 28(2), 329 (2010).

Jai78 Jain, S. C., Hughes, A. E., J. Mater. Sci. 13, p. 1611-1631 (1978).

Jbm11 J.B. Matovu, N.K. Penta, S. Peddeti, S.V. Babu, Journal of The Electrochemical Society, 158 (11) H1152-H1160 (2011).

Jdi10 J. Diaz-Reyes, R. J. Delgado-Macuil, V. Dorantes-Garcia, A Perez-Benitez, J. A. Balderas-Lopez, and J. A. Ariza-Ortega, Physical properties characterization of WO_3 films grown by hot-filament metal oxide deposition, Materials Science and Engineering B-Advanced functional solid-state materials, 74(1–3), 182 (2010).

Jdr87 J. Drxylama, J. Lekki, Powder Technology, 52, p. 251 (1987).

Jer13 Jerry Wu, Yin-Lin Shen, Kitt Reinhardt, Harold Szu, and Boqun Dong, Review Article A Nanotechnology Enhancement to Moore's Law, Applied Computational Intelligence and Soft Computing, Article ID 426962, 13 pages, (2013).

Jmi09 J. Mitard et al., Symposium on VLSI Technology, Digest of Technical Papers., 82, (2009).

Jos04 Joseph M. Steigerwald, Shyam P.Murarka, Ronald J. Gutmann, Chemical Mechanical Planarization of Microelectronic Materials, (2003).

Jru06 J. Ruzyllo, Substrates for the next generation electronics and photonics, ElectroChemical Society's Interface, 15(4), 21 (2006).

Jsp09 J.-S. Park, M. Curtin, J.M. Hydrick, J. Bai, J.-Li, Z. Cheng, M. Carrol, J.G. Fiorenza, and A. Lochtefeld, Electrochem.solid-state let., 12, H142-H144 (2009).

Jwc58 J. W. Cahn and J. E. Hilliard, J. Chem. Phys. 28, p. 258-267 (1958).

Jwc61 J. W. Cahn, Acta Met. 9, p. 795 - 801 (1961).

Jwc65 J. W. Cahn, J. Chem. Phys. 42, p. 93-99 (1965).

Kon00 Kondo, S.; Sakuma, N.; Homma, Y.; Goto, Y.; Ohashi, N.; Yamaguchi, H.; Owada, N. J. Electrochem. Soc.,147, 3907, (2000).

Kri10 M. Krishnan, J.W. Nalaskowski, L.M. Cook, Chemical mechanical planarization: slurry chemistry, materials, and mechanisms, Chem. Rev. 110, 178–204, (2010).

Lor11 Lorenz, M., Wencksten, H., Grundmann, M., Adv. Mater. 23, p. 5383-5386 (2011).

Leu14 P. Leunissen, Electronic Materials by BASF Chemistry innovation as an enabler, NIM2014, (2014).

Lgp54 L. G. Parratt, Surface Studies of Solids by Total Reflection of X-Rays, Phys. Rev. 95, 59 (1954).

Liu13 Y.Liu, M. Tourbin, S. Lachoize, P.Guiraud, Silica Nanoparticles Separation from water: aggregation by cetryltrimethylammoniumbromide(CTAB), Polymed, (2013).

Mac01 Machinski S. Wear characterization of polyurethane chemical mechanical polishing pads, MS Thesis, University of Central Florida, FL, Summer, (2001).

Mah09 Mahadevaiyer Krishnan, Jakub W. Nalaskowski, and Lee M. Cook, Chemical Mechanical Planarization: Slurry Chemistry, Materials, and Mechanisms,IBM (2009).

Mat03 Matsuda, T.; Takahashi, H.; Tsurugaya, M.; Miyazaki, K.; Doy, T. K.; Kinoshita, M. J. Electrochem. Soc., 150, G532, (2003).

Mbi00 M. Bielman, U. Mahajan, R. K. Singh, P. Agarwal, S. Mischler, E. Rosset, and D. Landolt, in Chemical Mechanical Polishing – Fundamentals and Challenges, S. V. Babu, S. Danyluk, M. Krishnan, and M. Tsujimura, Editors, PV 566, p. 97, Mater. Res. Soc. Proc., Pittsburgh, PA (2000).

Mkr10 M. Krishnan, J. W. Nalaskowski, and L. M. Cook, Chemical mechanical planarization: slurry chemistry, materials, and mechanisms, Chemical Reviews,110, 178 (2010).

Mlo11 M. Lorenz, H. Von Wenckstern, and M. Grundmann, Tungsten Oxide as Gate Dielectric for Highly Transparent and Temperature-Stable Zinc-Oxide-Based Thin Film Transistors, Advance Materials, 23, 5383 (2011).

Nkd09 N. K. Das, K. Suzuki, K. Ogawa, and T. Shoji, Early stage SCC initiation analysis of fcc Fe-Cr-Ni ternary alloy at 228 degrees C:Aquantum chemical molecular dynamics approach, Corrosion Science, 51(4), 908 (2009).

Nva05 N. V. Allov, Determination of the states of oxidation of metals in thin oxide films bu X-ray photoelectron spectroscopy, Journal of Analytical Chemistry, 60 431 (2005).

Ped12 Peddeti S et al., Chemical Mechanical Planarization of Germanium Shallow Trench Isolation Structures using Silica Based Dispersions, Microelectronic Engineering, (93) 61-66, (2012).

Pff03 P. F. Fewster, X-Ray Scattering from Semiconductors. Imperial College Press, London, p. 82, (2003).

Pon12 P.Ong et al., ICPT 2012, Grenoble, France, (2012).

Psa98 P. Sallagoity, F. Gaillard, M. Rivoire, M. Paoli, M. Haond, STI process steps for sub-quarter micron CMOS,Microelectron. Reliab. 38, 271 (1998).

Rdw11 R. D. White, A. J. Mueller, M. Shin, D. Gauthier, V. P. Manno, and C. B. Rogers, Measurement of microscale shear forces during chemical mechanical planarization, Journal of The Electrochemical Society, 158(10), 1041 (2011).

Rep05 ReportU.S. Geological Survey, Reston, Virginia (2005).

Rjw13 R. J. W. Hill, I. Ali C. Hobbs P.D. Kirsch – SEMATECH G. Whitener, B. Ward, B.Fortino – Cabot. High mobility channel materials: CMP challenges and opportunities (2013).

Ros89 M.J. Rosen, "Surfactants and Interfacial Phenomena," p. 337,Wiley, NewYork, (1989).

Ruz06 J. Ruzyllo, Interface, V.15, No.4, (2006).

Sad81 S. Adachi, Journal of The Electrochemical Society, 129, 609 (1981).

Scj78 S. C. Jain and A. E. Hughes, Ostwald ripening and its application to precipitates and colloids in ionic crystals and glasses, Journal of Materials Science, 13, 1611 (1978).

Sma10 S. Manciu Felicia, J. L. Enriquez, G. W. Durrer, Y. Yun, C. V. Ramana, and

S. K. Gullapalli, Spectroscopic analysis of tungsten oxide thin films, Journal of Material Research, 25(12), 188 (2010).

Spe11 S. Peddeti, P.Ong, L. H. A. Leunissen and S. V. Babu, "Chemical Mechanical Polishing of Ge Using Colloidal Silica Particles and H_2O_2", doi: 10.1149/1.3575166, Electrochem. Solid-State Lett., Volume 14, Issue 7, Pages H254-H257, (2011).

Spe12 S. Peddeti, P. Ong, L.H.A. Leunissen, S.V. Babu, "Chemical mechanical planarization of germanium shallow trench isolation structures using silica-based dispersions", Microelectronic Engineering 93, 61–66 (2012).

Ste04 J.M. Steigerwald, S.P. Murarka, R.J. Gutmann, Chemical Mechanical Planarization of Microelectronics Materials, Wiley-VCH, Weinheim, 2004. pp.15–33.

Str04 Strained Si, SiGe, and Ge on-insulator: review of wafer bonding fabrication techniques Gianni Taraschi *, Arthur J. Pitera, Eugene A. Fitzgerald- Solid-State Electronics 48,1297–1305(2004).

Swo91 S. Wolf, Silicon Processing for VLSI Era II, Process Integration 45, McGraw-Hill, New York, (1991).

Tht03 T.-H. Tsai, S.-C. Yen, Localized corrosion effects and modifications of acidic and alkaline slurries on copper chemical mechanical polishing, Appl. Surf. Sci. 210, (3– 4) (2003).

Thu94 T. Küpper, N. Masbaum, Acta Metall. Mater. 42 (6), p. 1847-1858 (1994).

Vac95 V. A. C. Haanappel, H. D. Vancorbach, T. Fransen, and P. J. Gellings, Scanning scratch tests for evaluating the adhesion of thin oxide films on stainless steel, Material Research Society Symposia Proceedings, 356 (1995).

Vak10 Vakarelski I. U., Brown, S.C, Basim G.B, Rabinovich, Y. I., and Moudgil B.M., Tailoring Silica Nanotribology for CMP Slurry Optimization: Ca^{2+} Cation Competition in C_{12}TAB Mediated Lubrication, ACS Applied Materials & Interfaces, Vol. 2, No 4, pp. 1228-1235, (2010).

Wbc11 W.B.Chen, C.H. Cheng, C.W. Lin, P.C. Chen, and A. Chin, Solid-State Electron.,55,64 (2011).

Wei09 Wei-En Fu,Tzeng-Yow Lin , Meng-Ke Chen , Chao-Chang A. Chen , Surface qualities after chemical–mechanical polishing on thin films, Thin Solid Films 517,4909–4915, (2009).

Wsh12 W. Shin, J. An, J. Kim, H. Jeong, Proceedings of ICPT 2012, October 15-17, p. 309-314, Grenoble, France (2012).

Ysk97 Y.S. Kim, US patent # 5595934, Samsung Electronics Co., Suwon, KR,(1997).

Zst97 Z. Stavreva, D. Zeidler, M. Plötner, K. Drescher, Characteristics in chemical-mechanical polishing of copper: comparison of polishing pads, Appl. Surface Sci. 108, 39–44, (1997).

BIOGRAPHICAL SKETCH

Ayse Karagoz was born on May 6, 1983, in Soma-Manisa, Turkey. She graduated first in the graduating class in 2001 from Muharrem Hasbi High Scholl in Balıkesir, Turkey. She then enrolled at Anadolu University in Eskişehir, Turkey. In July 2007 she graduated the graduating class with a Bachelor of Science degree in chemical engineering with a specialization in biodiesel production from Rape Seed Oil and characterization. Then, she focused on synthesis and characterization of polymeric biomaterials and their applications during her MS at Bioengineering Department at Yıldız Technical University (YTU), 2009. After her MS, she continued her academic career as a PhD student at YTU and transferred to Ozyegin University in January,2013. Since March 2010 she has been involved in a Marie Curie International Reintegration Grant project (Nano-Scale Protective Oxide Films for Semiconductor Applications & Beyond) under the advisory of Assoc. Prof. Dr. G.Bahar Başım at Ozyegin University. She has spent nine months at University of Florida Engineering Research Center for Particle Science & Technology to work on a research project on CMP founded by US National Institute for Standards and Technology. Moreover, she had worked as a part time PhD student at Bosch&Siemens Home Appliance(B/S/H) Company at Technology and Innovation Department from October 2011 to January 2013. In addition, she has also collaboration with the Siegen University for three months in an effort to realize the polymeric particle synthesis and nano-capsulation efforts for CMP applications. Her dissertation research concentrated on nano-scale chemically modified thin film characterization for chemical mechanical planarization applications. She graduated from Ozyegin University with a doctorate degree in mechanical engineering with electronic materials in January 2015.

I. APPENDIX

CENTRAL COMPOSITE DESIGN AND RESPONSES

Experimental variables:

A: Concentration of SDS (mM)

B: Solids loading (% wt)

C: pH

Responses:

Material removal rate (MRR) (Å/min)

Selectivity (nm)

Contact Angle (θ)

Final equations (* Significant factors in 95% confidence interval):

Ge Material removal rate =

$2717^{*} - 97\,A^{*} + 477\,B^{*} - 133\,C^{*} + 20\,A^{2*} - 733\,B^{2*} - 267\,C^{2*} + 332\,AB^{*} + 507\,AC^{*} + 86\,BC^{*}$

SiO_2 Material removal rate =

$3043^{*} - 63\,A^{*} + 572\,B^{*} + 209\,C^{*} + 48\,A^{2*} - 877\,B^{2*} - 82\,C^{2*} - 130\,AB^{*} - 28\,AC^{*} + 14\,BC^{*}$

Ge Selectivity =

$1.27^{*} - 0.043\,A^{*} + 0.029\,B^{*} + 0.23\,C^{*} - 0.21\,AB^{*} - 0.42\,AC^{*} - 0.056\,BC^{*}$

SiO_2 Selectivity =

$1.27^{*} - 0.032\,A^{*} + 0.000099\,B^{*} + 0.044\,C^{*} + 0.013\,A^{2*} - 0.031\,B^{2*} - 0.087\,C^{2*} - 0.00\,AB^{*} + 0.00075\,AC^{*} + 0.00\,BC^{*}$

Ge Contact Angle =

40.03*– 6.14 A*- 0.000894 B* - 0.93 C*

SiO_2 Selectivity =

47.00*– 6.39 A*- 0.0000322 B* - 0.75 C*

Run No	Pattern	SDS Conc. (mM)	Solids Conc. (%wt)	pH	Ge MRR (Å/min)	SiO_2 MRR (Å/min)	Ge CA (θ)	SiO2 CA (θ)	Ge Selectivity	SiO2 Selectivity
1	-00 Axial	2	3	6	2751	3074	37.88	47.69	1.117	1.259
2	0+0 Axial	2	3	6	2649	2917	37.88	47.69	1.010	1.259
3	000 Center	2	3	6	2716	3141	37.88	47.69	1.157	1.259
4	-++ Face	2	3	3	1392	2102	43.98	43.31	1.510	0.986
5	+-- Face	3.2	1.2	4.2	951	1538	36.68	40.64	1.618	1.108
6	--+ Face	3.2	1.2	7.8	1158	1743	37.74	44.52	1.505	1.180
7	000 Center	2	6	6	977	1151	37.88	47.69	1.178	1.259
8	++- Face	0.8	4.8	4.2	2864	2881	45.46	47.96	1.006	1.055
9	-+- Face	2	3	6	2830	3073	37.88	47.69	1.086	1.259
10	+-+ Face	0.8	4.8	7.8	1388	3253	46.41	50.93	2.343	1.097
11	000 Center	4	3	6	2021	2853	29.03	41.33	1.412	1.424
12	--- Face	2	0.1	6	0	0	37.88	47.69	1	1.259
13	00- Axial	0.8	1.2	7.8	658	1527	46.41	50.93	2.321	1.097
14	00+ Axial	2	3	6	2741	3058	37.88	47.69	1.116	1.259
15	+00 Axial	2	3	9	2015	3266	34.00	41.18	1.621	1.211
16	000 Center	0.8	1.2	4.2	2636	1338	45.46	47.96	0.508	1.055
17	0-0 Axial	2	3	6	2738	3046	37.88	47.69	1.113	1.259
18	000 Center	3.2	4.8	7.8	3061	2824	37.74	44.52	0.923	1.180
19	+++ Face	3.2	4.8	4.2	2665	2689	36.68	40.64	1.009	1.108
20	000 Center	0	3	6	2987	3239	58.06	76.85	1.085	1.325